

AN ABSTRACT OF THE THESIS OF

William George McDougal for the degree of Doctor of Philosophy in
Civil Engineering presented on September 11, 1981.

Title: Ocean Wave-Soil-Geotextile Interaction

Abstract approved: **Redacted for privacy**
Dr. Charles K. Sollitt

Geotextiles are synthetic fabrics which may be substituted for graded aggregate to protect ocean and coastal structures from erosion and soil instability adjacent to the structure. They are commonly used as a filter and as a structural membrane between an undisturbed sediment surface below and an erosion resistant coarse aggregate above. Geotextiles provide a cost effective alternative to graded aggregate in marine foundations. The need for rational design procedures has led to a theoretical description of the combined soil-geotextile behavior which quantifies failure potential and facilitates optimum geotextile selection. A two-dimensional analytical model has been developed for a three layered system; two different soils separated by a geotextile. The soil response is modeled by Biot consolidation theory and an unsteady form of Darcy's equation in which each soil is considered homogeneous, isotropic and linearly elastic. The soil layers are coupled through the geotextile which acts as an elastic permeable membrane. Soil displacements and stresses and fluid pressures and flows are determined analytically. Potential failure conditions are identified from the cyclic shear stress ratio and from a Mohr-Coulomb stress analysis.

Two series of laboratory experiments were conducted at the Oregon State University Wave Research Facility to verify the model. The large scale facility includes a wave channel which is 12 feet wide, 15 feet deep and 342 feet long. A test section 36 feet long was constructed in the wave channel and filled with approximately three feet of fine sand, a geotextile and one foot of gravel. The test section was exposed to simple harmonic and random waves with heights up to four and one-half feet and periods to eight seconds in water depths to eight feet. The pore water pressure was monitored continuously at seven to ten soil depths and three to five lateral positions and recorded on magnetic tape along with the displacement of the free surface. Four geotextile conditions were tested including woven, impermeable, semi-rigid and no geotextile. Wave-induced liquefaction was observed for a low permeability geotextile.

The experimental results verify the soil-geotextile interaction model and also provide insight into the dynamic response of horizontally layered soils. Results indicate that for the permeabilities of commonly available geotextiles that the hydraulic properties of the geotextile are dominated by the adjacent soil properties. However, clogging of the geotextile increases the potential for soil failure. The pore pressure amplitude response is frequency selective, the higher frequencies being more highly damped. For a given soil condition a "worst" wave period may exist which produces maximum failure potential. Conversely, for a given design wave, there is a "worst" combination of backfill and armor in terms of potential failure.

Ocean Wave-Soil-Geotextile
Interaction

by

William George McDougal

A THESIS

submitted to

Department of Civil Engineering
Oregon State University

in partial fulfillment of
the requirements for the
degree of

Doctor of Philosophy

Completed September 11, 1981

Commencement June 1982

APPROVED:

Redacted for privacy

Professor of Civil Engineering in Charge of Major

Redacted for privacy

Head of Department of Civil Engineering

Redacted for privacy

Dean of Graduate School

Date thesis is presented _____ September 11, 1981

Typed by Connie Best and Connie Wilson for _____ William G. McDougal

ACKNOWLEDGEMENTS

Thank you C.K. Sollitt, T.S. Vinson, D.L. Thielen and J.F. McDougal.

This research was supported by the Oregon State University Sea Grant College Program, National Oceanic and Atmospheric Administration Office of Sea Grant, Department of Commerce, under Grant No. NA79AA-D-00106.

TABLE OF CONTENTS

	<u>Page</u>
1.0 INTRODUCTION	1
1.1 Motivation	2
1.2 Scope	3
1.3 Literature Review	3
1.3.a Ocean Engineering Literature	4
1.3.b Geotechnical Literature	8
1.3.c Geotextile Literature	8
1.3.d Relevant Literature Synopsis	9
1.4 Geotextile Properties	10
2.0 DEFINING EQUATIONS	12
2.1 Elastic Soil Equations	12
2.2 Storage Equation	17
2.3 Boundary Conditions	21
2.3.a Mudline Boundary Conditions	21
2.3.b Geotextile Boundary Conditions	23
2.3.c Impermeable Bottom Boundary Conditions	25
3.0 SOLUTIONS TO THE BIOT EQUATIONS	27
3.1 Earthquake Consolidation Equation Model	27
3.2 Potential Pressure Model	32
3.3 Periodic, Two-Dimensional Biot Model	38
3.3.a Computer Program	47
4.0 ANALYTICAL SOLUTION BEHAVIOR	50
4.1 Single Soil Layer Response	50
4.2 Two Soil Layer Response	62

TABLE OF CONTENTS (continued)

	<u>Page</u>
5.0 EXPERIMENTAL RESULTS	71
5.1 Laboratory Setup	71
5.1.a Oregon State University Wave Research Facility	71
5.1.b Test Section	71
5.1.c Pressure Transducers	79
5.2 Laboratory Measurements	79
5.3 Comparison of Theory and Observations	83
5.4 Wave-Induced Failure	94
6.0 CONCLUSIONS	99
6.1 Summary	99
6.2 Applications	100
6.3 Future Research	101
REFERENCES	103
APPENDIX A. List of Notations	109
APPENDIX B. Computer Programs	113
B.1 Program GEOTEX	113
B.2 Program PLOTT	128
APPENDIX C. Determination of Test Section Length	132
APPENDIX D. Laboratory Measurements	136
D.1 1980 Measurements	136
D.2 1981 Measurements	142
APPENDIX E. English/SI Unit Conversions	143

LIST OF FIGURES

<u>Figure</u>	<u>Page</u>
2.1 Definition sketch for the coordinate system and stress notation	13
2.2 Soil layer definition sketch	13
3.1 Rate of pore water pressure build-up in simple cyclic shear tests	31
3.2 Dimensionless pore water pressure accumulation profiles	31
3.3 Idealized wave-induced soil failure due to periodic and mean accumulation of pore water pressure	34
3.4 Vertical pore water pressure profiles from the potential pressure model for stream function wave cases 5B, 7B and 8B	37
3.5 Computer program block diagram	49
4.1 Wave-induced horizontal displacement, vertical displacement, excess pore water pressure and horizontal effective stress for the case A conditions	52
4.2 Wave-induced vertical effective stress, shear stress, horizontal discharge velocity and vertical discharge velocity for the case A conditions	53
4.3 Wave-induced shear stress ratio and shear stress angle for the case A conditions	54
4.4 Frequency dependency of pore water pressure profiles for the case A conditions	56
4.5 Transfer function for the dimensionless pore water pressure from the potential pressure model	56
4.6 Frequency dependency of the maximum displacements and shear stress for the case A conditions	57
4.7 Maximum displacements and stresses as a function of the shear modulus for the case A conditions	57
4.8 Maximum displacements as a function of the degree of bottom slip for the case A conditions	59

LIST OF FIGURES (continued)

<u>Figure</u>	<u>Page</u>
4.9 Pore water pressure profiles as a function of the degree of bottom slip for the case A conditions	59
4.10 Pore water pressure profiles as a function of the degrees of saturation for the case A conditions	60
4.11 Maximum displacements and shear stress as a function of the degree of saturation for the case A conditions	60
4.12 Pore water pressure profiles as a function of the soil thickness for the case A conditions	61
4.13 Maximum displacements and shear stress as a function of the soil thickness for the case A conditions	61
4.14 Pore water pressure profiles as a function of the geotextile permeability for the case B conditions	63
4.15 Maximum displacements and shear stress as a function of the geotextile permeability for the case B conditions	63
4.16 Pore water pressure profiles as a function of the relative permeability for the case B conditions ($K_2 = 0.01$ ft/s)	65
4.17 Maximum displacements and shear stress as a function of the relative permeability for the case B conditions ($K_2 = 0.01$ ft/s)	65
4.18 Pore water pressure profiles as a function of the relative permeability for the case B conditions ($K_1 = 0.01$ ft/s)	66
4.19 Maximum displacements and shear stress as a function of the relative permeability for the case B conditions ($K_1 = 0.01$ ft/s)	66
4.20 Maximum displacements and shear stress as a function of the geotextile elasticity for the case B conditions	68
4.21 Maximum displacements and shear stress as a function of geotextile tension for the case B conditions	68

LIST OF FIGURES (continued)

<u>Figure</u>	<u>Page</u>
4.22 Pore water pressure profiles as a function of the degree of saturation of the upper layer for the case B conditions	70
5.1 In place photograph of the test section before the addition of the soil layers	73
5.2 Typical cross-section of the test section	73
5.3 Shear modulus and Poisson's ratio in lower soil layer as a function of porosity for different confining pressure	74
5.4 Buoyant weight and permeability for the lower soil layer as a function of porosity	74
5.5 Monofilament woven geotextile (Polyfiber GB, Carthage Mills)	75
5.6 Needle punch nonwoven geotextile (Bidim C42, Monsanto)	75
5.7 Heat bonded nonwoven geotextile (Tygar, Dupont)	76
5.8 Combination woven/nonwoven geotextile (Terrafix 500N, Terrafix)	76
5.9 Definition diagram for Dean's stream function wave cases	82
5.10 Dimensionless measured pore water pressure profiles for stream function wave cases 8A, 8B and 8C	84
5.11 Average dimensionless measured pore water pressure profiles for stream function wave cases 8A, 8B and 8C as a function of geotextile conditions	84
5.12 Comparison of theory and measurements for the no geotextile condition	85
5.13 Comparison of theory and measurements for the no geotextile condition	86
5.14 Comparison of theory and measurements for Polyfilter GB geotextile	88
5.15 Comparison of theory and measurements for Polyfilter GB geotextile	89

LIST OF FIGURES (continued)

<u>Figure</u>	<u>Page</u>
5.16 Comparison of theory and measurements for the compliant impermeable geotextile	90
5.17 Comparison of theory and measurements for the compliant impermeable geotextile	91
5.18 Comparison of theory and measurements for the semi-rigid geotextile	92
5.19 Comparison of theory and measurements for the semi-rigid geotextile	93
5.20 Pore water pressure profiles as a function of the armor layer thickness for approximately the experimental conditions and wave case 7B	95
5.21 Maximum displacements and shear stress as a function of the armor layer thickness for approximately the experimental conditions and wave case 7B	95
5.22 Laboratory measurements of wave-induced liquefaction	97
5.23 Geotextile before failure	98
5.24 Geotextile after failure	98
C.1 Portion of the test section with less than 5% error due to the end effects as a function of different wave and test section lengths	135

LIST OF TABLES

<u>Table</u>		<u>Page</u>
1.1	Categorization of ocean engineering wave-bottom interaction literature	6
3.1	Non-dimensionalizing scaling factors	48
4.1	Case A wave and soil conditions	50
4.2	Case B wave and soil conditions	62
5.1	Test section upper layer soil properties	72
5.2	Geotextile properties	77
5.3	Lower soil layer porosities for the 1980 tests	78
5.4	Mean lower soil properties	78
5.5	Pressure transducer locations	80
5.6	Simple periodic waves tested for a water depth of four feet	80
5.7	Simple periodic waves tested for a water depth of eight feet	81

OCEAN WAVE-SOIL-GEOTEXTILE INTERACTION

1.0 INTRODUCTION

Geotextiles are synthetic fabrics which may be substituted for graded aggregate to protect ocean and coastal structures from erosion and soil instability. Geotextiles are commonly used as a structural membrane and as a filter between an undisturbed sediment surface below and an erosion resistant coarse aggregate placed above. Applications in coastal engineering include: erosion protection at piers, dolphins, dikes and tidal channels; foundation stabilization under sea walls, caissons and outfalls; intermediate layers in composite breakwaters, jetties and groins; and reinforcement of buried pipeline back-fill material.

Geotextile fabrics are derived from polymers which are constructed as woven, nonwoven or a combination. The mechanical and hydraulic properties of the geotextile vary with the fabric type and may be adjusted to focus on five important performance functions: drainage, filtration, reinforcement, separation and armor. In addition, a geotextile composition must be selected to provide satisfactory placement and longevity for the design life of the structure. Thus, properties such as resistance to ultraviolet deterioration, biofouling, tearing, puncturing, etc. must also be considered in the selection of the optimum geotextile. It is readily apparent that the performance functions, constructability and longevity impose a great number of constraints on the desirable fabric properties for a particular application. This problem is compounded by the recent advent of hundreds of durable and economical geotextiles suitable for both marine and terrestrial application.

1.1 Motivation

Most ocean and coastal structures require protection from erosion and soil instability effects adjacent to the structure. A common practice is to riprap the sediment surface near the structure with graded geologic materials. The geologic materials are placed in layers with the smallest in contact with the undisturbed sediment surface and with each layer increasing in size up to the final armor layer at the top. The armor layer material is selected to provide a stable surface at the design wave and current conditions. The other layer sizes are selected to minimize the exchange of geologic material between adjacent layers.

An alternative to graded riprap filters is the use of synthetic filter fabrics or geotextiles. A geotextile may replace several intermediate layers of graded materials and thereby reduce the construction costs. In the construction of deep water marine structures, the placement of graded riprap filters becomes very difficult. This difficulty may be reduced through the use of geotextiles. A third benefit of geotextiles is that they confine the movement of the soil. Buried pipelines may be held down by fabric tension.

Geotextiles provide a cost-effective alternative to graded riprap filters, are less difficult to work with in deeper water and provide an additional mode of soil stabilization. As a result, geotextiles are being used in an increasing number of marine structures. However, the use of these materials has preceded a well-defined analysis, design and construction procedures required to insure their successful performance in the field [Heerten (1981)].

This study responds to the need for a comprehensive examination of synthetic geotextile behavior in coastal and ocean engineering applications. A theoretical description of the combined wave-soil-geotextile interaction is developed which provides the framework to develop meaningful design procedures.

1.2 Scope

An analytical model is developed to quantify the response of a horizontal, three-layered soil-geotextile-soil system to wave excitation. The differential equations describe each soil layer as a homogeneous, isotropic, linearly elastic medium. The fluid flow in the interstices of the soil is described by an unsteady, compressible fluid form of Darcy's equation. The two soil layers are coupled through the geotextile which acts as an elastic permeable membrane. A general solution to the differential equations is obtained assuming simple harmonic dependence in time and the horizontal direction of surface wave propagation. This reduces the system of partial differential equations to ordinary differential equations in depth which have exponential solutions. The model is verified with experimental results. The behavior of the solution is examined for a variety of soil and geotextile characteristics.

1.3 Literature Review

Fluid flow in porous media is common to many areas of science and engineering. However, most of the literature is the result of four areas of research: ground water flow, geotechnical engineering, mechanics and ocean engineering. The systems being modeled by each discipline are similar but the relative importance of individual processes varies among the fields. In ground water problems the rate of flow may be of interest while in geotechnical engineering the soil settlement or consolidation due to the expulsion of the pore fluid is of major interest. In the mechanics literature more emphasis is placed on soil stresses and displacements while in ocean engineering wave damping and sub-bottom failures are of interest. The diversity of application has, unfortunately, fragmented the literature.

The present study, while falling in the ocean engineering category, is an attempt to draw concepts from all four disciplines to develop a physically meaningful set of defining equations with a tractable solution. An overview of the ocean engineering literature is

presented, followed by a review of geotechnical literature, a review of geotextile literature and a summary of the literature relevant to the present wave-soil interaction study.

1.3.a Ocean Engineering Literature

The interaction of water waves and the bottom has been observed in the field [Gade (1958), Bennett and Faris (1979), Bea et al. (1980)], and demonstrated in the laboratory [Nakamura et al. (1973) and Nath et al. (1977)]. Heerten (1981) suggests that significant profile changes and slope reduction of a revetment was caused by wave-induced liquefaction. Wave-induced failures associated with large storms observed in the Mississippi delta and have resulted in pipeline failures [Bea et al. (1980)]. In a soft permeable sediment excess pore water pressures are developed and the bottom deforms in response to the wave pressure. Either or both of these mechanisms may lead to a soil failure. Since energy is dissipated at the fluid-soil interface and in the soil layer, the water wave height is attenuated. This attenuation may be significant if the bottom is very soft or the wave travel distance in shallow water is long. The magnitude of the wave bottom interaction is a function of the wave conditions and the soil matrix properties. A variety of theories have been proposed within the framework of these variables; permeable or impermeable bottom, rigid or deformable soil skeleton, compressible pore fluid and the degree of wave-bottom interaction. A number of theories are categorized by these assumptions in Table 1.1.

The simplest assumptions are that the bottom is rigid, impermeable and smooth. This leads to a no wave-bottom interaction solution [Lamb (1932)]. A number of solutions have been developed which include bottom friction [Putnam and Johnson (1949), Hunt (1952, 1964), Case and Parkinson (1957), Ippen (1966), Van Dorn (1966), Johns (1968), Treloar and Bebnier (1970), Mei and Liu (1973), Isaacson (1977), and Kamphus (1978)]. Wave heights are attenuated due to viscous dissipation.

The impermeable soil assumption has also been applied to deformable bottoms [Mallard and Dalrymple (1977), Dawson (1978), and Dawson et al. (1981)]. The soil is assumed to be an elastic solid which deforms in response to wave pressures. An alternative is to treat the bottom as a viscous fluid [Gade (1958) and Dalrymple and Liu (1978)]. As in the case of the elastic solid, the bottom deforms in response to wave pressures. Viscous dissipation in the bottom fluid results in wave attenuation. Hsiao and Shemdin (1980) and MacPherson (1980) have developed solutions for a soil which is modeled as an impermeable viscoelastic medium.

A number of solutions have been developed for a porous, rigid bottom. Putnam (1949) developed a solution for the pore water velocity potential from fluid continuity and Darcy's equation. The wave and bottom were not coupled. An estimation of wave decay was made by calculating the mechanical energy dissipated in the pore fluid. Reid and Kajiura (1957) extended this analysis to include wave-bottom interaction which resulted in an exponential decay of wave height with travel distance. Pressure and vertical flux of fluid were matched at the mudline. This led to a solution in which there is a discontinuity in the horizontal component of velocity at the mudline. Hunt (1959), Murraray (1965), Liu (1973), Dalrymple (1974), McClain et al. (1977), and Puri (1980) have resolved this difficulty by allowing for the development of a viscous boundary layer at the mudline.

Porous rigid bottom solutions have also been developed for anisotropic soils [Sleath (1970)], turbulent flow in the bed [Massel (1976)] and a compressible pore fluid [Nakamura et al. (1972) and Moshagen and Torum (1975)]. The extension to anisotropic soils is useful since in most sedimentary sea beds the horizontal and vertical flow properties are different. The turbulent flow model is applicable when the sediment grain size is large and the flow is less restricted. A compressible pore fluid and an incompressible soil skeleton is usually an inappropriate assumption since the skeleton is often more deformable [Prevost et al. (1965)].

A recent series of papers stimulated by Yamamoto (1977) treat the bottom as porous and deformable. He developed a solution from the

Table 1.1. Categorization of ocean engineering wave-bottom interaction literature

Soil:	Impermeable		Porous		
Skeleton:	Rigid	Deformable	Rigid		Deformable
Fluid:			Compressible	Incompressible	Compressible
	Lamb (1932)	Gade (1958)	Nakamura <i>et al.</i> (1972)	Putnam (1949)	Yamamoto (1977, 1978, 1981a, 1981b)
	Putnam and Johnson (1949)	Mallard and Dalrymple (1977)	Moshagen and Torum (1975)	Reid and Kajiura (1957)	Yamamoto <i>et al.</i> (1978)
	Hunt (1952)	Dawson (1978)		Hunt (1959)	Madsen (1973)
	Case and Parkinson (1957)	Dalrymple and Liu (1978)		Murray (1965)	Mei and Foda (1975)
	Hunt (1964)	MacPherson (1980)		Sleath (1970)	Dalrymple and Liu (1979)
	Ippen (1966)	Hsiao and Shemdin (1980)		Liu (1973)	Hudspeth and Patton (personal communication)
	Van Dorn (1966)	Dawson <i>et al.</i> (1981)		Dalrymple (1974)	Yamamoto and Suzuki (1980)
	Johns (1968)			Massel (1976)	Rousseau (1981)
	Treloar and Brebner (1970)			Puri (1980)	
	Mei and Liu (1973)				
	Isaacson (1977)				
	Kamphuis (1978)				

quasi-static theory of consolidation proposed by Biot (1941). It is assumed that the soil skeleton behaves as a linearly elastic medium and that the fluid flow is modeled by Darcy's equation. The inertia terms are neglected in the stress equilibrium equations. The continuity or storage equation was taken from Verruijt (1969) and accounts for the partial saturation of the pore fluid. The theory predicted stresses, displacements and pore pressures for an infinitely thick soil deposit in which the water waves were decoupled from the soil response. Depth profiles of pressure amplitude and phase agreed with laboratory observations. Madsen (1978) developed a solution by a different mathematical approach and extended the model conceptually to anisotropic permeability and layered soils. Yamamoto (1978) extended the results of his earlier work to soil deposits of finite thickness. For soil layers of finite thickness, the permeability was shown to be more important.

Yamamoto has recently developed a multi-layered model [Yamamoto and Suzuki (1980) and Yamamoto (1981a)]. This model approximates vertically inhomogeneous soil deposits. Yamamoto has also examined the potential for sea bed liquefaction using a Mohr circle analysis. Hudspeth and Patton (personal communication) have extended the Biot theory to allow for wave-bottom interaction and the development of a bottom boundary layer. Wave height attenuation is determined for the combined effects of viscous dissipation at the mudline and wave induced flow in the sea bed. Rousseau (1981) has solved the coupled wave-bottom interaction problem for a soil with anisotropic permeability.

Biot (1956a,b) extended his earlier work to include the inertia terms. The solution to these equations revealed the existence of three waves: one rotational or shear wave, and two dilational or compression waves. Dalrymple and Liu (1979) solved the coupled wave-soil problem including the inertia terms. The inertia terms were found to be unimportant, except for the case of very soft sediments in which the water wave celerity approaches the Raleigh wave speed of the sediment. Noting that one of the dilational waves is rapidly attenuated, Mei and Foda (1979) developed a boundary layer type formulation. Outside the boundary layer there is little relative motion between the

fluid and soil and the inertia terms are unimportant. The approximate solution was within five percent of the Yamamoto et al. (1978) results. Yamamoto (1981b) has also developed a solution to the Biot equations including the inertia terms and internal Coulumb friction. This solution agreed well with field measurements.

1.3.b Geotechnical Literature

Geotechnical engineers have also studied the wave-soil interaction phenomenon. Primarily, two aspects of wave-soil interaction have been analyzed: 1) wave-induced slope instability and 2) wave-induced liquefaction. For the slope stability analyses a failure surface is constructed and the load is prescribed as a combination of the static overburden and the dynamic wave pressure [e.g., Henkel (1970)]. For the wave-induced liquefaction models, concepts are drawn from earthquake engineering and the development of excess pore water pressure due to cyclic stressing of the soil [Seed et al. (1976)]. Terzaghi's one-dimensional consolidation equation [Terzaghi and Peck (1967)] is time-averaged over one wave period and a semi-empirical pore pressure source term is included to account for the pore water pressure accumulation due to the cyclic stressing of the soil [Finn et al. (1977), Rahman et al. (1977), Seed and Rahman (1978), Finn et al. (1980)]. The random sea surface is reduced to a simple periodic loading by estimating the equivalent number of cycles associated with each loading. As the pore pressure accumulates a liquefaction failure is predicted.

1.3.c Geotextile Literature

The geotextile literature identifies a variety of applications: highway construction, erosion control, soil stabilization, drainage and ocean engineering. However, the vast majority of the literature is related to highway engineering. In ocean engineering the first geotextile applications were in coastal protection on sand beaches [Agerschon (1961) and Crowell (1963)]. The geotextiles were placed beneath an armor layer to prevent washout of the underlying beach

sands. Cathage Mills, a major manufacturer of geotextiles, identified a variety of applications in ocean engineering including revetments, seawalls, bulkheads, groins and jetties [Barrett (1963)]. A number of coastal structures using filter fabrics are discussed by Barrett (1966) suggesting that geotextiles were becoming an integral component in many coastal construction projects. Other marine experiences with geotextiles are reported by Lee (1972), Dunham and Barrett (1974), DeMent (1978), Welsh and Koerner (1979), and Heerten (1981). Heerten also identifies a lack of technical recommendations and testing regulations for specific applications of geotextiles in marine structures. He presents a technique for selecting fabrics on the basis of permeability and soil separation. An excellent bibliography of geotextile properties and all areas of geotextile applications by J.R. Bell is given in a Transportation Research Circular (1979). This circular also identifies literature related to soil-geotextile interaction models.

Broms (1977) showed that geotextile layers in soils increase the lateral strength analytically and experimentally. Several models have been developed which indicate that geotextiles increase the bearing capacity of soils [e.g., Nieuwenhuis (1977) and Jessberger (1977)]. However, the geotextile must be very strong to perform this function. A number of finite element numerical models have been developed to analyze the states of stress in soil-geotextile systems [Al-Hussaini and Johnson (1977), Bell *et al.* (1977) and Barvashov and Fedorovsky (1977)]. The pretension in the geotextile increases stability, but this tension must be large.

Most of the soil-geotextile models are for static conditions in foundations or highway engineering. No models have been developed addressing the dynamic, marine application of this investigation.

1.3.d Relevant Literature Synopsis

The Biot consolidation equations [Biot (1941)] coupled with the storage equation [Verruijt (1969)] provide the best description of wave-induced soil response [Yamamoto (1981b)]. The inertia terms may be neglected as they have little influence except for very soft muds

[Dalrymple and Liu (1979)]. The equations presented in Yamamoto (1977) are appropriate for the present study. The coupling of the soil layers is conceptually similar to that suggested by Madsen (1978), Yamamoto and Suzuki (1980) and Yamamoto (1981a) except that the influence of the geotextile must also be considered. Rather than considering the geotextile as a fabric element as in the finite element soil-geotextile models, the fabric is modeled as a thin permeable, elastic membrane.

1.4 Geotextile Properties

The development of geotextiles and their engineering applications has occurred very rapidly within the past 15 years. Initial applications were primarily terrestrial but marine applications are becoming increasingly more common. This rapid development has led to confusion with regard to design procedures and geotextile properties. These problems are particularly apparent in the marine environment due to the limited field experience. These problems are further complicated by the large number of commercially available geotextiles.

To help remedy this situation the Federal Highway Administration awarded a contract to Hicks and Bell at Oregon State University to develop test methods and use criteria for geotextiles. In an interim report, Bell and Hicks (1980) categorize fabrics by construction method: woven, knitted, nonwoven, combinations and special. Woven geotextiles tend to have high strengths, high moduli and low strain at failure. The single strand fabrics have simple pore structures and are less susceptible to swelling in water than multiple strand fabrics. Knitted geotextiles may be constructed of either single or multiple strand fabrics. These fabrics tend to be less expensive than woven geotextiles and may be knitted into tubes or sacks. Nonwoven fabrics encompass a number of construction methods: needle punching, heat bonding and resin bonding. Nonwoven tend to be less expensive than woven geotextiles and have lower strengths. Combination fabrics are combinations of the above techniques. A typical example is a light weight needle punch in combination with a stronger woven backing or scrim. Special geotextiles include construction methods not outlined

above. An example of this type is an extruded plastic mesh.

Most geotextiles are formed from polyester or polypropylene fibers. However, the individual fabric hydraulic and mechanical properties are highly variable due to the different construction techniques. Important properties include pore size, permeability, elastic modulus, strength, friction and tear and puncture resistance. Pore size is important for determining the separation capabilities of the fabric and the potential for clogging. The geotextile permeability determines the drainage condition. In general, a drained condition is desired to allow for the release of pore water pressure. Modulus and strength indicate the stretching of the fabric and the ultimate failure. If the friction between the soil and geotextile is large, then the fabric may increase structural strength. Tear and puncture resistance are important during construction when the geotextile may be exposed to very high concentrated loads such as in the placement of riprap.

Geotextile physical properties employed in this study are permittivity, elasticity and in situ fabric tension. The permittivity is a single hydraulic fabric parameter which indicates the effectiveness of pressure transmission through the geotextile. It incorporates both the permeability and the fabric thickness.

2.0 DEFINING EQUATIONS

The physical system under consideration in this study is two horizontal layers of soil separated by a geotextile. The dynamic response of this system to ocean waves is to be modeled. The model will be used to predict states of soil stress and identify potential failure conditions as a function of wave, soil and geotextile conditions. Biot (1941) developed a set of equations describing the three-dimensional consolidation of a poro-elastic soil subjected to a time varying load. The Biot equations are used to model the dynamic response of the soil skeleton. The pore water pressure is modeled by the storage equation [Verruijt (1969)]. This system of equations provides information on soil displacements and stresses and on fluid flows and pressure.

2.1 Elastic Soil Skeleton

The Biot equations are derived by substituting stress expressed as a function of displacement through Hooke's Law into the equations of stress equilibrium. Important assumptions are that the soil is linearly elastic, that the soil inertia is small, and that the body forces are small. A short derivation of the Biot equations is presented for completeness.

The convention for identifying stresses is shown in Figure 2.1. A stress on a positive face acting in a positive direction is considered positive. A stress on a negative face acting in a negative direction is also considered positive. Therefore, the convention that tension is positive is being used. Stresses are excess values in that they are the stress levels above static conditions.

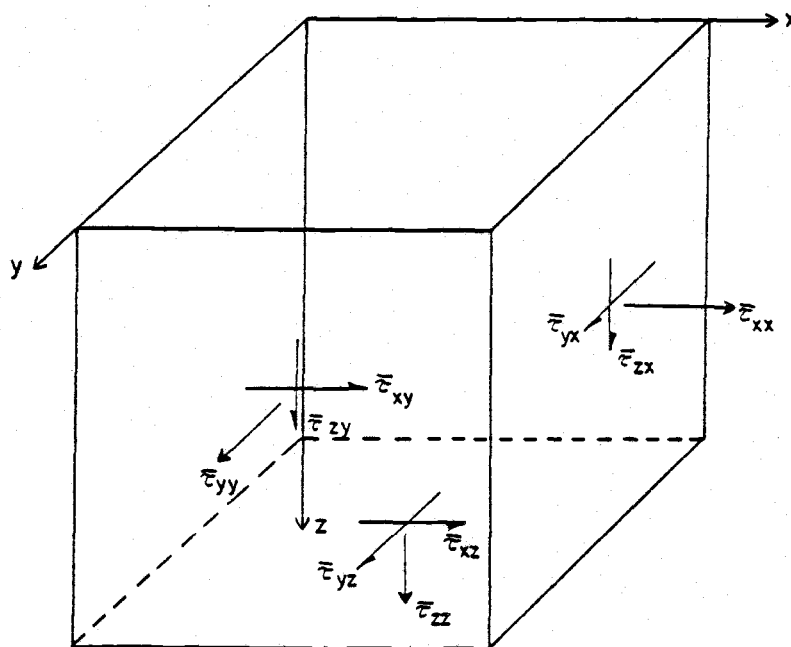


Figure 2.1. Definition sketch for the coordinate system and stress notation.

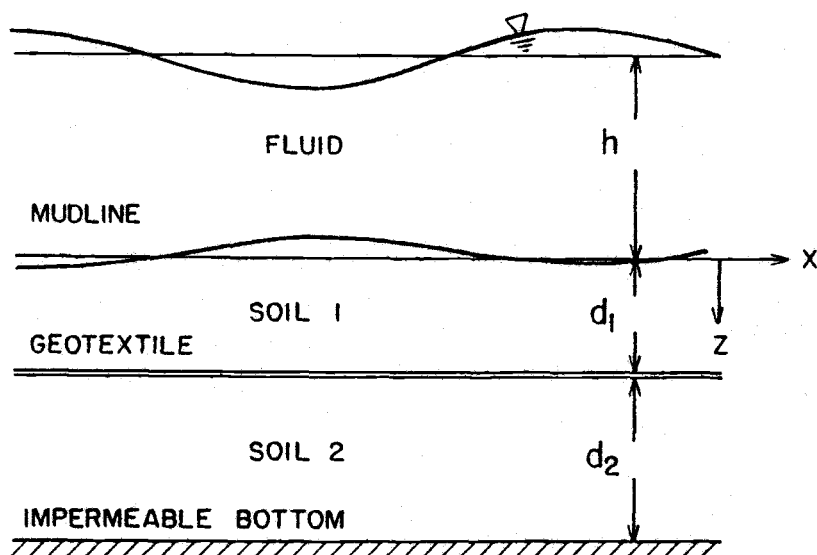


Figure 2.2. Soil layer definition sketch

The components of the total stress tensor, $\bar{\tau}_{ij}$, are denoted by

$$\bar{\tau}_{ij} = \begin{bmatrix} \bar{\tau}_{xx} & \bar{\tau}_{xy} & \bar{\tau}_{xz} \\ \bar{\tau}_{yx} & \bar{\tau}_{yy} & \bar{\tau}_{yz} \\ \bar{\tau}_{zx} & \bar{\tau}_{zy} & \bar{\tau}_{zz} \end{bmatrix} \quad (2.1.1)$$

Columns represent surface faces and rows indicate stress directions.

Assuming that the elemental volume shown in Figure 2.1 is small and that the volume is in equilibrium, taking moments about each axis yields

$$\bar{\tau}_{ij} = \bar{\tau}_{ji} \quad (2.1.2)$$

Since the stress tensor is symmetric, the following notation is adopted

$$\bar{\tau}_{ij} = \begin{bmatrix} \bar{\sigma}_x & \bar{\tau}_z & \bar{\tau}_y \\ \bar{\tau}_z & \bar{\sigma}_y & \bar{\tau}_x \\ \bar{\tau}_y & \bar{\tau}_x & \bar{\sigma}_z \end{bmatrix} \quad (2.1.3)$$

The total stress may be decomposed as

$$\bar{\sigma}_x = \sigma_x - p \quad (2.1.4a)$$

$$\bar{\sigma}_y = \sigma_y - p \quad (2.1.4b)$$

$$\bar{\sigma}_z = \sigma_z - p \quad (2.1.4c)$$

$$\bar{\tau}_x = \tau_x \quad (2.1.4d)$$

$$\bar{\tau}_y = \tau_y \quad (2.1.4e)$$

$$\bar{\tau}_z = \tau_z \quad (2.1.4f)$$

in which σ_x, σ_y and σ_z are the x, y and z components of the effective normal stress, respectively, τ_x, τ_y and τ_z are the components of the shear stress and p is fluid pressure.

The sum of the forces in each direction is equal to the product of mass and acceleration of the elemental volume in that direction. Expanding the stresses in a Taylor series, evaluating forces as the product of the stress with the area it acts over and retaining first order terms gives the equations of stress equilibrium. If the inertia is small and body forces are separated as a static load, the dynamic equations are given by

$$\frac{\partial \sigma_x}{\partial x} + \frac{\partial \tau_z}{\partial y} + \frac{\partial \tau_y}{\partial z} = \frac{\partial p}{\partial x} \quad (2.1.5a)$$

$$\frac{\partial \tau_z}{\partial x} + \frac{\partial \sigma_y}{\partial y} + \frac{\partial \tau_x}{\partial z} = \frac{\partial p}{\partial y} \quad (2.1.5b)$$

$$\frac{\partial \tau_y}{\partial x} + \frac{\partial \tau_x}{\partial y} + \frac{\partial \sigma_z}{\partial z} = \frac{\partial p}{\partial z} \quad (2.1.5c)$$

The strains in the soil are, by definition, gradients of the soil displacements. Defining ξ, χ and ζ as the components of soil displacement in the x, y, and z directions, respectively, then the strains are given as

$$e_x = \frac{\partial \xi}{\partial x} \quad (2.1.6a)$$

$$e_y = \frac{\partial \chi}{\partial y} \quad (2.1.6b)$$

$$e_z = \frac{\partial \zeta}{\partial z} \quad (2.1.6c)$$

$$\gamma_x = 1/2 \left(\frac{\partial \zeta}{\partial y} + \frac{\partial \chi}{\partial z} \right) \quad (2.1.6d)$$

$$\gamma_y = 1/2 \left(\frac{\partial \zeta}{\partial x} + \frac{\partial \xi}{\partial z} \right) \quad (2.1.6e)$$

$$\gamma_z = 1/2 \left(\frac{\partial \chi}{\partial x} + \frac{\partial \xi}{\partial y} \right) \quad (2.1.6f)$$

in which e_x, e_y and e_z are the components of normal strain and γ_x, γ_y and γ_z are the shear strains. Only the linear terms in the strain tensor have been retained which requires that the strains are small. For small

strains and displacements the soil is assumed to be linearly elastic and obey Hooke's Law. Hooke's Law relates strains to longitudinal and lateral stresses according to

$$e_x = [\sigma_x - \nu(\sigma_y + \sigma_z)]/E \quad (2.1.7a)$$

$$e_y = [\sigma_y - \nu(\sigma_x + \sigma_z)]/E \quad (2.1.7b)$$

$$e_z = [\sigma_z - \nu(\sigma_x + \sigma_y)]/E \quad (2.1.7c)$$

$$\gamma_x = \tau_x / (2G) \quad (2.1.7d)$$

$$\gamma_y = \tau_y / (2G) \quad (2.1.7e)$$

$$\gamma_z = \tau_z / (2G) \quad (2.1.7f)$$

in which E is Young's modulus, G is the shear modulus and ν is Poisson's ratio. Symmetry in isotropic materials assures that normal stresses produce only normal strains [equations (2.1.7a-2.1.7c)] and that shear stresses produce only shear strains [equations (2.1.7d-2.1.7f)]. The relationship between E and G is

$$G = \frac{E}{2(\nu+1)} \quad (2.1.8)$$

Hooke's Law may also be inverted to express stresses as functions of strains according to

$$\sigma_x = 2G(e_x + \frac{\nu E}{1-2\nu}) \quad (2.1.9a)$$

$$\sigma_y = 2G(e_y + \frac{\nu E}{1-2\nu}) \quad (2.1.9b)$$

$$\sigma_z = 2G(e_z + \frac{\nu E}{1-2\nu}) \quad (2.1.9c)$$

$$\tau_x = 2G\gamma_x \quad (2.1.9d)$$

$$\tau_y = 2G\gamma_y \quad (2.1.9e)$$

$$\tau_z = 2G\gamma_z \quad (2.1.9f)$$

in which

$$\varepsilon = e_x + e_y + e_z \quad (2.1.10)$$

and is termed the volume strain. Substituting the strains expressed in terms of displacements into the above form of Hooke's Law yields

$$\sigma_x = 2G \left[\frac{\partial \xi}{\partial x} + \frac{\nu}{1-2\nu} \left(\frac{\partial \xi}{\partial x} + \frac{\partial \chi}{\partial y} + \frac{\partial \zeta}{\partial z} \right) \right] \quad (2.1.11a)$$

$$\sigma_y = 2G \left[\frac{\partial \chi}{\partial y} + \frac{\nu}{1-2\nu} \left(\frac{\partial \xi}{\partial x} + \frac{\partial \chi}{\partial y} + \frac{\partial \zeta}{\partial z} \right) \right] \quad (2.1.11b)$$

$$\sigma_z = 2G \left[\frac{\partial \zeta}{\partial z} + \frac{\nu}{1-2\nu} \left(\frac{\partial \xi}{\partial x} + \frac{\partial \chi}{\partial y} + \frac{\partial \zeta}{\partial z} \right) \right] \quad (2.1.11c)$$

$$\tau_x = G \left(\frac{\partial \chi}{\partial z} + \frac{\partial \zeta}{\partial y} \right) \quad (2.1.11d)$$

$$\tau_y = G \left(\frac{\partial \zeta}{\partial x} + \frac{\partial \xi}{\partial z} \right) \quad (2.1.11e)$$

$$\tau_z = G \left(\frac{\partial \chi}{\partial x} + \frac{\partial \xi}{\partial y} \right) \quad (2.1.11f)$$

Using these relationships, the equations-of equilibrium may be written in terms of the displacements

$$G \nabla^2 \xi + \frac{G}{1-2\nu} \frac{\partial}{\partial x} \left(\frac{\partial \xi}{\partial x} + \frac{\partial \chi}{\partial y} + \frac{\partial \zeta}{\partial z} \right) = \frac{\partial p}{\partial x} \quad (2.1.12a)$$

$$G \nabla^2 \chi + \frac{G}{1-2\nu} \frac{\partial}{\partial y} \left(\frac{\partial \xi}{\partial x} + \frac{\partial \chi}{\partial y} + \frac{\partial \zeta}{\partial z} \right) = \frac{\partial p}{\partial y} \quad (2.1.12b)$$

$$G \nabla^2 \zeta + \frac{G}{1-2\nu} \frac{\partial}{\partial z} \left(\frac{\partial \xi}{\partial x} + \frac{\partial \chi}{\partial y} + \frac{\partial \zeta}{\partial z} \right) = \frac{\partial p}{\partial z} \quad (2.1.12c)$$

in which ∇^2 is the Laplacian operator defined in Cartesian coordinates as

$$\nabla^2(\cdot) \equiv \frac{\partial^2(\cdot)}{\partial x^2} + \frac{\partial^2(\cdot)}{\partial y^2} + \frac{\partial^2(\cdot)}{\partial z^2} \quad (2.1.13)$$

Equations (2.1.12a), (2.1.12b) and (2.1.12c) define the response of the soil skeleton. The equation for pore pressure must now be derived.

2.2 Storage Equation

The relationship between an elemental volume change and the fluid pressure is modeled by the storage equation [Verruijt (1969)]. The porous media is assumed to consist of three components: 1) soil grains, 2) pore liquid and 3) pore gas. Properties which are related to each of these components are denoted by subscript A, B and C, respectively. The relative mass of each fraction, ψ , in a fixed volume is

$$\psi_A = (1-n)\rho_A \quad (2.2.1a)$$

$$\psi_B = nS\rho_B \quad (2.2.1b)$$

$$\psi_C = n(1-S)\rho_C \quad (2.2.1c)$$

in which n is the porosity, S is the degree of saturation and ρ is the density of each fraction. The time rate of change of each component of the relative mass in a fixed volume must be balanced by the mass flux of that fraction across the boundaries of the volume, i.e., each component of the relative mass must satisfy conservation of mass.

$$\frac{\partial}{\partial t} [(1-n)\rho_A] + \nabla \cdot [(1-n)\rho_A \vec{v}_A] = 0 \quad (2.2.2a)$$

$$\frac{\partial}{\partial t} [nS\rho_B] + \nabla \cdot [nS\rho_B \vec{v}_B] = 0 \quad (2.2.2b)$$

$$\frac{\partial}{\partial t} [n(1-S)\rho_C] + \nabla \cdot [n(1-S)\rho_C \vec{v}_C] = 0 \quad (2.2.2c)$$

in which \vec{v} is the vector velocity of each component and $\nabla \cdot (\cdot)$ is the divergence operator.

Assuming that the grains are incompressible (not the soil skeleton) relative to the fluids, that the liquid is only slightly compressible and that the gas is ideal and obeys Boyles Law, the equations of state are given as

$$\rho_A = \text{constant} \quad (2.2.3a)$$

$$\rho_B = \rho_0 e^{\beta p} \quad (2.2.3b)$$

$$\rho_C = \rho_g \frac{p}{p_g} \quad (2.2.3c)$$

where ρ_0 and ρ_g are reference densities, p_g is a reference pressure and β is the liquid compressibility which is a function of the degree of saturation.

If the volume of air in the water is small, then the velocity of the pore gas will be the same as the pore liquid. Employing this assumption and the equations of state, the conservation of mass equations may be written

$$\frac{\partial n}{\partial t} + \vec{v}_A \cdot \nabla n - (1-n) \nabla \cdot \vec{v}_A = 0 \quad (2.2.4a)$$

$$\frac{1}{n} \frac{\partial n}{\partial t} + \frac{1}{S} \frac{\partial S}{\partial t} + \beta \frac{\partial p}{\partial t} + \nabla \cdot \vec{v}_B + \frac{\nabla(\rho_B S n) \cdot \vec{v}_B}{\rho_B S n} = 0 \quad (2.2.4b)$$

$$\frac{1}{n} \frac{\partial n}{\partial t} - \frac{1}{(1-S)} \frac{\partial S}{\partial t} + \frac{1}{p} \frac{\partial p}{\partial t} + \nabla \cdot \vec{v}_C + \frac{\nabla[\rho_C (1-S)n] \cdot \vec{v}_B}{\rho_C (1-S)n} = 0 \quad (2.2.4c)$$

in which $\nabla(\cdot)$ is the gradient operator. Elimination of the $\frac{\partial S}{\partial t}$ term from equations (2.2.4b) and (2.2.4c) gives

$$\frac{1}{n} \frac{\partial n}{\partial t} + \frac{1-S+S\beta p}{p} \frac{\partial p}{\partial t} + \nabla \cdot \vec{v}_B + \left(\frac{1}{n} \nabla n + \frac{1-S+S\beta p}{p} \nabla p \right) \cdot \vec{v}_B = 0 \quad (2.2.5)$$

The fluid discharge velocity (relative to the soil) is given by Darcy's equation for small relative pore fluid velocities. Previous

applications of Biot's theory to the wave-soil problem have ignored the effect of pore water acceleration in Darcy's equation. However, Sollitt and Cross (1972) and Hannoura and McCorquodale (1978) have shown this effect may be significant for unsteady flows in coarse aggregate. A more complete, but linearized, form of the equation of motion of the pore fluid is

$$(1+C_m) \frac{\partial}{\partial t} \vec{q} = - \frac{n}{\rho} \nabla p - \frac{gn}{\hat{K}} \vec{q} \quad (2.2.6)$$

in which C_m is an inertial coefficient, \vec{q} is the two-dimensional vector discharge velocity and \hat{K} is the steady permeability. The wave-induced flows are periodic in x and t and therefore

$$\vec{q}(x,z,t) = \vec{Q}(z) e^{i(\lambda x - \omega t)} \quad (2.2.7)$$

Substituting this periodic form of the discharge velocity into equation (2.2.6) yields

$$\left[\frac{-i\omega(1+C_m)}{gn} + \frac{1}{\hat{K}} \right] \vec{q} = - \frac{1}{\rho g} \nabla p \quad (2.2.8)$$

Defining an apparent unsteady permeability, K , as

$$\frac{1}{K} = \frac{1}{\hat{K}} - \frac{i\omega(1+C_m)}{gn} \quad (2.2.9)$$

the equation of motion yields an unsteady form for Darcy's equation

$$\vec{q} = - \frac{K}{\rho g} \nabla p \quad (2.2.10)$$

Taking the divergence of equation (2.2.10) yields

$$\begin{aligned} \frac{K}{\rho_B g} \nabla^2 p = & - (\vec{v}_B - \vec{v}_A) \cdot \nabla (Sn) - Sn \nabla \cdot (\vec{v}_B - \vec{v}_A) \\ & + \frac{\beta K}{\rho_B g} \nabla p \cdot \nabla p \end{aligned} \quad (2.2.11)$$

Eliminating $\nabla \cdot \vec{v}_B$ between equations (2.2.5) and (2.2.11) and using equation (2.2.4b) to eliminate $S \frac{\partial n}{\partial t}$ gives

$$\begin{aligned} \frac{K}{\rho_B g} \nabla^2 p = & S \nabla \cdot \vec{v}_A + Sn \left(\frac{1-S+\beta p}{p} \right) \frac{\partial p}{\partial t} + n \vec{v}_A \cdot \nabla S \\ & + n \vec{v}_B \cdot \left[-\nabla S + S \left(\frac{1-S+\beta p}{p} \right) \nabla p \right] \\ & + \frac{\beta K}{\rho_B g} \nabla p \cdot \nabla p \end{aligned} \quad (2.2.12)$$

It has been assumed that the volume of air in the water is small and therefore, $S \approx 1$. Since pure water is nearly incompressible, $p\beta \ll 1$. It has also been assumed that the soil skeleton deformations are small and second order terms were neglected. Adhering to the same order of approximation, second order terms are also neglected in the storage equation. Equation (2.2.12), for these assumptions, is

$$\frac{K}{\rho_B g} \nabla^2 p = \nabla \cdot \vec{v}_A + n\beta' \frac{\partial p}{\partial t} \quad (2.2.13)$$

in which

$$\beta' = \beta + \frac{1-S}{p} \quad (2.2.14)$$

For wave-induced pressure fluctuations in soils the pressure in equation (2.2.14) may be approximated by the absolute static pressure, p_S . The combined air-water compressibility, β' , is given by

$$\beta' = \frac{1}{K_W} + \frac{1-S}{p_S} \quad (2.2.15)$$

in which K_W is the bulk modulus of elasticity of pure water. Noting that the divergence of \vec{v}_A is equivalent to the time rate of change of ϵ , the final form of the storage equation is

$$\frac{K}{\gamma} \nabla^2 p = \frac{\partial}{\partial t} \left(\frac{\partial \xi}{\partial x} + \frac{\partial \chi}{\partial y} + \frac{\partial \zeta}{\partial z} \right) + n\beta' \frac{\partial p}{\partial t} \quad (2.2.16)$$

in which γ is the weight of density of the fluid, not to be confused with the shear strains, γ_x , γ_y and γ_z , in equations (2.1.7d-2.1.7f). The first term in equation (2.2.16) models the pressure response in a rigid soil matrix, the second term accounts for the soil matrix deformation and the third term includes the pore fluid compressibility.

2.3 Boundary Conditions

In two dimensions the Biot consolidation equations are second order in three variables: ξ , ζ and p . If a simple harmonic solution is required in x and t , then six boundary conditions are required for the z dependence in each soil layer. For two soil layers separated by a geotextile, as shown in Figure 2.2, 12 boundary conditions are required; three at the mudline, three at the impermeable bottom and six at the geotextile.

2.3 Boundary Conditions

In two dimensions the Biot consolidation equations are second order in three variables: ξ , ζ and p . Therefore, six boundary conditions are required for each soil layer. For two soil layers separated by a geotextile, as shown in Figure 2.2, 12 boundary conditions are required; three at the mudline, three at the impermeable bottom and six at the geotextile.

2.3.a Mudline Boundary Conditions

At the mudline the pore fluid pressure is matched with the dynamic component of the wave-induced pressure. The dynamic pressure is periodic in the direction of wave propagation, x , and in time, t . The pressure boundary condition is given by

$$p_1(x,0,t) = p_0 e^{i(\lambda x - \omega t)} \quad (2.3.a.1)$$

in which i is the square root of -1 , λ is the wave number, ω is the radian wave frequency and p_0 is the amplitude of the wave-induced bottom pressure. Subscripts 1 and 2 denote values in the upper and lower soil layers, respectively. The component of pressure due to the elevation changes of the mudline are very small and are therefore neglected.

Also at the mudline, the vertical component of effective stress vanishes

$$\sigma_{z1}(x,0,t) = 0 \quad (2.3.a.2)$$

and the horizontal shear stress on the bottom due to flow in the fluid layer is balanced by the shear stress in the soil. The shear stress is conventionally expressed proportional to the velocity squared, however, using Lorentz principle of equivalent work [Lorentz (1926)], a linear stress which dissipates the same amount of energy per wave period is given by

$$\tau_1(x,0,t) = \frac{8}{3\pi} \rho C_D u_0^2 e^{i(\lambda x - \omega t)} \quad (2.3.a.3)$$

in which π is a numerical constant, C_D is a drag coefficient of order 0.01, ρ is the fluid density and u_0 is the amplitude of the near bottom horizontal velocity. As with the pore pressure, stresses associated with the small displacement of the mudline are small and are neglected.

2.3.b Geotextile Boundary Conditions

Geotextiles usually have rough surfaces or pores which provide a no-slip surface between the fabric and the soil. Also, the fabric is thin so that no gradients in fabric extension occur across the thickness of the fabric. Therefore, the horizontal and vertical components of displacement are matched across the geotextile.

$$\xi_1(x, d_1, t) = \xi_2(x, d_1, t) \quad (2.3.b.1a)$$

$$\zeta_1(x, d_1, t) = \zeta_2(x, d_1, t) \quad (2.3.b.1b)$$

Both the mechanical and the hydraulic behavior of the geotextile must be determined to quantify its effect on the adjacent soil layers. The mechanical behavior of the geotextile may be idealized as a membrane in tension. For the two-dimensional Biot problem, the state of stress in the geotextile is described by the one-dimensional wave equation [Hildebrand (1964)]

$$\hat{T} \frac{\partial^2}{\partial x^2} \mu + \left(\frac{\partial}{\partial x} \hat{T} \right) \left(\frac{\partial}{\partial x} \mu \right) + f = 0 \quad (2.3.b.2)$$

in which \hat{T} is the tension per unit width in the geotextile, μ is the vertical geotextile displacement and f is the normal stress. The second term in equation (2.3.b.2) is negligible if the horizontal gradients are small. As an alternative, the gradient of the tension may be approximated by a spring constant, K_S . The normal stress on the geotextile is the result of the total vertical stresses in the adjacent soil layers. The vertical displacements of the soil layers are continuous across the geotextile and therefore equal to the fabric displacement. Balancing vertical forces across the geotextile, equation (2.3.b.2) may be written

$$\begin{aligned} (1-n_1) \sigma_{z1}(x, d_1, t) + n_1 p_1(x, d_1, t) &= (1-n_2) \sigma_{z2}(x, d_1, t) \\ + n_2 p_2(x, d_1, t) + \left(\hat{T} \frac{\partial^2}{\partial x^2} + K_S \frac{\partial}{\partial x} \right) \zeta_2(x, d_1, t) & \end{aligned} \quad (2.3.b.3)$$

The elasticity of the geotextile also resists horizontal displacement. Balancing horizontal forces across the geotextile yields

$$\tau_1(x, d_1, t) = \tau_2(x, d_1, t) + K_S \frac{\partial}{\partial x} \xi_2(x, d_1, t) \quad (2.3.b.4)$$

The volume of water for thin fabrics in the pore spaces of the geotextile remains approximately constant. Therefore, by conservation of mass, the vertical volume flow of water must match across the fabric. From Darcy's equation

$$\frac{\partial}{\partial z} p_1(x, d_1, t) = \frac{K_2}{K_1} \frac{\partial}{\partial z} p_2(x, d_1, t) \quad (2.3.b.5)$$

in which K_1 and K_2 are the permeabilities of soil layers 1 and 2, respectively.

The hydraulic behavior of the geotextile is characterized by the fluid energy dissipated in the flow through the fabric. From the energy equation, the pressure drop across the geotextile is due to a head loss in the geotextile. An estimate of this pressure drop is obtained from Darcy's equation and conservation of mass between the fabric and the lower soil layer

$$\frac{K_f}{\gamma} \frac{\Delta p}{\Delta z_f} = \frac{K_2}{\gamma} \frac{\partial}{\partial z} p_2(x, d_1, t) \quad (2.3.b.6)$$

in which K_f is the fabric permeability, Δp is the pressure drop across the fabric and Δz_f is the fabric thickness. Defining the permittivity C_ℓ , as

$$C_\ell = \frac{\Delta z_f}{K_f} \quad (2.3.b.7)$$

the energy equation across the fabric yields

$$p_1(x, d_1, t) = p_2(x, d_1, t) - C_\ell K_2 \frac{\partial}{\partial z} p_2(x, d_1, t) \quad (2.3.b.8)$$

2.3.c Impermeable Bottom Boundary Conditions

At the rigid impermeable bottom there is no vertical flow of pore fluid.

$$\frac{\partial}{\partial z} p_2(x, d_1 + d_2, t) = 0 \quad (2.3.c.1)$$

Also at this boundary there is no vertical displacement.

$$\xi_2(x, d_1 + d_2, t) = 0 \quad (2.3.c.2)$$

The impermeable bottom may be clay or rock in the field or wood or concrete in the laboratory. For field conditions, due to the interlocking between the soil grains and the bottom, a no horizontal displacement boundary condition may be appropriate. However, for smooth bottom surfaces in the laboratory a limited amount of slip may occur. Therefore, a boundary condition which will allow for partial slip is employed.

$$\alpha[\xi_2(x, d_1 + d_2, t)] + (1 - \alpha)(d_1 + d_2) \frac{\partial}{\partial z} [\xi_2(x, d_1 + d_2, t)] = 0 \quad (2.3.c.3)$$

This allows for the full range of slip conditions as a function of the constant, α .

$$\alpha = 0 \quad \text{free slip} \quad (2.3.c.4a)$$

$$0 < \alpha < 1 \quad \text{partial slip} \quad (2.3.c.4b)$$

$$\alpha = 1 \quad \text{no slip} \quad (2.3.c.4c)$$

The gradient term, with $\alpha = 0$, assures that the free slip boundary condition is allowed to penetrate to the full depth of the bottom layer.

3.0 SOLUTIONS TO THE BIOT EQUATIONS

The Biot consolidation equations provide a very general description of dynamic soil response. It is of interest to note that a number of simplified methods developed for analyzing pore pressure response in marine soils are based on reduced forms of the Biot equations. An examination of the "unseen" assumptions in the aforementioned methods provides insight into their range of validity or application. Two such examples, the earthquake consolidation equation and the potential pressure model, are examined before developing solutions to the full set of Biot equations.

3.1 Earthquake Consolidation Equation Model

The solutions developed by Yamamoto (1977) and others (see Table 1.1) for the Biot consolidation equations are strictly periodic in time. However, it has been observed that soils subjected to simple periodic cyclic loading may not respond in a strictly periodic sense. The mean excess pore water pressure in a loose saturated silt or fine sand may increase with the number of cyclic loads [Seed and Lee (1966), Seed et al. (1978)].

These soils exhibit a tendency for volume reduction when cyclically loaded. As the volume decreases, the excess pore water pressure increases. If the accumulation of pore pressure per cycle of loading exceeds the dissipation by drainage a net accumulation results. The pore pressure may increase to the point that most of the overburden is carried by the fluid and grain effective stress is very small. Since water is incapable of supporting substantial shear stresses, an increase in the applied load may result in a soil failure. Such a failure has been termed liquefaction because the soil behaves as a liquid. Liquefaction due to cyclic earthquake loading has been well documented [Seed and Idriss (1967)]. This problem has been analyzed by earthquake engineers using a modified form of Terzaghi's one-dimensional consolidation equation [Terzaghi and Peck (1967)]. More recently this technique has been applied to model the response of marine soils due to the cyclic

loading of water waves [Finn, et al. (1977), Rahman, et al. (1977), Seed Rahman (1978), Finn, et al. (1980)]. The derivation of the consolidation equation is not based on the Biot equations and the resulting boundary value problem is solved numerically although for simple cases analytic solutions are possible.

The three-dimensional Biot consolidation equations were derived in Chapter 2. The earthquake consolidation equation may be derived from equations (2.1.39), (2.1.40), (2.1.41) and (2.2.12) by seeking a one-dimensional solution. That is, all gradients with respect to the x and y coordinate directions are assumed to be zero. The resulting equations are

$$G \frac{2-2\nu}{1-2\nu} \frac{\partial^2 \zeta}{\partial z^2} = \frac{\partial p}{\partial z} \quad (3.1.1a)$$

$$\frac{K}{\gamma} \frac{\partial^2 p}{\partial z^2} = \frac{\partial^2 \zeta}{\partial z \partial t} + n \beta' \frac{\partial p}{\partial t} \quad (3.1.1b)$$

Differentiating equation (3.1.1a) with respect to t and equation (3.1.1b) with respect to z and eliminating ζ from equation (3.1.1b) yields

$$\frac{\partial^2 p}{\partial z \partial t} = c \frac{\partial^3 p}{\partial z^3} \quad (3.1.2)$$

in which

$$c = \frac{GK}{\gamma} \frac{(2-2\nu)}{(1-2\nu) + (2-2\nu)n\beta'G} \quad (3.1.3)$$

and is termed the coefficient of consolidation. Integrating with respect to z yields the earthquake consolidation equation

$$\frac{\partial p}{\partial t} = c \frac{\partial^2 p}{\partial z^2} + s \quad (3.1.4)$$

in which s is an integration constant in z, functioning as a pore pressure source term and may be time dependent. However, for generality (and

because of the form of the source term used by earthquake engineers) s will be considered a function of time and depth in each soil layer. The pressure is composed of a fluctuating component (in time) and a mean drift component. The mean drift or pore pressure accumulation may be more clearly examined by removing the fluctuating component by time averaging over one wave period. The mean pore pressure accumulation, \bar{p} , is given by

$$\bar{p} = \frac{1}{T} \int_t^{t+T} p dt \quad (3.1.5)$$

The boundary value problem for the pore pressure accumulation for a homogenous soil of thickness, d , over an impermeable bed material is given by

$$\frac{\partial \bar{p}}{\partial t} = c \frac{\partial^2 \bar{p}}{\partial z^2} + s \quad (3.1.6a)$$

$$\bar{p}(0, t) = 0 \quad (3.1.6b)$$

$$\frac{\partial}{\partial z} \bar{p}(d, z) = 0 \quad (3.1.6c)$$

$$\bar{p}(z, 0) = f(z) \quad (3.1.6d)$$

in which $f(z)$ is the initial vertical profile of the pore water pressure. The pore pressure at the mudline time-averages out. Therefore, the pore pressure is only driven by the source term. An eigenseries solution to this problem obtained by separation of variables and application of the boundary conditions is given by

$$p = \sum_{n=1}^{\infty} \frac{2}{d} e^{-c\kappa_n^2 t} \left\{ \int_0^t e^{c\kappa_n^2 \tau} \left[\int_0^d s(z, \tau) \sin(\kappa_n z) dz \right] d\tau \right\} \times \sin(\kappa_n z) \quad (3.1.7)$$

in which the eigenvalues are given by

$$\kappa_n = \frac{2n-1}{2} \frac{\pi}{d} \quad (3.1.8)$$

This solution applies for an arbitrary pore water pressure source term. For the solution to be physically meaningful an analytic expression for the source term must be determined. The laboratory results of De Alba, Chan and Seed (1975) relate the development of pore water pressure to the number of load cycles in simple shear. This relationship is given by

$$\frac{\bar{p}_g}{\sigma'_0} = \frac{1}{2} + \frac{1}{\pi} \sin^{-1} \left[2 \left(\frac{N}{N_\ell} \right)^{1/\alpha} - 1 \right] \quad (3.1.9)$$

in which \bar{p}_g is the pore water pressure generated due to the cyclic loading, σ'_0 is the effective overburden stress corresponding to static conditions, N is the number of cyclic loadings, N_ℓ is the number of cycles to liquefaction, and α is a shape factor. This family of curves is shown in Figure 3.1 as a function of α . Seed, et al. (1975) suggest using a value of $\alpha = 0.7$ for which there is a somewhat linear relationship between the pore pressure ratio \bar{p}_g/σ'_0 and the cyclic ratio N/N_ℓ (the dashed line in Figure 3.1). For a linear relationship

$$\bar{p}_g = \sigma'_0 \frac{N}{N_\ell} \quad (3.1.10)$$

The pore pressure source term in equation (3.1.6a) is given by Seed, et al. (1974) as

$$s = \frac{\partial}{\partial t} \left(\sigma'_0 \frac{N}{N_\ell} \right) \quad (3.1.11)$$

The effective overburden stress is

$$\sigma'_0 = \gamma_B z \quad (3.1.12)$$

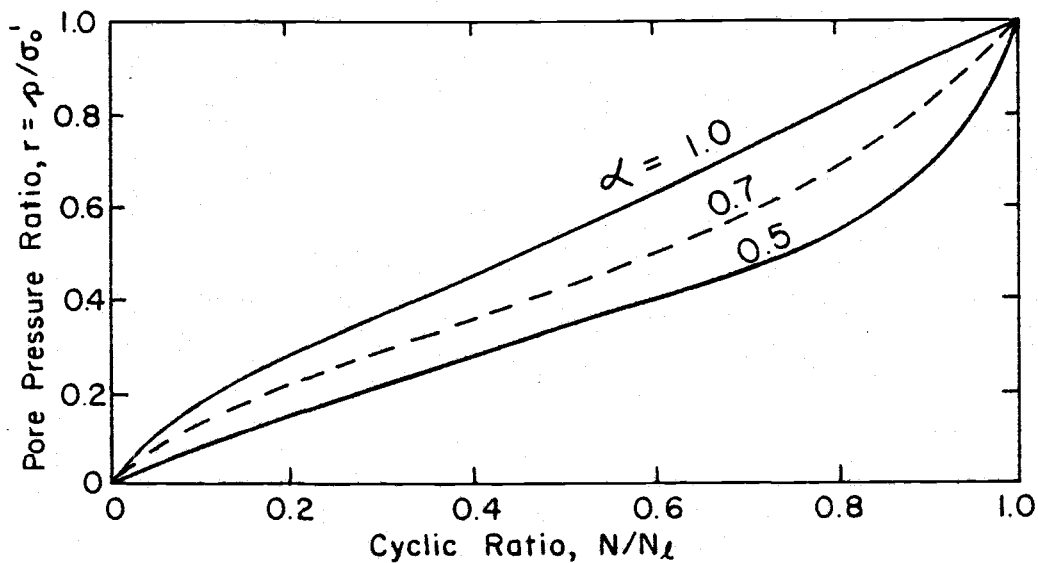


Figure 3.1 Rate of pore water pressure buildup in cyclic simple shear tests.
[Seed, et al. (1975)]

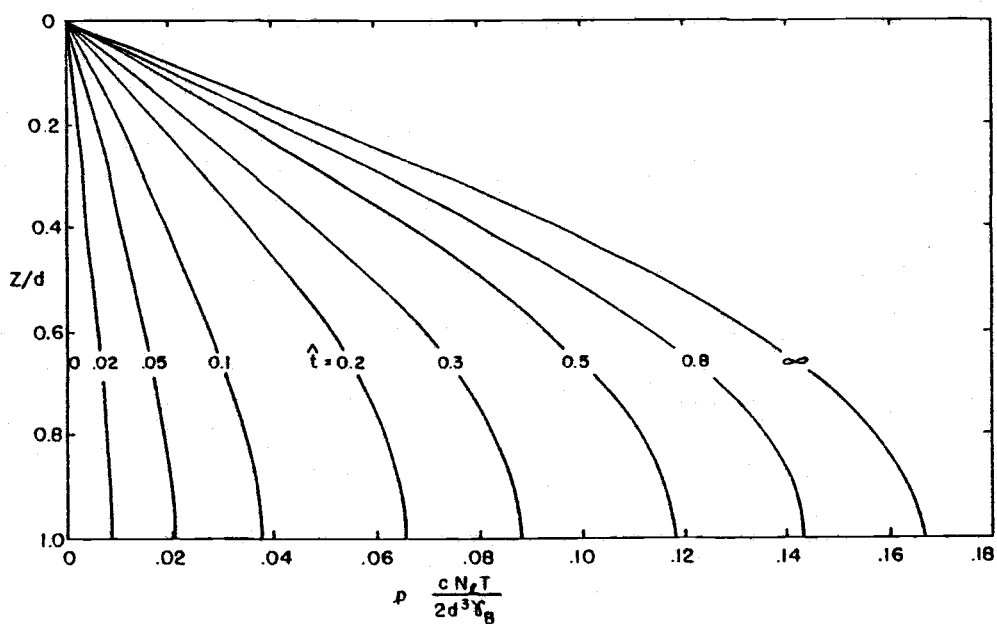


Figure 3.2 Dimensionless pore water pressure accumulation profiles.

and the cyclic ratio as a continuous function of time is given by

$$\frac{N}{N_\ell} = \frac{t}{N_\ell T} \quad (3.1.13)$$

in which t is time and T is the wave period. Therefore, the pore pressure source term is given by

$$s = \frac{\gamma_B}{N_\ell T} z \quad (3.1.14)$$

For this source term, the solution to the earthquake consolidation equation given by equation (3.1.7) is

$$\bar{p} = \sum_{n=1}^{\infty} \frac{(-1)^n}{\kappa_n^4} \frac{2\gamma_B}{cdN_\ell T} (1 - e^{-c\kappa_n^2 t}) \sin(\kappa_n z) \quad (3.1.15)$$

It is convenient to express the pressure in a dimensionless form by introducing the following variables

$$\hat{z} = z/d \quad (3.1.16a)$$

$$\hat{t} = t(c/d^2) \quad (3.1.16b)$$

$$\hat{\kappa}_n = \frac{2n-1}{2} \pi \quad (3.1.16c)$$

$$\hat{p} = \bar{p} \frac{cN_\ell T}{2d^3 \gamma_B} \quad (3.1.16d)$$

A dimensionless solution, which applies for all soils and wave conditions, is

$$\hat{p} = \sum_{n=1}^{\infty} \frac{(-1)^n}{\hat{\kappa}_n^4} (1 - e^{-\hat{\kappa}_n^2 \hat{t}}) \sin(\hat{\kappa}_n \hat{z}) \quad (3.1.17)$$

Dimensionless vertical pressure profiles are shown in Figure 3.2 as a function of dimensionless time. These profiles apply for all soils that have a tendency for volume reduction and pore pressure accumulation when cyclically loaded. The pressure scaling term in equation (3.1.16d) contains fluid properties, flow properties, static and dynamic soil properties, geometric and wave properties.

The one-dimensional earthquake consolidation equation provides information on the accumulation of pore pressure not revealed by other solutions of the Biot equations. However, by itself this approach may not provide adequate pore water pressure information to predict failure. Specifically, if the periodic pore pressure amplitude is large a failure would be observed before the accumulated pressure reaches a failure level. This type of failure is shown in Figure 3.3. Instantaneous or momentary failures occur before the mean drift failure. Even for rapid pore pressure accumulation, complete failure may be preceded by momentary failures associated with the periodic component of pore water pressure. If design estimates are based only on the earthquake consolidation equation, failure may be observed in the field before the predicted number of cycles.

This failure mechanism suggests a coupling of the earthquake consolidation equation to determine mean pore pressure accumulation with the two-dimensional periodic solutions to the Biot equations for the cyclic pore pressure. Such a model is an anticipated extension of the present study.

3.2 Potential Pressure Model

Moshagen and Torum (1975) developed a two-dimensional heat equation for modeling wave-induced pressures in marine soils. This equation is a simplified form of the Biot equations for compressible pore fluid but an incompressible or rigid soil skeleton. The resulting equation is

$$\frac{K}{\gamma} \nabla^2 p = n\beta' \frac{\partial p}{\partial t} \quad (3.2.1)$$

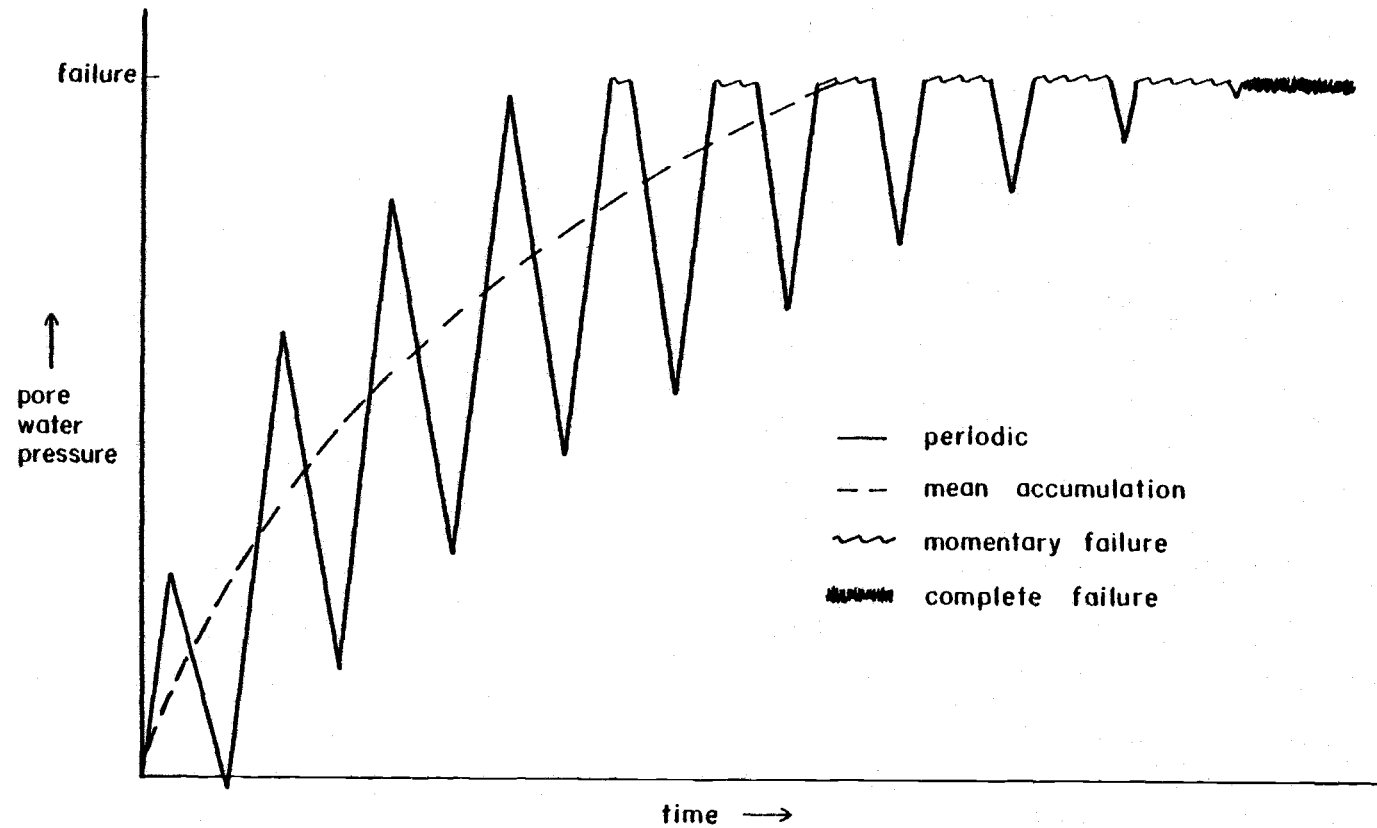


Figure 3.3 Idealized wave-induced soil failure due to periodic and mean accumulation of pore water pressure.

The assumption that the fluid is more compressible than the skeleton is physically unrealistic for most saturated marine soils [Prevost, Eide and Anderson (1975)]. A more physically consistent assumption is that the pore fluid is also incompressible. This yields the potential pressure model.

$$\nabla^2 p = 0 \quad (3.2.2)$$

A number of investigators have examined soil response to waves by assuming that the field equation for pressure is Laplace's equation [cf. Putnam (1974), Reid and Kajura (1957), Hunt (1959), Murray (1965) Liu (1973), Dalrymple (1974), McClain, et al. (1977), Puri (1980)]. The most common derivation of this relationship is from Darcy's equations for horizontal and vertical flow.

$$u = - \frac{K}{\gamma} \frac{\partial p}{\partial x} \quad (3.2.3a)$$

$$w = - \frac{K}{\gamma} \frac{\partial p}{\partial z} \quad (3.2.3b)$$

Taking the derivative of equation (3.2.3a) with respect to x and the derivative of equation (3.2.3b) with respect to z and adding, for a homogeneous soil and assuming continuity, yields

$$\nabla^2 p = 0 \quad (3.2.4)$$

It is interesting to note that the equation for the pressure is independent of the soil properties. Relative soil properties are introduced through the boundary conditions.

The boundary conditions for pressure for a three layered system, two soils separated by a geotextile, as shown in Figure 2.2, are given by equations (2.3a.1), (2.3b.3), (2.3b.6) and 2.3c.1). They correspond to pressure matching at the mudline, fluid continuity and a pressure head loss at the geotextile and a no flow bottom boundary condition, respectively. For these boundary conditions, a solution obtained by

separation of variables to equation (3.2.4) is

$$p_1 = p_0 [\text{ch}(\lambda z) + R2 \text{ sh}(\lambda z)] e^{i(\lambda x - \omega t)} \quad (3.2.5a)$$

$$p_2 = p_0 \frac{K_1}{K_2} R1 [1 + R2 \text{ th}(\lambda d_1)] [\text{ch}(\lambda z) - \text{th}(\lambda \bar{d}) \text{ sh}(\lambda z)] e^{i(\lambda x - \omega t)} \quad (3.2.5b)$$

in which

$$R1 = \frac{K_2}{K_1} [1 - \text{th}(\lambda d_1) \text{ th}(\lambda \bar{d}) + R3]^{-1} \quad (3.2.6a)$$

$$R2 = \frac{R1 [\text{th}(\lambda d_1) - \text{th}(\lambda \bar{d})] - \text{th}(\lambda d_1)}{1 - R1 \text{ th}(\lambda d_1) [\text{th}(\lambda d_1) - \text{th}(\lambda \bar{d})]} \quad (3.2.6b)$$

$$R3 = K_2 C_d [\text{th}(\lambda d_1) - \text{th}(\lambda \bar{d})] \lambda \quad (3.2.6c)$$

$$\bar{d} = d_1 + d_2 \quad (3.2.6d)$$

and p_1 is the pore pressure in soil layer 1 and p_2 is the pore pressure in layer 2. Vertical profiles of the pressure amplitude are shown in Figure 3.4 for a test condition of one foot of pea gravel above three feet of silt separated by a very permeable fabric. This configuration approximately corresponds to the laboratory conditions for several of the experiments. Stream function [Dean (1974)] wave cases 5B, 7B and 8B for a water depth of eight feet are shown. The wave heights and periods for these wave cases are summarized in Table 4.4. Figure 3.4 indicates that the decay of pressure response with depth is exponential [in accordance with equations (3.2.5a) and (3.2.5b)] and that the shorter wave lengths are more highly damped.

The potential pressure model provides reasonable estimates of pore pressure for sands [Liu (personal communication)] which are relatively permeable and stiff. However, no information on the phase shift with depth is obtained from this solution.

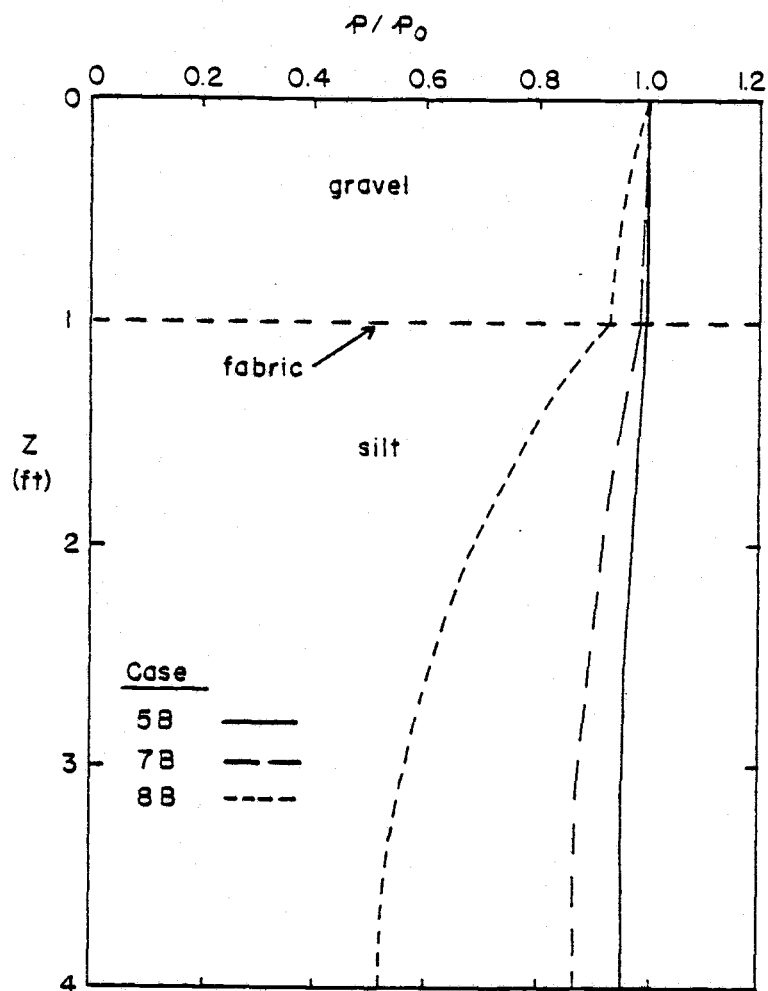


Figure 3.4 Vertical pore water pressure profiles from the potential pressure model for stream function wave cases 5B, 7B and 8B.

3.3 Periodic, Two-Dimensional Biot Model

The most general analytic solutions to the Biot equations for wave-induced marine soil response have considered a periodic, two-dimensional case [eg. Yamamoto (1977)]. If the solution is assumed to be periodic in x and t , with the same frequencies as the wave, the Biot equations (2.1.12a), (2.1.12c) and (2.2.16) reduce to the matrix form

$$\begin{bmatrix} (D^2 - \frac{2-2\nu}{1-2\nu} \lambda^2) & (\frac{i\lambda}{1-2\nu} D) & (-i \frac{\lambda}{G}) \\ (\frac{i\lambda}{2-2\nu} D) & (D^2 - \frac{1-2\nu}{2-2\nu} \lambda^2) & (-\frac{1}{G} \frac{1-2\nu}{2-2\nu} D) \\ (-\frac{\gamma}{K} \lambda \omega) & (i \frac{\gamma}{K} \omega D) & [D^2 + (i \frac{\gamma}{K} \omega n \beta' \lambda^2)] \end{bmatrix} \begin{bmatrix} \xi \\ \zeta \\ p \end{bmatrix} = \begin{bmatrix} 0 \\ 0 \\ 0 \end{bmatrix} \quad (3.3.1)$$

in which

$$D(\cdot) \equiv \frac{d}{dz} (\cdot) \quad (3.3.2)$$

The existence of a non-trivial solution requires that the determinant of the coefficient matrix vanish [Wylie (1975)]. The eigenvalues corresponding to the roots are

$$\lambda_1 = \pm \lambda \quad (3.3.3a)$$

$$\lambda_2 = \pm \lambda \quad (3.3.3b)$$

$$\lambda_3 = \pm \lambda' = [\lambda^2 - i \frac{\gamma}{K} \frac{\omega}{G} (n \beta' G + \frac{1-2\nu}{2-2\nu})]^{1/2} \quad (3.3.3c)$$

With the eigenvalues known, general solutions for horizontal displacement, vertical displacement and pressure in the two soil layers are

$$\begin{aligned}\xi_1 = & [a_1 \operatorname{ch}(\lambda z) + a_2 \operatorname{sh}(\lambda z) + a_3 z \operatorname{ch}(\lambda z) + a_4 z \operatorname{sh}(\lambda z) + a_5 \operatorname{ch}(\lambda'_1 z) \\ & + a_6 \operatorname{sh}(\lambda'_1 z)] e^{i(\lambda x - \omega t)}\end{aligned}\quad (3.3.4a)$$

$$\begin{aligned}\zeta_1 = & [b_1 \operatorname{ch}(\lambda z) + b_2 \operatorname{sh}(\lambda z) + b_3 z \operatorname{ch}(\lambda z) + b_4 z \operatorname{sh}(\lambda z) + b_5 \operatorname{ch}(\lambda'_1 z) \\ & + b_6 \operatorname{sh}(\lambda'_1 z)] e^{i(\lambda x - \omega t)}\end{aligned}\quad (3.3.4b)$$

$$\begin{aligned}p_1 = & [c_1 \operatorname{ch}(\lambda z) + c_2 \operatorname{sh}(\lambda z) + c_3 z \operatorname{ch}(\lambda z) + c_4 z \operatorname{sh}(\lambda z) + c_5 \operatorname{ch}(\lambda'_1 z) \\ & + c_6 \operatorname{sh}(\lambda'_1 z)] e^{i(\lambda x - \omega t)}\end{aligned}\quad (3.3.4c)$$

$$\begin{aligned}\xi_2 = & [a_7 \operatorname{ch}(\lambda z) + a_8 \operatorname{sh}(\lambda z) + a_9 z \operatorname{ch}(\lambda z) + a_{10} z \operatorname{sh}(\lambda z) + a_{11} \operatorname{ch}(\lambda'_2 z) \\ & + a_{12} \operatorname{sh}(\lambda'_2 z)] e^{i(\lambda x - \omega t)}\end{aligned}\quad (3.3.4d)$$

$$\begin{aligned}\zeta_2 = & [b_7 \operatorname{ch}(\lambda z) + b_8 \operatorname{sh}(\lambda z) + b_9 z \operatorname{ch}(\lambda z) + b_{10} z \operatorname{sh}(\lambda z) + b_{11} \operatorname{ch}(\lambda'_2 z) \\ & + b_{12} \operatorname{sh}(\lambda'_2 z)] e^{i(\lambda x - \omega t)}\end{aligned}\quad (3.3.4e)$$

$$\begin{aligned}p_2 = & [c_7 \operatorname{ch}(\lambda z) + c_8 \operatorname{sh}(\lambda z) + c_9 z \operatorname{ch}(\lambda z) + c_{10} z \operatorname{sh}(\lambda z) + c_{11} \operatorname{ch}(\lambda'_2 z) \\ & + c_{12} \operatorname{sh}(\lambda'_2 z)] e^{i(\lambda x - \omega t)}\end{aligned}\quad (3.3.4f)$$

in which the subscripts on ξ , ζ and p refer to the soil layer.

There are 36 integration constants but only 12 boundary conditions (see section 2.3). This suggests that 24 of the constants are not independent. This dependency may be determined by substituting the general solutions into the governing equations (3.3.1) and collecting

like terms in $\text{ch}(\lambda z)$, $\text{sh}(\lambda z)$, etc. The resulting system of equations can be solved to yield the vertical displacement and pressure integration constants as functions of the horizontal displacement constants. These relationships are

$$b_1 = -ia_2 + iA1 a_3 \quad (3.3.5a)$$

$$b_2 = -ia_1 + iA1 a_4 \quad (3.3.5b)$$

$$b_3 = -i a_4 \quad (3.3.5c)$$

$$b_4 = -i a_3 \quad (3.3.5d)$$

$$b_5 = -i \frac{\lambda'_1}{\lambda} a_6 \quad (3.3.5e)$$

$$b_6 = -i \frac{\lambda'_1}{\lambda} a_5 \quad (3.3.5f)$$

$$b_7 = -i a_8 + iB1 a_{11} \quad (3.3.5g)$$

$$b_8 = -i a_7 + iB1 a_{10} \quad (3.3.5h)$$

$$b_9 = -i a_{10} \quad (3.3.5i)$$

$$b_{10} = -i a_9 \quad (3.3.5j)$$

$$b_{11} = -i \frac{\lambda'_2}{\lambda} a_{12} \quad (3.3.5k)$$

$$b_{12} = -i \frac{\lambda'_2}{\lambda} a_{11} \quad (3.3.5l)$$

$$c_1 = -i A2 a_4 \quad (3.3.5m)$$

$$c_2 = -i A2 a_3 \quad (3.3.5n)$$

$$c_3 = 0 \quad (3.3.5o)$$

$$c_4 = 0 \quad (3.3.5p)$$

$$c_5 = -A3 \ a_5 \quad (3.3.5q)$$

$$c_6 = -A3 \ a_6 \quad (3.3.5r)$$

$$c_7 = -i \ B2 \ a_{10} \quad (3.3.5s)$$

$$c_8 = -i \ B2 \ a_9 \quad (3.3.5t)$$

$$c_9 = 0 \quad (3.3.5u)$$

$$c_{10} = 0 \quad (3.3.5v)$$

$$c_{11} = -B3 \ a_{11} \quad (3.3.5w)$$

$$c_{12} = -B3 \ a_{12} \quad (3.3.5x)$$

in which

$$A1 = \frac{1}{\lambda} \frac{1+C1 (3-4\nu_1)}{1+C1} \quad (3.3.6a)$$

$$A2 = \frac{2G_1}{1+C1} \quad (3.3.6b)$$

$$A3 = \frac{\gamma}{K_1} \frac{\omega}{\lambda} [1+C1(2-2\nu_1)] \quad (3.3.6c)$$

$$C1 = \frac{n_1 \beta'_{11} G_1}{1-2\nu_1} \quad (3.3.6d)$$

$$B1 = \frac{1}{\lambda} \frac{1+C2(3-4\nu_2)}{1+C2} \quad (3.3.6e)$$

$$B2 = \frac{2G_2}{1+C2} \quad (3.3.6f)$$

$$B3 = \frac{\lambda}{K_2} \frac{\omega}{\lambda} [1 + C2(2 - 2\nu_2)] \quad (3.3.6g)$$

$$C2 = \frac{n_2 \beta'_2 G_2}{1 - 2\nu_2} \quad (3.3.6h)$$

and the subscripts on ν , G , K , n and β refer to the soil layer. The 12 boundary conditions are now imposed to determine the remaining 12 unknown horizontal displacement integration constants. The resulting system of 12 simultaneous equations is solved numerically.

$$-i A2 a_4 - A3 a_5 = p_0 \quad (3.3.7a)$$

$$a_1 + \frac{(1 - \nu_1)(1 - \lambda A1)}{\lambda(1 - 2\nu_1)} a_4 + \frac{(1 - \nu_1)\lambda'^2_1 - \nu_1\lambda^2}{\lambda^2(1 - 2\nu_1)} a_5 = 0 \quad (3.3.7b)$$

$$2\lambda a_2 + (1 - \lambda A1) a_3 + 2\lambda'_1 a_6 = \frac{1}{G_1} \frac{8}{3\pi} \rho c_f u_0^2 \quad (3.3.7c)$$

$$\begin{aligned} & a_1 + \text{th}(\lambda d_1) a_2 + d_1 a_3 + d_1 \text{th}(\lambda d_1) a_4 + \frac{\text{ch}(\lambda'_1 d_1)}{\text{ch}(\lambda d_1)} a_5 \\ & + \frac{\text{sh}(\lambda'_1 d_1)}{\text{ch}(\lambda d_1)} a_6 - a_7 - \text{th}(\lambda d_1) a_8 \\ & - d_1 a_9 + d_1 \text{th}(\lambda d_1) a_{10} - \frac{\text{ch}(\lambda'_2 d_1)}{\text{ch}(\lambda d_1)} a_{11} \\ & - \frac{\text{sh}(\lambda'_2 d_1)}{\text{ch}(\lambda d_1)} a_{12} = 0 \end{aligned} \quad (3.3.7d)$$

$$\operatorname{th}(\lambda d_1) a_1 + a_2 + [d_1 \operatorname{th}(\lambda d_1) - A_1] a_3 + [d_1 - A_1 \operatorname{th}(\lambda d_1)] a_4$$

$$+ \frac{\lambda'_1}{\lambda} \frac{\operatorname{sh}(\lambda'_1 d_1)}{\operatorname{ch}(\lambda d_1)} a_5 + \frac{\lambda'_1}{\lambda} \frac{\operatorname{ch}(\lambda'_1 d_1)}{\operatorname{ch}(\lambda d_1)} a_6$$

$$- \operatorname{th}(\lambda d_1) a_7 - a_8 - [d_1 \operatorname{th} \lambda d_1 - B_1] a_9 \quad (3.3.7e)$$

$$- [d_1 - B_1 \operatorname{th}(\lambda d_1)] a_{10} - \frac{\lambda'_2}{\lambda} \frac{\operatorname{sh}(\lambda'_2 d_1)}{\operatorname{ch}(\lambda d_1)} a_{11}$$

$$- \frac{\lambda'_2}{\lambda} \frac{\operatorname{ch}(\lambda'_2 d_1)}{\operatorname{ch}(\lambda d_1)} a_{12} = 0$$

$$- a_1 - \operatorname{th}(\lambda d_1) a_2 + \left\{ \left[\frac{1-\nu_1}{1-2\nu_1} \left(A_1 - \frac{1}{\lambda} \right) \operatorname{th}(\lambda d_1) - d_1 \right] - \frac{n_1 A_2 \operatorname{th}(\lambda d_1)}{2\lambda G_1 (1-n_1)} \right\} a_3$$

$$+ \left\{ \left[\frac{1-\nu_1}{1-2\nu_1} \left(A_1 - \frac{1}{\lambda} \right) - d_1 \operatorname{th}(\lambda d_1) \right] - \frac{n_1 A_2}{2\lambda G_1 (1-n_1)} \right\} a_4$$

$$+ \left[\frac{\nu_1 \lambda^2 - (1-\nu_1) \lambda'^1_1{}^2}{\lambda^2 (1-2\nu_1)} - \frac{n_1 A_3}{i 2\lambda G_1 (1-n_1)} \right] \frac{\operatorname{ch}(\lambda'_1 d_1)}{\operatorname{ch}(\lambda d_1)} a_5 +$$

$$+ \left[\frac{\nu_1 \lambda^2 - (1-\nu_1) \lambda'^1_1{}^2}{\lambda^2 (1-2\nu_1)} - \frac{n_1 A_3}{i 2\lambda G_1 (1-n_1)} \right] \frac{\operatorname{sh}(\lambda'_1 d_1)}{\operatorname{ch}(\lambda d_1)} a_6 \quad (3.3.7f)$$

(continued)

$$+ \left[\frac{1-n_2}{1-n_1} \frac{G_2}{G_1} + \bar{\phi} \operatorname{th}(\lambda d_1) \right] a_7 + \left[\frac{1-n_2}{1-n_1} \frac{G_2}{G_1} \operatorname{th} \lambda d_1 + \bar{\phi} \right] a_8$$

(3.3.7f)
(continued)

$$- \left\{ \frac{1-n_2}{1-n_1} \frac{G_2}{G_1} \left[\frac{1-\nu_2}{1-2\nu_2} \left(B1 - \frac{1}{\lambda} \right) \operatorname{th}(\lambda d_1) - d_1 \right] - \frac{n_2 B_2}{2\lambda G_1 (1-n_1)} \right.$$

$$+ \left[\bar{\phi} B1 - \bar{\phi} d_1 \operatorname{th}(\lambda d_1) \right] a_9$$

$$- \left\{ \frac{1-n_2}{1-n_1} \frac{G_2}{G_1} \left[\frac{1-\nu_2}{1-2\nu_2} \left(B1 - \frac{1}{\lambda} \right) - d_1 \operatorname{th}(\lambda d_1) \right] - \frac{n_2 B_2}{2\lambda G_1 (1-n_1)} \right.$$

$$+ \left[\bar{\phi} B1 \operatorname{th}(\lambda d_1) - d_1 \bar{\phi} \right] a_{10}$$

$$- \left\{ \left[\frac{1-n_2}{1-n_1} \frac{G_2}{G_1} \frac{\nu_2 \lambda^2 - (1-\nu_2) \lambda'^2_2}{\lambda^2 (1-2\nu_2)} - \frac{n_2 B_3}{i 2\lambda G_1 (1-n_1)} \right] \frac{\operatorname{ch}(\lambda'_2 d_1)}{\operatorname{ch}(\lambda d_1)} \right.$$

$$- \left. \bar{\phi} \frac{\lambda'_2}{\lambda} \frac{\operatorname{sh}(\lambda'_2 d_1)}{\operatorname{ch}(\lambda d_1)} \right\} a_{11}$$

$$+ \left\{ \left[\frac{1-n_2}{1-n_1} \frac{G_2}{G_1} \frac{\nu_2 \lambda^2 - (1-\nu_2) \lambda'^2_2}{\lambda^2 (1-2\nu_2)} - \frac{n_2 B_2}{i 2\lambda G_1 (1-n_1)} \right] \frac{\operatorname{sh}(\lambda'_2 d_1)}{\operatorname{ch}(\lambda d_1)} \right.$$

$$- \left. \bar{\phi} \frac{\lambda'_2}{\lambda} \frac{\operatorname{ch}(\lambda'_2 d_1)}{\operatorname{ch}(\lambda d_1)} \right\} a_{12} = 0$$

$$\begin{aligned}
& \text{th}(\lambda d_1) a_1 + a_2 + \left[\frac{1-\lambda A_1}{2\lambda} + d_1 \text{th}(\lambda d_1) \right] a_3 + \left[\frac{1-\lambda A_1}{2\lambda} \text{th}(\lambda d_1) + d_1 \right] a_4 \\
& + \frac{\lambda'_1}{\lambda} \frac{\text{sh}(\lambda'_1 d_1)}{\text{ch}(\lambda d_1)} a_5 + \frac{\lambda'_1}{\lambda} \frac{\text{ch}(\lambda'_1 d_1)}{\text{ch}(\lambda d_1)} a_6 \\
& - \frac{G_2}{G_1} \left(1 + \frac{\lambda K_s}{G_2} \right) \text{th}(\lambda d_1) a_7 - \frac{G_2}{G_1} \left(1 + \frac{\lambda K_s}{G_2} \right) a_8 \\
& - \frac{G_2}{G_1} \left\{ \frac{1-\lambda B_1}{2\lambda} + d_1 \text{th}(\lambda d_1) + \frac{K_s}{G_2} [1 + \lambda d_1 \text{th}(\lambda d_1)] \right\} a_9
\end{aligned} \tag{3.3.7g}$$

$$- \frac{G_2}{G_1} \left\{ \frac{1-\lambda B_1}{2\lambda} \text{th}(\lambda d_1) + d_1 + \frac{K_s}{G_2} [\text{th}(\lambda d_1) + \lambda d_1] \right\} a_{10}$$

$$- \frac{G_2}{G_1} \left(\frac{\lambda'_2}{\lambda} + \frac{\lambda'_2 K_s}{G_2} \right) \frac{\text{sh}(\lambda'_2 d_1)}{\text{ch}(\lambda d_1)} a_{11}$$

$$- \frac{G_2}{G_1} \left(\frac{\lambda'_2}{\lambda} + \frac{\lambda'_2 K_s}{G_2} \right) \frac{\text{ch}(\lambda'_2 d_1)}{\text{ch}(\lambda d_1)} a_{12} = 0$$

$$- i A_2 \text{th}(\lambda d_1) a_3 - i A_2 a_4 - A_3 \frac{\text{ch}(\lambda'_1 d_1)}{\text{ch}(\lambda d_1)} a_5 - A_3 \frac{\text{sh}(\lambda'_1 d_1)}{\text{ch}(\lambda d_1)} a_6$$

$$+ i B_2 [\text{th}(\lambda d_1) - \lambda K_2 C_2] a_9 + i B_2 [1 - \lambda K_2 C_2 \text{th}(\lambda d_1)] a_{10}$$

(3.3.7h)

$$+ B_3 \left[\frac{\text{ch}(\lambda'_2 d_1)}{\text{ch}(\lambda d_1)} - \lambda'_2 K_2 C_2 \frac{\text{sh}(\lambda'_2 d_1)}{\text{ch}(\lambda d_1)} \right] a_{11}$$

$$+ B_3 \left[\frac{\text{sh}(\lambda'_2 d_1)}{\text{ch}(\lambda d_1)} - \lambda'_2 K_2 C_2 \frac{\text{ch}(\lambda'_2 d_1)}{\text{ch}(\lambda d_1)} \right] a_{12} = 0$$

$$\begin{aligned}
& -i A_2 a_3 - i A_2 \operatorname{th}(\lambda d_1) a_4 - \frac{\lambda'_1}{\lambda} A_3 \frac{\operatorname{sh}(\lambda'_1 d_1)}{\operatorname{ch}(\lambda d_1)} a_5 - \frac{\lambda'_1}{\lambda} A_3 \frac{\operatorname{ch}(\lambda'_1 d_1)}{\operatorname{ch}(\lambda d_1)} a_6 \\
& + i \frac{K_2}{K_1} B_2 a_9 + i \frac{K_2}{K_1} B_2 \operatorname{th}(\lambda d_1) a_{10} + \frac{K_2}{K_1} \frac{\lambda'_2}{\lambda} B_3 \frac{\operatorname{sh}(\lambda'_2 d_1)}{\operatorname{ch}(\lambda d_1)} a_{11} \quad (3.3.7i) \\
& + \frac{K_2}{K_1} \frac{\lambda'_2}{\lambda} \frac{\operatorname{ch}(\lambda'_2 d_1)}{\operatorname{ch}(\lambda d_1)} a_{12} = 0
\end{aligned}$$

$$\begin{aligned}
& [\alpha + (1-\alpha) \lambda \bar{d} \operatorname{th}(\lambda \bar{d})] a_7 + [\alpha \operatorname{th}(\lambda \bar{d}) + (1-\alpha) \lambda \bar{d}] a_8 \\
& + \{\alpha \bar{d} + (1-\alpha) \bar{d} [1 + \lambda \bar{d} \operatorname{th}(\lambda \bar{d})]\} a_9 + \{\alpha \bar{d} \operatorname{th}(\lambda \bar{d}) + \\
& (1-\alpha) \bar{d} [\operatorname{th}(\lambda \bar{d}) - \lambda \bar{d}]\} a_{10} \quad (3.3.7j)
\end{aligned}$$

$$\begin{aligned}
& + \left[\alpha \frac{\operatorname{ch}(\lambda'_2 \bar{d})}{\operatorname{ch}(\lambda \bar{d})} + (1-\alpha) \lambda'_2 \bar{d} \frac{\operatorname{sh}(\lambda'_2 \bar{d})}{\operatorname{ch} \lambda \bar{d}} \right] a_{11} \\
& + \left[\alpha \frac{\operatorname{sh}(\lambda'_2 \bar{d})}{\operatorname{ch}(\lambda \bar{d})} + (1-\alpha) \lambda'_2 \bar{d} \frac{\operatorname{ch}(\lambda'_2 \bar{d})}{\operatorname{ch}(\lambda \bar{d})} \right] a_{12} = 0
\end{aligned}$$

$$\begin{aligned}
& \operatorname{th}(\lambda \bar{d}) a_7 + a_8 - [B_1 - \bar{d} \operatorname{th}(\lambda \bar{d})] a_9 - [B_1 \operatorname{th}(\lambda \bar{d}) - \bar{d}] a_{10} \\
& + \frac{\lambda'_2}{\lambda} \frac{\operatorname{sh}(\lambda'_2 \bar{d})}{\operatorname{ch}(\lambda \bar{d})} a_{11} + \frac{\lambda'_2}{\lambda} \frac{\operatorname{ch}(\lambda'_2 \bar{d})}{\operatorname{ch}(\lambda \bar{d})} a_{12} = 0 \quad (3.3.7k)
\end{aligned}$$

$$\begin{aligned}
 & i B_2 a_9 + i B_2 \operatorname{th}(\lambda \bar{d}) a_{10} + B_3 \frac{\lambda'_2}{\lambda} \frac{\operatorname{sh}(\lambda'_2 \bar{d})}{\operatorname{ch}(\lambda \bar{d})} a_{11} \\
 & + B_3 \frac{\lambda'_2}{\lambda} \frac{\operatorname{ch}(\lambda'_2 \bar{d})}{\operatorname{ch}(\lambda \bar{d})} a_{12} = 0
 \end{aligned}
 \tag{3.3.71}$$

in which

$$\bar{\phi} = \frac{-\hat{T}\lambda + iK_s}{2G_1(1-n_1)} \tag{3.3.8}$$

3.3.a Computer Program

Although the solution to the Biot equations is analytic, the actual numerical computation requires the use of the computer. The horizontal displacement integration constants are determined from equations (3.3.7a)-(3.3.71) using the International Mathematics and Science Library subroutine LEQT2C. The remaining integration constants for vertical displacement and pressure are determined by back substitution into equations (3.3.5a)-(3.3.5x). Stresses are calculated from equations (2.1.11a), (2.1.11c) and (2.1.11e). Fluid flows are determined from equation (2.2.7). The shear stress ratio, r , is defined as the ratio of the maximum shear stress, τ_m , to the effective overburden, σ'_0 , and is useful for identifying potential soil failure conditions.

$$r = \frac{\tau_m}{\sigma'_0} \tag{3.3.9}$$

in which τ_m is given by [Jumikis (1969)]

$$\tau_m = \left[\left(\frac{\sigma_z - \sigma_x}{2} \right)^2 - \tau^2 \right]^{1/2} \tag{3.3.10}$$

Another parameter useful for identifying potential failure conditions is the shear stress angle, ϕ [Jumikis (1969)].

$$\phi = \tan^{-1} \frac{\tau_m^2}{\left(\frac{\sigma_x + \sigma_z}{2} + \tau_m\right) \left(\frac{\sigma_x + \sigma_z}{2} - \tau_m\right)} \quad (3.3.11)$$

The computer program gives both dimensional and dimensionless results. The scaling used for each variable is listed in Table 3.1.

Table 3.1 Non-dimensionalizing scaling factors.

<u>Variable</u>	<u>Scaling</u>
ξ	Lp_0/G_1
ζ	Lp_0/G_1
p	p_0
σ_x	p_0
σ_z	p_0
τ	p_0
u	$Kp_0/\gamma L$
w	$Kp_0/\gamma L$
z	L

A listing of the computer program is given in Appendix B.

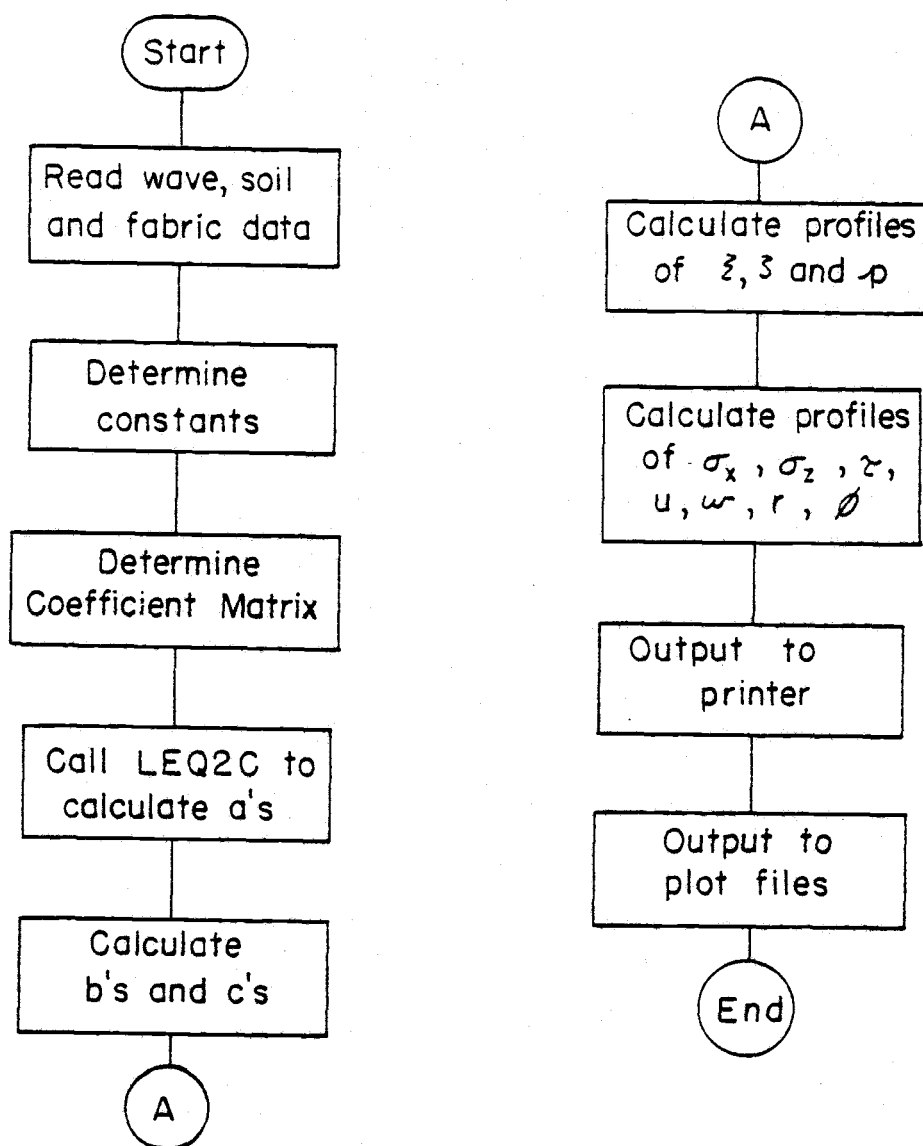


Figure 3.5 Computer program block diagram.

4.0 ANALYTICAL SOLUTION BEHAVIOR

The response of the soil-geotextile system to waves is not readily apparent from the analytical solution. Therefore, the general solution behavior and response to changes in wave and soil properties are examined. These responses are first presented for a single soil layer. An examination of this simplified case provides insight into the more complex case: two different soils separated by a "non-transparent" geotextile. For a three layered system examined at the end of this chapter, it is shown that the relative properties of the soils also influence the response.

4.1 Single Soil Layer Response

The dynamic response of a single, homogeneous soil layer may be examined using the soil-geotextile interaction model. This is the case for which both soils have identical properties and the geotextile does not resist displacement or fluid flow. A single soil layer 40 feet thick is examined. The specific wave and soil characteristics are listed in Table 4.1 and are denoted as the case A condition. This soil is generally described as a coarse sand [Creager et al. (1955)].

Table 4.1. Case A wave and soil conditions.

$G = 10^6 \text{ lb/ft}^2$	$\gamma_B = 60 \text{ lb/ft}^3$	$H = 19.8 \text{ ft}$
$\nu = 0.33$	$d = 40 \text{ ft}$	$T = 10 \text{ s}$
$n = 0.40$	$\alpha = 1.0$	$h = 50 \text{ ft}$
$K = 0.01 \text{ ft/s}$		

The vertical profiles of displacements, stresses and flows are shown in Figures 4.1 - 4.3. The dimensionless depth is the depth scaled by the wave length.

The amplitudes of the displacements tend to decrease with depth. For the case A conditions the maximum horizontal and vertical displacements are 4.4×10^{-3} ft and 1.3×10^{-3} ft, respectively. The maximum horizontal displacement may occur at intermediate depths. However, the maximum vertical displacement always occurs at the mudline. For this case, no-slip bottom boundary conditions were imposed so both components of displacement vanish at the lower boundary of the soil layer.

The pore water pressure also decreases with depth for this case. However, for certain wave-soil conditions the pressure may increase near the impermeable bottom boundary. For this case, and in general, there is little phase shift with depth.

The stress profiles for this case are typical for a single soil layer system. The horizontal effective stress is a maximum at the mudline and has a large phase shift near the bottom boundary. The vertical effective stress is zero at the mudline as specified by the boundary condition and attains a maximum at intermediate depths. The shear stress increases approximately linearly with depth.

The horizontal velocity is proportional to the pressure because of the periodicity assumption in x . Therefore, the form of the horizontal discharge velocity is similar to the pore pressure profile. The vertical discharge velocity decreases almost linearly from a maximum at the mudline to zero at the bottom impermeable boundary.

The cyclic shear stress ratio is commonly used by earthquake engineers in estimating soil failure. Values larger than 0.25 for a drained soil indicate a potential failure condition. For this case, failure would be anticipated in the upper 5 or 6 feet of soil.

Another indicator of failure conditions is the shear stress angle. For cohesionless soils such as silts, sands and gravels, if this angle is exceeded the soil will fail. Failure is predicted for the upper 2 feet of soil. It is of interest to note that even though the maximum displacements are small (approximately 1/20 and 1/60 in.

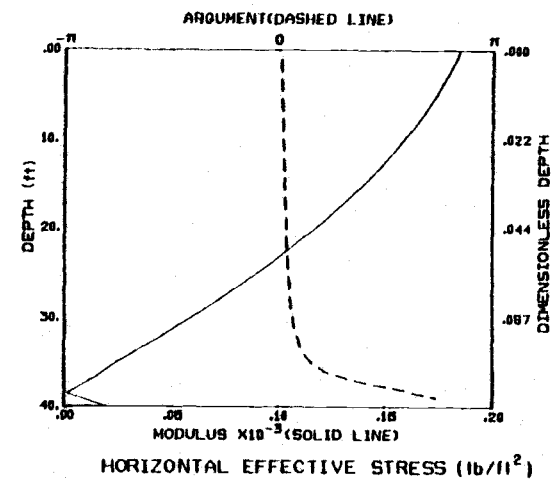
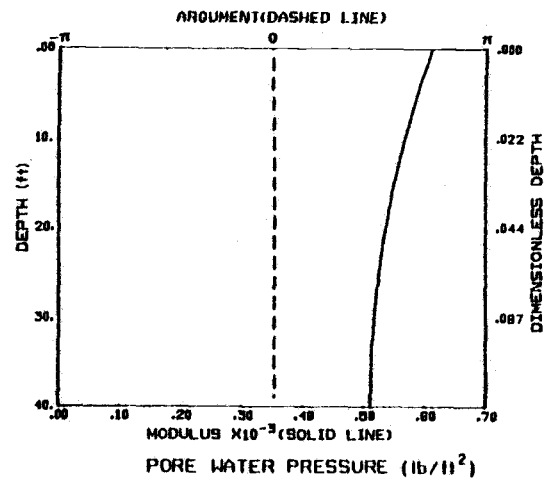
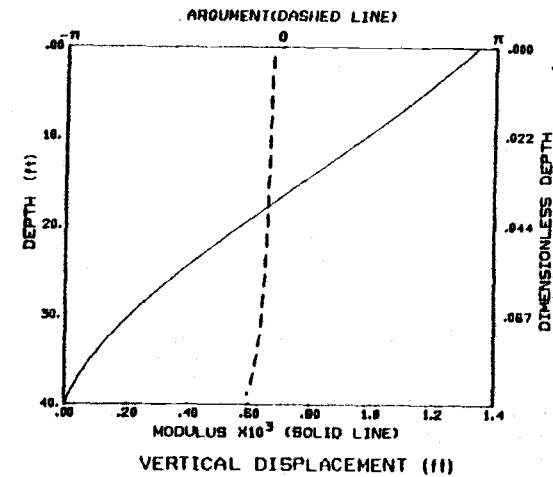
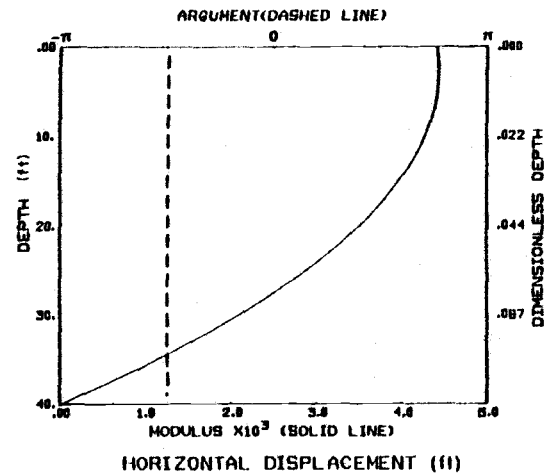


Figure 4.1. Wave-induced horizontal displacement, vertical displacement, excess pore water pressure and horizontal effective stress for the case A conditions.

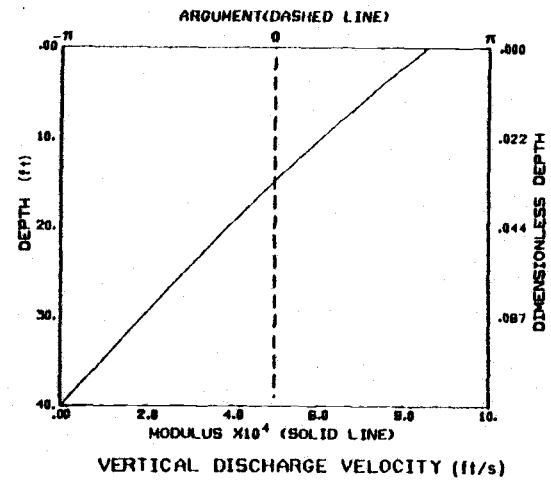
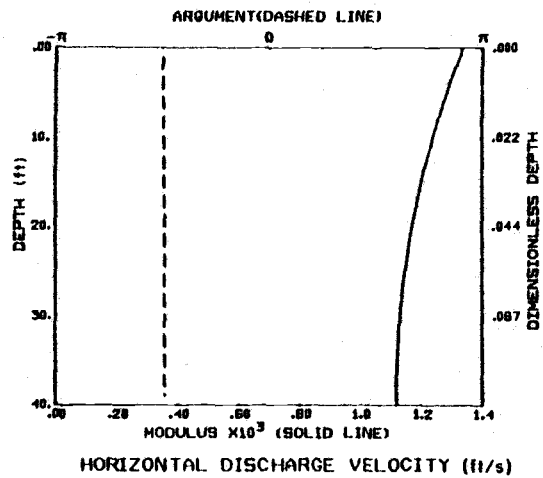
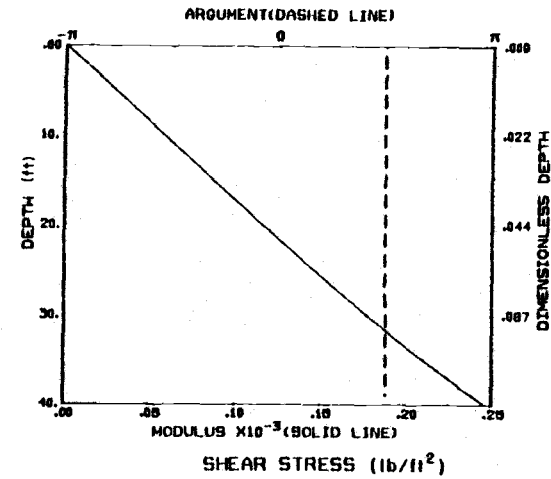
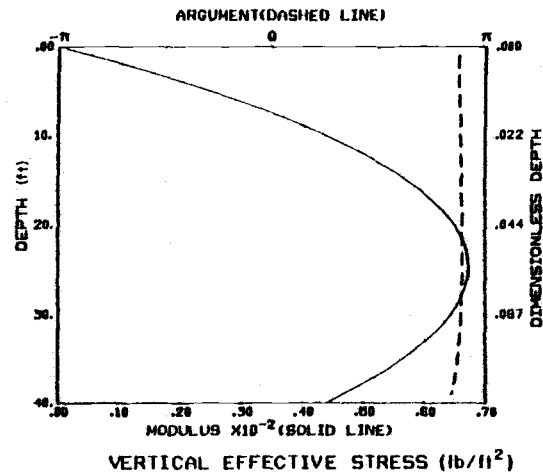


Figure 4.2. Wave-induced vertical effective stress, shear stress, horizontal discharge velocity and vertical discharge velocity for the case A conditions.

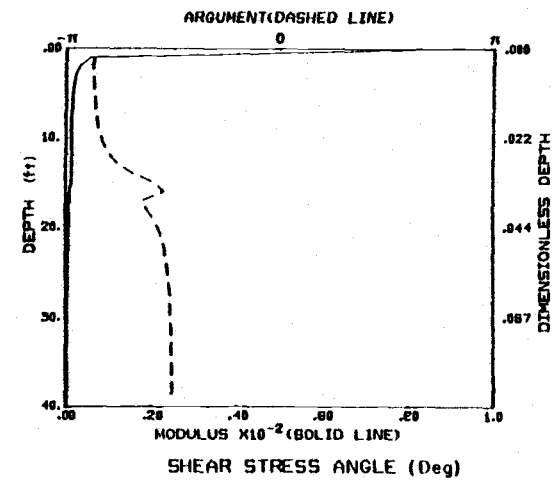
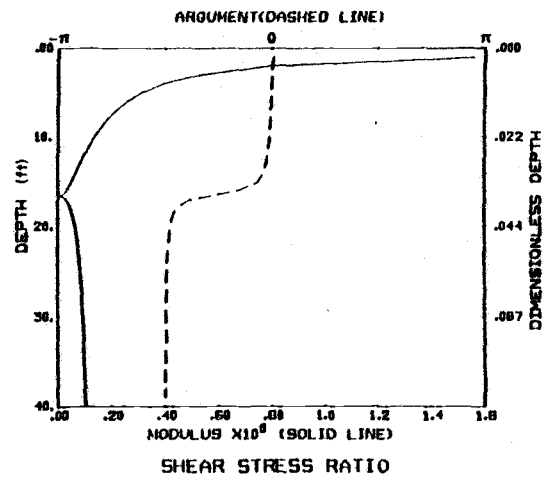


Figure 4.3. Wave-induced shear stress ratio and shear stress angle for the case A conditions.

for the horizontal and vertical, respectively) that failures may occur.

The amplitude of the pore pressure response is frequency selective, the higher frequencies being more highly damped. This response is shown in Figure 4.4 for the case A conditions but allowing the wave period to vary. The soil acts as a low pass filter preferentially removing the higher frequencies. This behavior is characterized by a frequency and depth dependent transfer function. For a single soil layer of thickness, d , the transfer function for dimensionless pressure from the potential pressure model, T , is

$$T = \frac{ch^2 [\lambda(d-z)]}{ch^2 (\lambda d)} \quad (4.1.1)$$

This transfer function is shown in Figure 4.5 for the case A conditions. The higher frequencies are very highly damped. The frequency dependency is also given as a function of d/L which is a common scaling. The depth of the soil may be classified as shallow, intermediate or deep with respect to the wave length by examining the asymptotic behavior of the transfer function. These domains are labeled using the same criteria as used in linear wave theory. For a shallow soil the amplitude of the dynamic pore water pressure is constant with depth, for a deep soil the dependency is exponential and for an intermediate depth soil the dependency is hyperbolic.

The magnitudes of the maximum soil displacements and of the maximum shear stress are also frequency selective. Both components of displacement have a critical frequency at which a maximum occurs. For the case A conditions, the maximum horizontal and vertical displacements and shear stress occur at approximately 12, 8 and 11 seconds, respectively, as shown in Figure 4.6.

The magnitudes of the maximum soil displacements are inversely related to the shear modulus, the stiffer soils being more resistant to displacement. This dependency is shown in Figure 4.7 for the case A conditions, but with variable shear modulus. For these conditions, the displacements are approximately linear functions of the modulus. It is also shown that for values of the modulus greater than 10^{10} lb/ft² the stresses are constant.

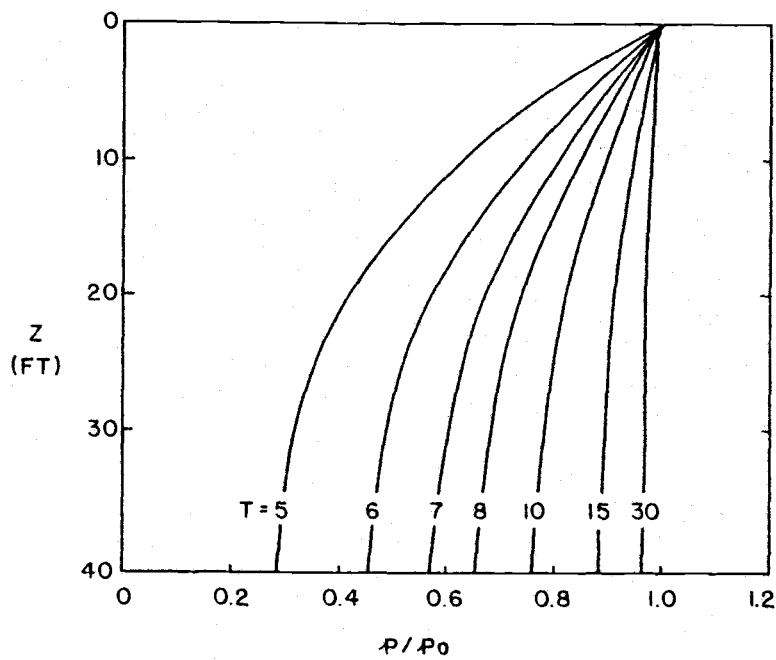


Figure 4.4. Frequency dependency of pore water pressure profiles for the case A conditions.

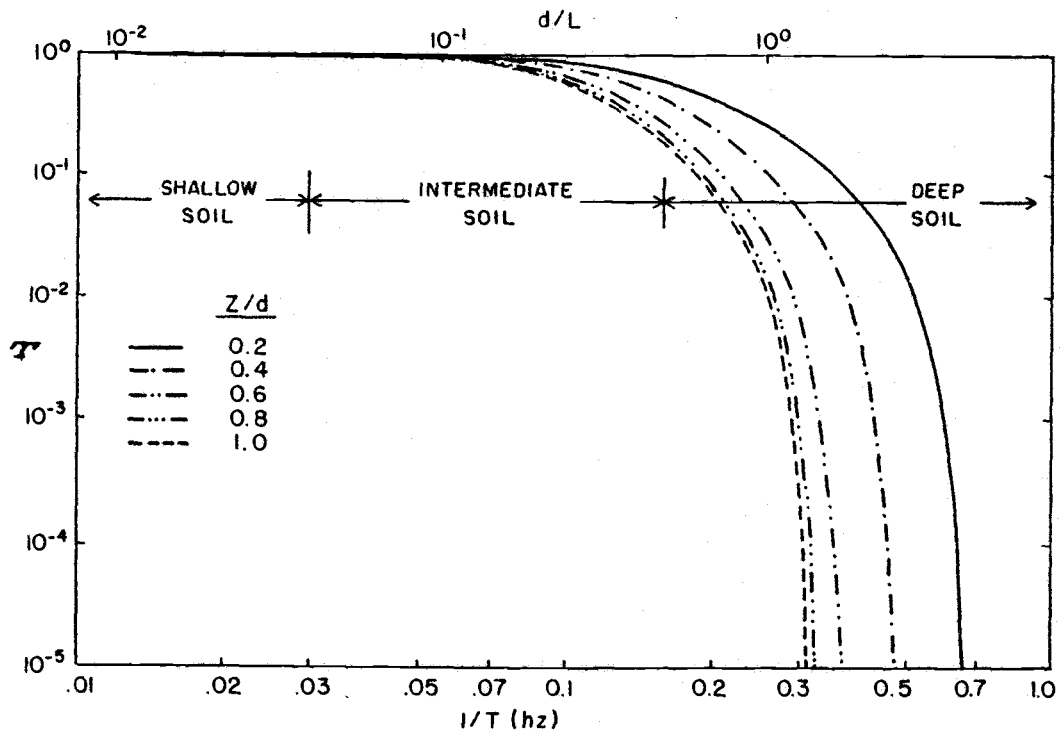


Figure 4.5. Transfer function for the dimensionless pore water pressure from the potential pressure model.

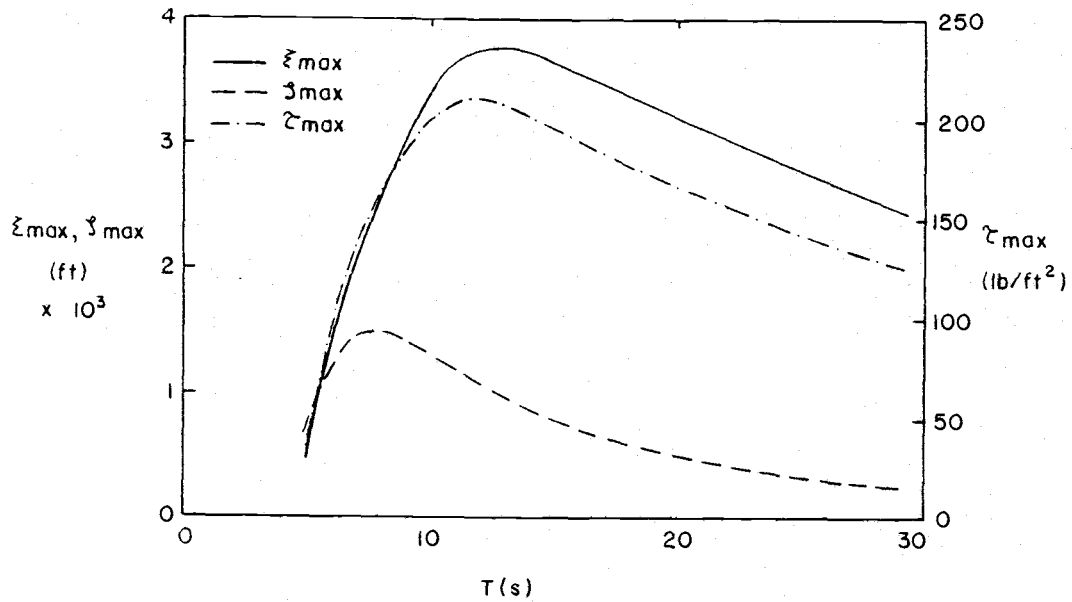


Figure 4.6. Frequency dependency of the maximum displacements and shear stress for the case A conditions.

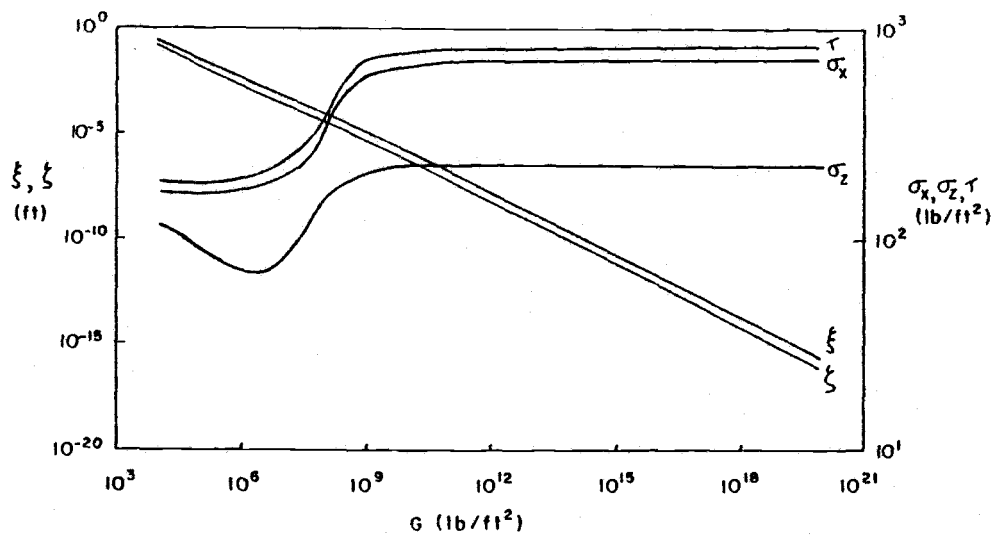


Figure 4.7. Maximum displacements and stresses as a function of the shear modulus for the case A conditions.

The magnitudes of the displacements are a function of the degree of slip at the bottom. The maximum horizontal and vertical displacements and the horizontal displacement at the bottom are shown in Figure 4.8 as a function of the degree of slip for the case A conditions. Free slip corresponds to $\alpha = 0$ and no slip corresponds to $\alpha = 1$. In the field, the impermeable bottom boundary (clay, rock, etc.) may interlock with the soil restricting the soil motion. However, in the laboratory the impermeable bottom may be wood or smooth concrete which provides little resistance to horizontal soil displacement. In this case, the form and magnitude of the soil displacements (and the associated stresses) are dependent on the empirical coefficient, α . The value of α must be determined from experiments. However, this determination is difficult to make if the only measurements are the pore pressure profiles because the pore pressure is relatively insensitive to this coefficient (see Figure 4.9).

The degree of saturation of the pore water has a major effect on the pore pressure response. Air is much more compressible than pure water so even small amounts influence the response. Pore water pressure profiles are shown in Figure 4.10 for the case A conditions as a function of the degree of saturation. The air easily compresses when the soil deforms so the responses are not transmitted as efficiently down through the soil column. However, the displacements near the mudline tend to be larger (see Figure 4.11). An increase in the volume of air in the pore water results in an increase in failure potential.

Pore water pressure profiles are shown in Figure 4.12 for the case A conditions with variable soil depth. For shallow soils ($d/L < 0.05$) the response is nearly constant in z . For deep soils ($d/L > 0.5$) the decay with depth is exponential. The magnitudes of the displacements and shear are also a function of the soil layer thickness. Figure 4.13 indicates that for the case A conditions a maximum failure potential occurs for a soil depth which is approximately 15% of the wave length.

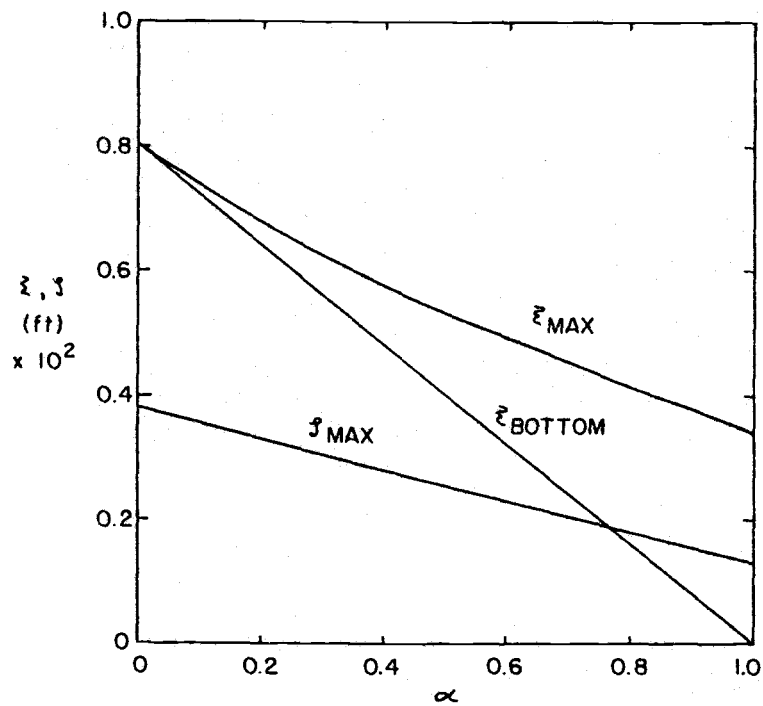


Figure 4.8. Maximum displacements as a function of the degree of bottom slip for the case A conditions.

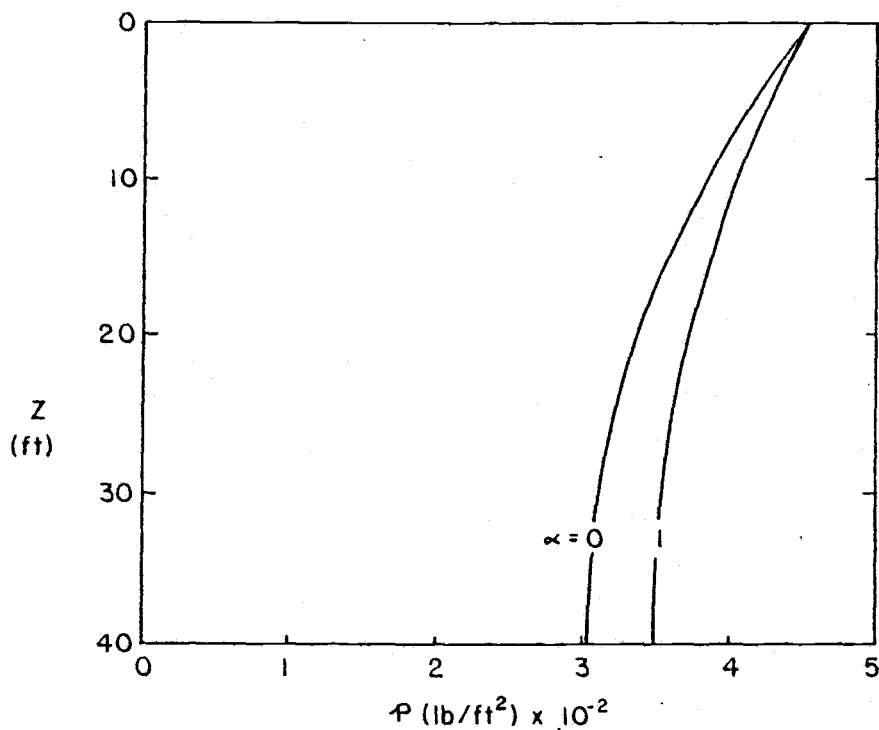


Figure 4.9. Pore water pressure profiles as a function of the degree of bottom slip for the case A conditions.

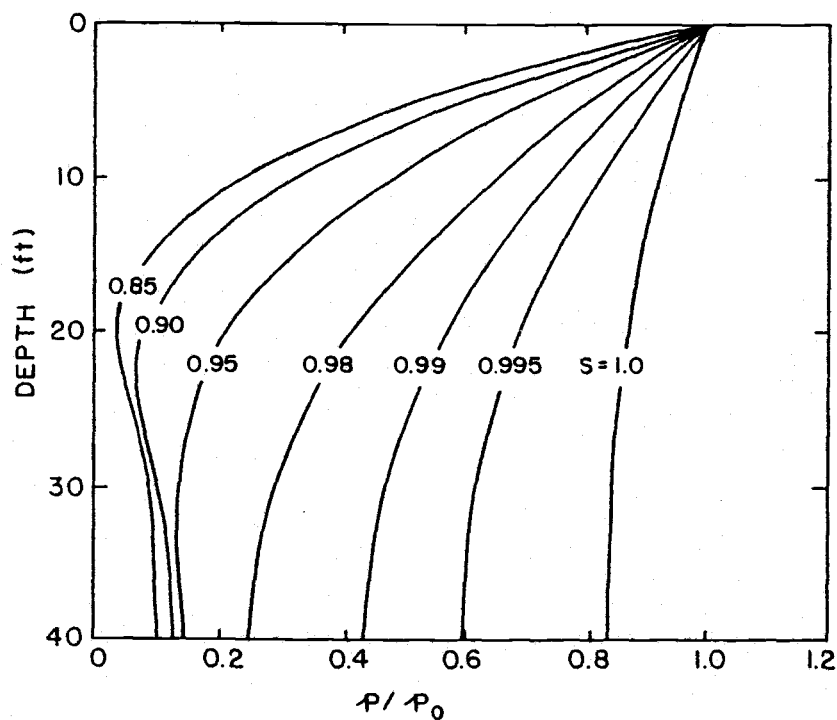


Figure 4.10. Pore water pressure profiles as a function of the degree of saturation for the case A conditions.

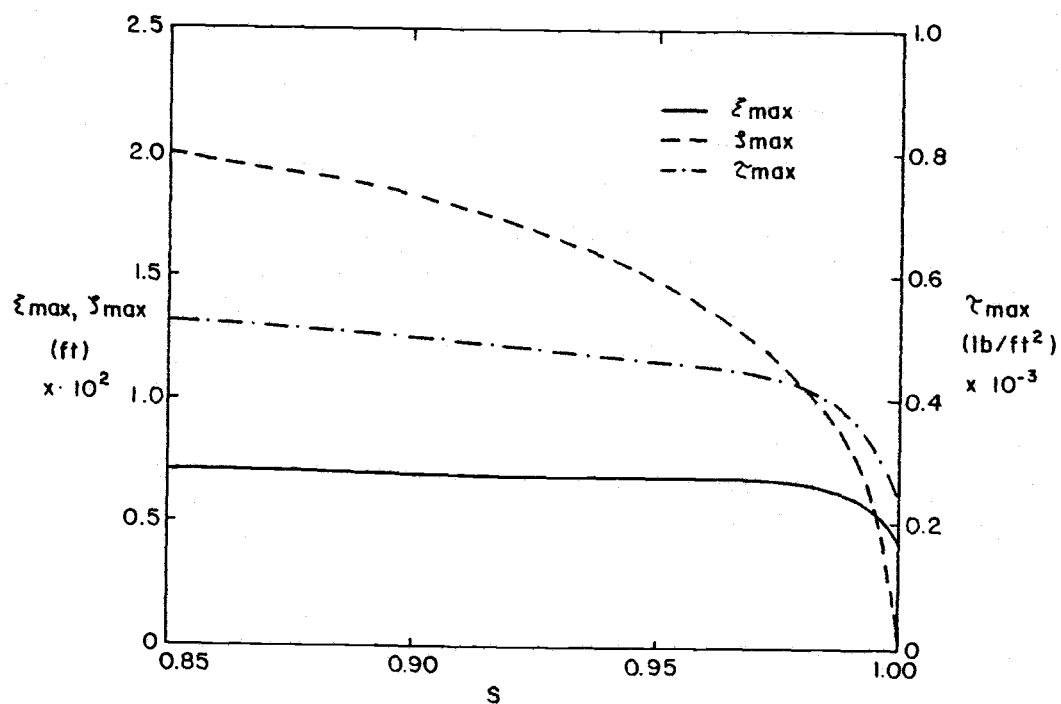


Figure 4.11. Maximum displacements and shear stress as a function of the degree of saturation for the case A conditions.

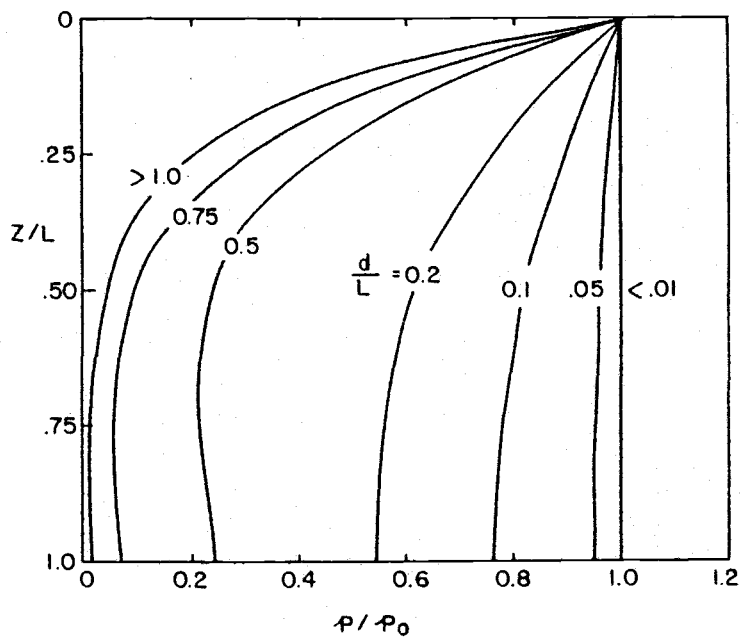


Figure 4.12. Pore water pressure profiles as a function of the soil thickness for the case A conditions.

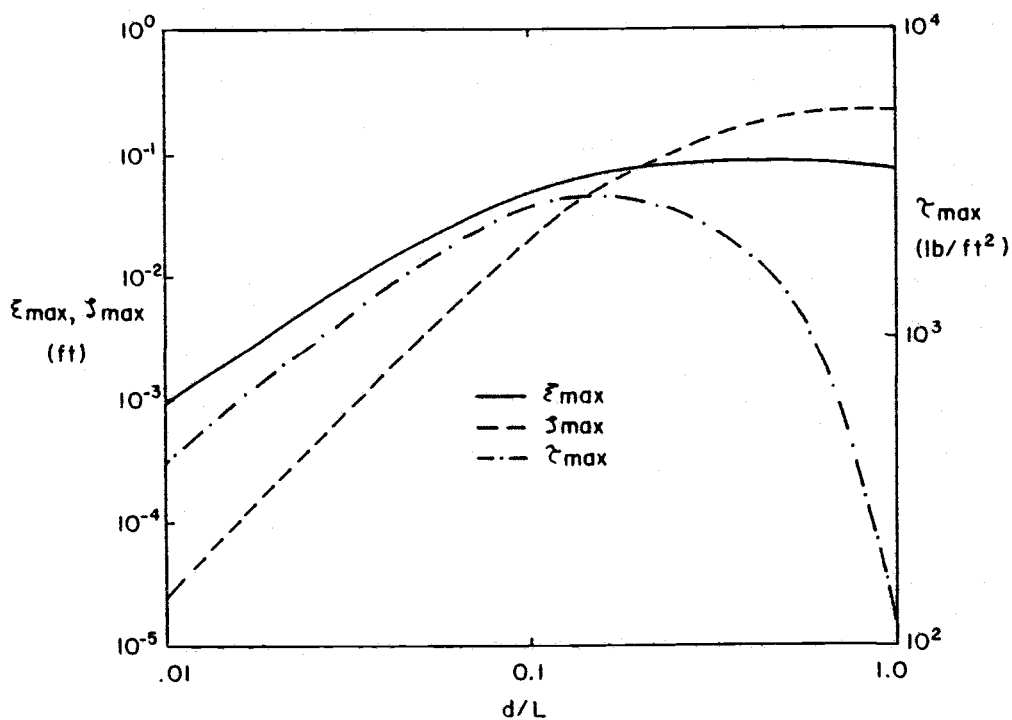


Figure 4.13. Maximum displacements and shear stress as a function of the soil thickness for the case A conditions.

4.2 Two Soil Layer Response

The general responses of a two soil layer system are similar to the one layer system but are complicated by the geotextile properties and the coupling of the two soil layers. A three layered system (two identical soil layers separated by a geotextile) with geometry similar to the conditions tested in the wave channel is examined in detail. These conditions are denoted as the case B conditions and are summarized in Table 4.2. The soils may again be described as a coarse sand.

Table 4.2. Case B wave and soil conditions.

$G_1 = 2.5 \times 10^5 \text{ lb/ft}^2$	$G_2 = 2.5 \times 10^5 \text{ lb/ft}^2$	$H = 2.03 \text{ ft}$
$v_1 = 0.33$	$v_2 = 0.33$	$T = 1.77 \text{ s}$
$n_1 = 0.4$	$n_2 = 0.4$	$h = 8.0 \text{ ft}$
$K_1 = 0.01 \text{ ft/s}$	$K_2 = 0.01 \text{ ft/s}$	$\alpha = 1.0$
$\gamma_{B1} = 50 \text{ lb/ft}$	$\gamma_{B2} = 50 \text{ lb/ft}$	
$d_1 = 1.0 \text{ ft}$	$d_2 = 3.0 \text{ ft}$	

The fluid energy dissipated in the geotextile is characterized by the permittivity. This coefficient is primarily a function of the fabric permeability. Pore water pressure profiles are shown in Figure 4.14 for the case B conditions as a function of the geotextile permeability for a geotextile with a thickness of 0.01 ft. The fabric location is shown by the hashed line. When the geotextile permeability is of the same order or greater than the soil permeability, the fabric is transparent. As the geotextile permeability decreases the transmission of pressure is significantly reduced. The resulting displacements and shear stress are shown in Figure 4.15. Decreasing geotextile permeability results in a decreased failure potential from the cyclic stresses. However, as the permeability of the geotextile

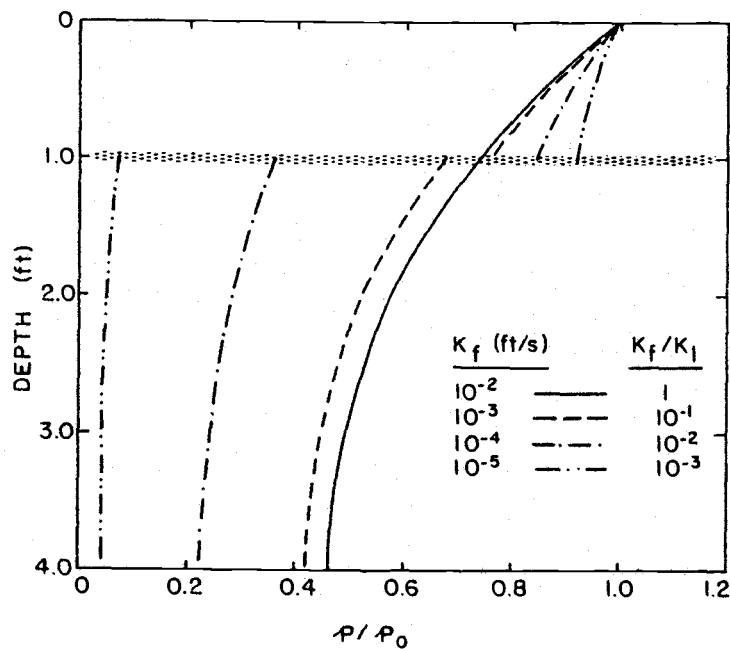


Figure 4.14. Pore water pressure profiles as a function of the geotextile permeability for the case B conditions.

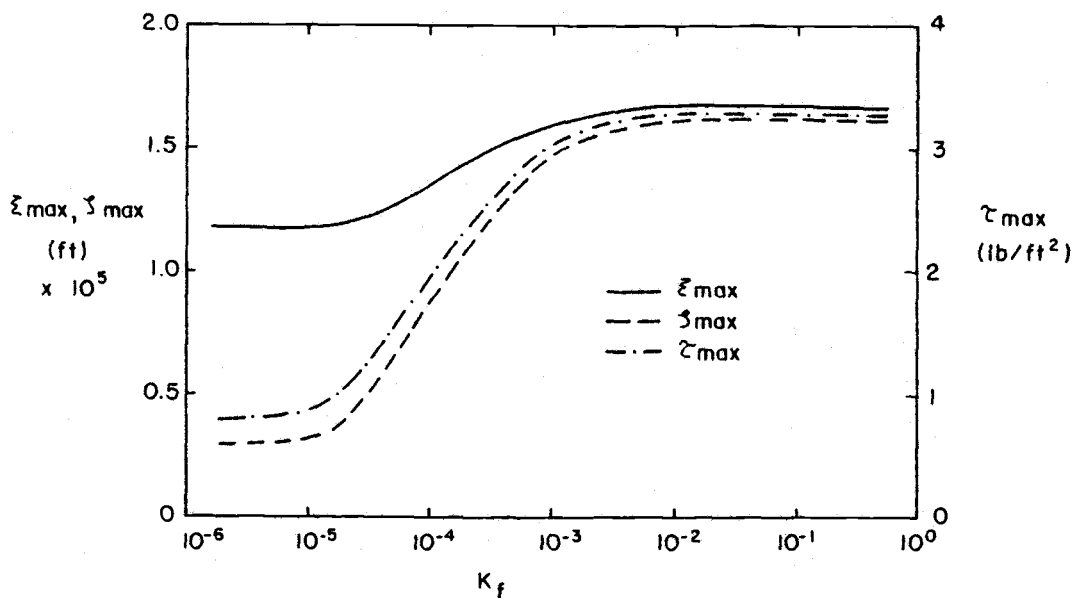


Figure 4.15. Maximum displacements and shear as a function of the geotextile permeability for the case B conditions.

decreases the failure potential due to the accumulation of pore water pressure increases significantly. A low permeability fabric is an undrained condition and the accumulating pore pressure is unable to dissipate. If the permeability of the geotextile is of the same order or greater than that of the adjacent soils the geotextile permeability will have little or no influence on the soil response. Most commercially available geotextiles are more permeable than sands and silts and therefore are transparent in the transmission of pressure. However, the geotextile pores can clog with soil particles which reduces the fabric permeability. A clogged geotextile is more susceptible to a pore water pressure accumulation failure.

The geotextile permeability may be defined to include the effect of the fluid acceleration in the same way unsteady soil permeabilities were defined. The imaginary portion of the permeability indicates the importance of the acceleration. For a physically realistic values for the inertial coefficient, C_m , the imaginary portion of the geotextile permeability has no influence on the soil response. The sensitivity to the inertial coefficient has been examined for the range $-6 < C_m < 6$. No discernible change in soil response was noted.

The solution is also influenced by the ratio of the soil permeabilities. Pore water pressure profiles are shown in Figures 4.16 for the case B conditions with variable K_1 . The pressure response in the lower layer is decreased as the upper layer becomes less permeable. Figure 4.17 shows the maximum displacements and shear. When the permeabilities are within an order of magnitude of each other the solution is sensitive to changes in the relative permeability. However, as the difference in permeability exceeds an order of magnitude, equilibrium values are quickly reached which are associated with the less permeable layer. Figures 4.18 and 4.19 are similar to Figures 4.17 and 4.18 except K_2 is held constant and K_1 is allowed to vary. It is of interest to note that for a relative permeability of approximately 10, a maximum pore water pressure profile results. This maximum is also observed in the horizontal displacement and shear stress. This corresponds to a worst combination of grain sizes in terms of failure potential. The permeabilities for this worst case (for the case B

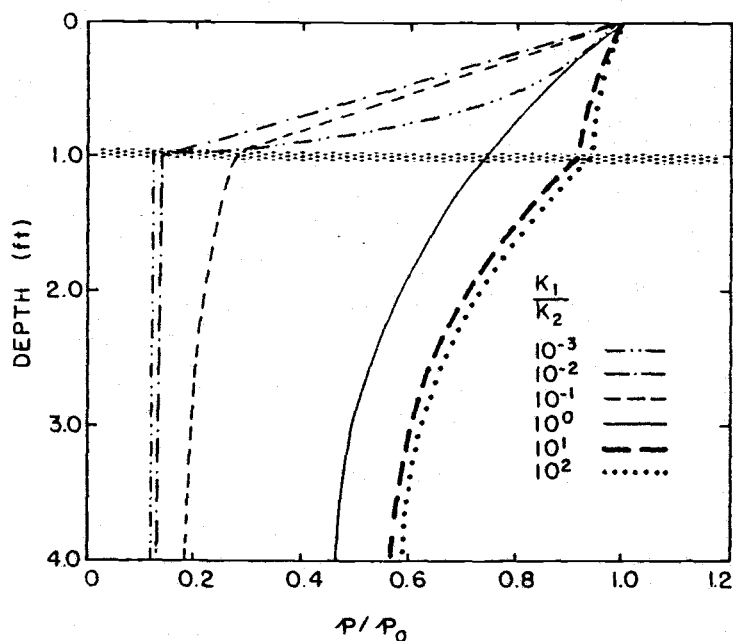


Figure 4.16. Pore water pressure profiles as a function of the relative permeability for the case B conditions ($K_2 = 0.01$ ft/s).

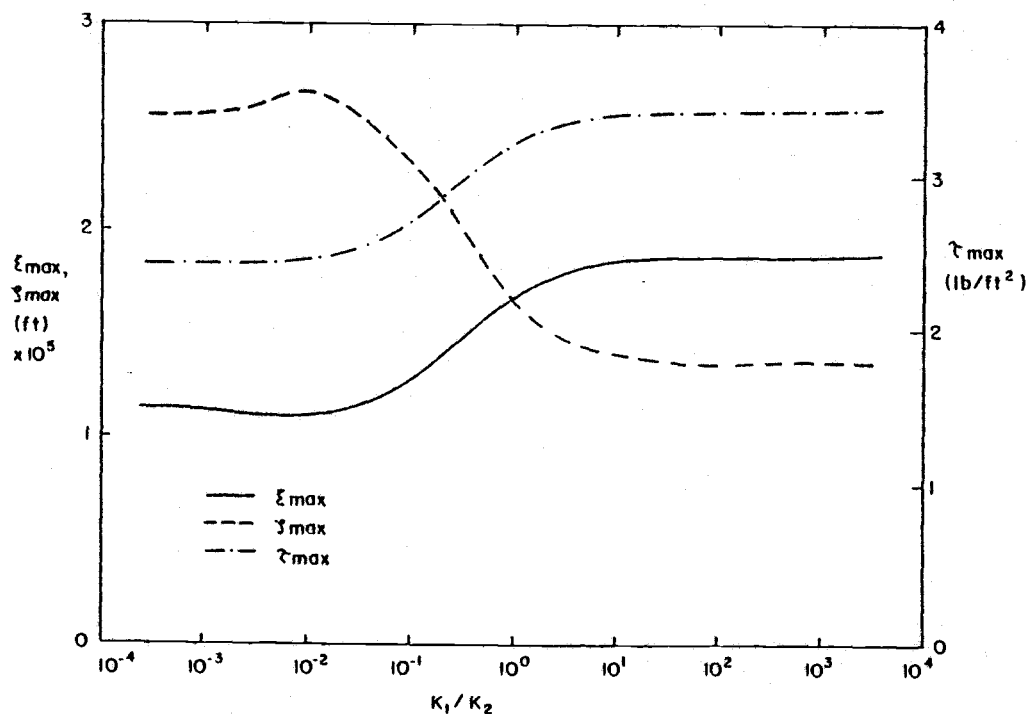


Figure 4.17. Maximum displacements and stresses as a function of the relative permeability for the case B conditions ($K_2 = 0.01$ ft/s).

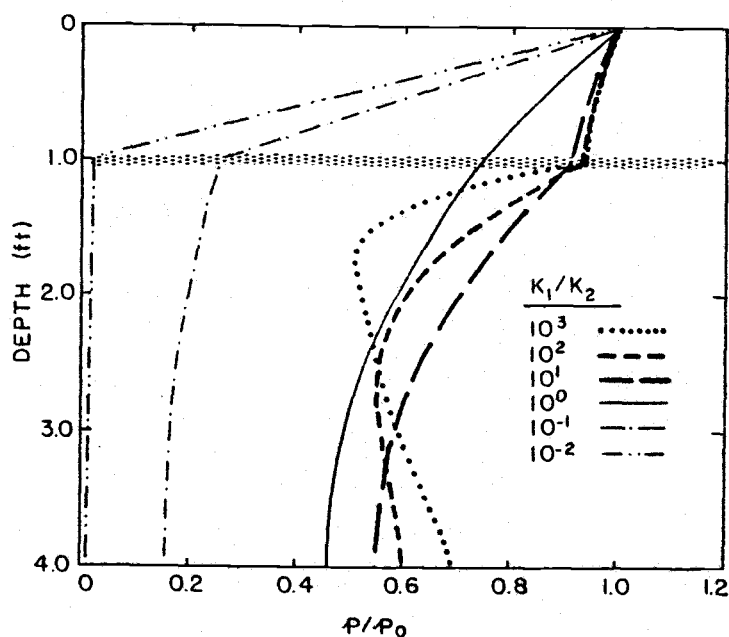


Figure 4.18. Pore water pressure profiles as a function of the relative permeability for the case B conditions ($K_1 = 0.01$ ft/s).

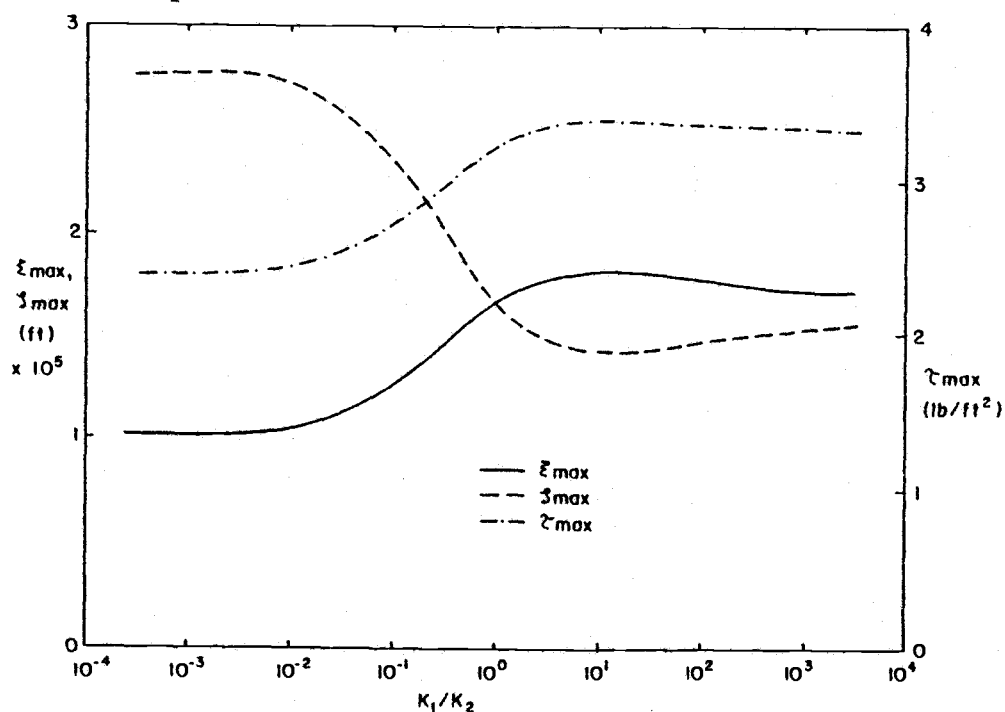


Figure 4.19. Maximum displacements and shear stress as a function of the relative permeability for the case B conditions ($K_1 = 0.01$ ft/s).

conditions) are representative of a gravel covering a coarse sand.

The imaginary portion of the soil permeability has a minor influence on the soil response. Hannoura and McCorquodale (1978) present experimental results that indicate the inertia coefficient for coarse granular media is between -6 and 6. The pressure profiles for this range of inertia coefficient are not influenced by the acceleration. The influence on the magnitude of the displacements and stresses is also very small for the test wave and soil conditions. However, the relative importance of the inertial term is given by $\omega C_m k/gn$. For most marine soils, the added mass and porosity show little variation. Therefore, the inertial term is primarily a function of the soil permeability and the wave frequency; high permeability (associated with larger sediment size) and higher wave frequency tending to increase the relative importance. For the case B conditions this coefficient has a value near 10^{-4} , while for gravel it is near 10^{-2} and for riprap it may approach unity.

The mechanical properties of the geotextile are described in terms of the elasticity and tension. The elasticity has little influence on the pore water pressure; less than 2% decrease for very stiff fabrics. However, the maximum displacements and shear stress are dependent on the elasticity (see Figure 4.21). The primary influence on the vertical displacement and shear stress occurs for very compliant geotextiles while the influence on the horizontal displacement is a maximum as the geotextile elasticity approaches the shear modulus of the soil. As with the elasticity, the pore water pressure profiles are only weakly dependent on the geotextile tension. The maximum change occurs for fabric tensions less than 100 lb/ft. Figure 4.21 shows that pretensioning the geotextile to 100 lb/ft for the case B condition results in a 30% reduction in shear stress.

It was shown in Figure 4.10 that the degree of saturation of the pore water influences the soil response. In a marine sediment, biological activity or chemical decomposition of organics may produce gas. The influence of these bio-chemical processes on the soil pressure response is shown in Figure 4.22 for the case B conditions with variable saturation in the upper layer. The soil response is a

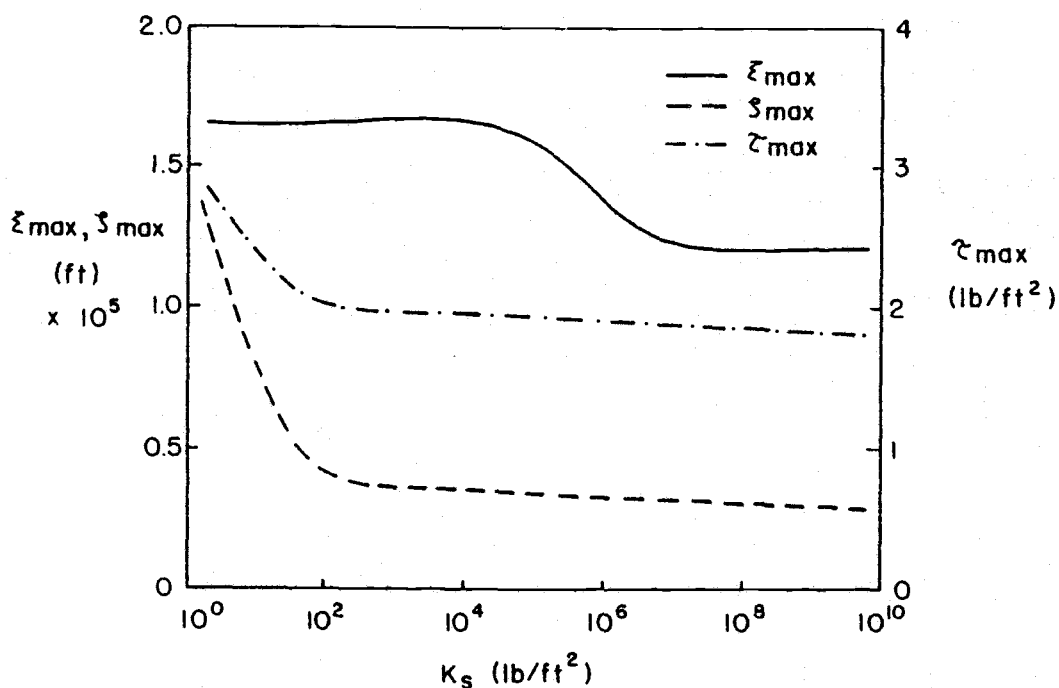


Figure 4.20. Maximum displacements and shear stress as a function of geotextile elasticity for the case B conditions.

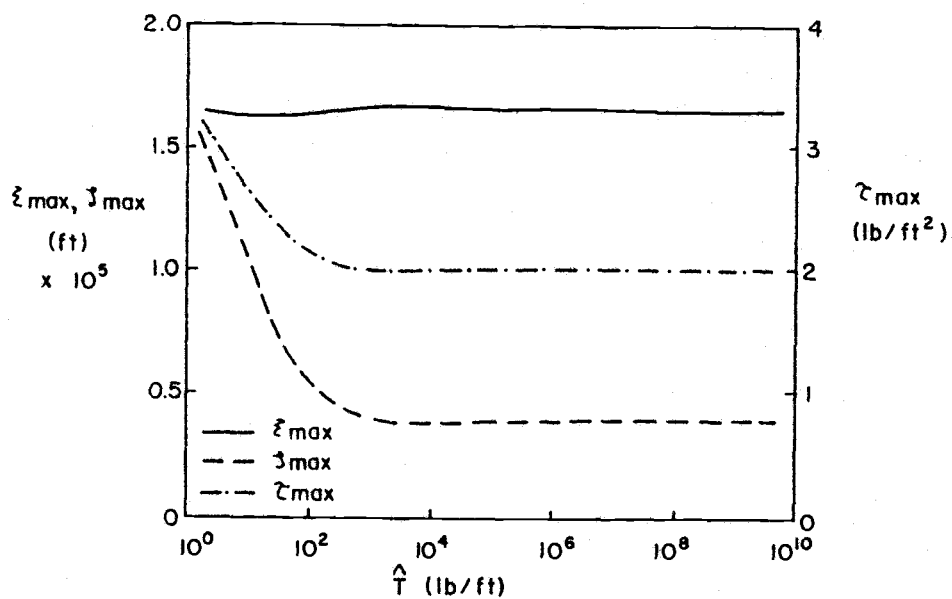


Figure 4.21. Maximum displacements and shear stress as a function of the geotextile tension for the case B conditions.

function of the degree of saturation in the upper layer, but the influence on the pressure profile is small even for a large variation in saturation. However, the shear stress increases in the upper layer in response to increasing gas content in the pore water. The sensitivity of both the shear stress and pore water pressure responses increase as the thickness of the organic layer increases.

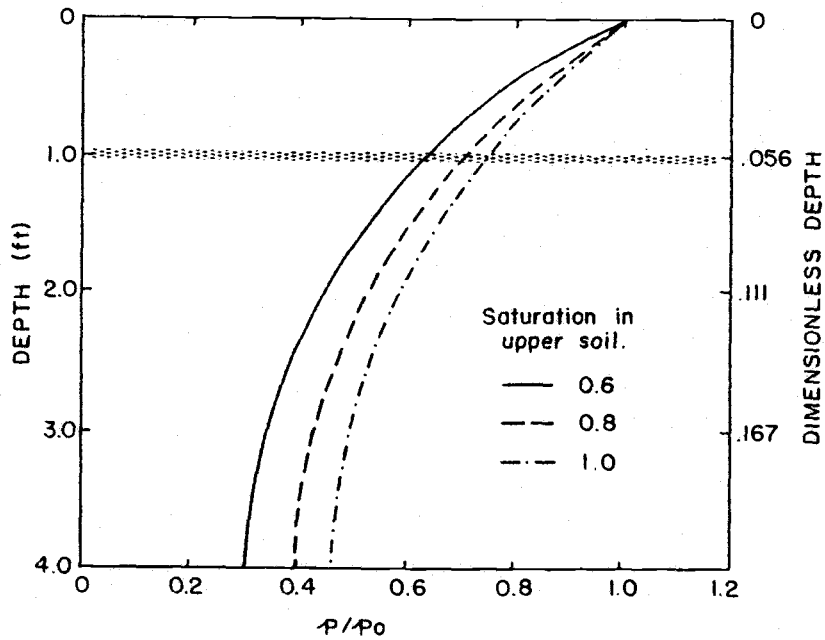


Figure 4.22. Pore water pressure profiles as a function of the degree of saturation of the upper layer for the case B conditions.

5.0 EXPERIMENTAL RESULTS

Two series of laboratory experiments were conducted at the Oregon State University Wave Research Facility (WRF) during the spring of 1980 and 1981. In both cases the pore pressure response was measured in a three layered system; two different soils separated by a geotextile. However, in the first series of experiments only the periodic responses were measured while in the second series of experiments both the periodic and mean change in pore water pressure were monitored.

5.1 Laboratory Setup

5.1.a Oregon State University Wave Research Facility

The WRF is a large scale open air wave channel 12 feet wide, 15 feet deep and 342 feet long. The hinged wave board is driven by an MTS servo hydraulic piston. The facility is capable of producing simple periodic waves with periods exceeding eight seconds and heights to five feet. Random waves can also be generated using the on-site PDP 11 computer to generate the wave spectrum and transfer function for the board motion. Wave heights are measured with a sonic surface profiler. The wave energy is dissipated through breaking on a concrete beach with slope 1:12.

5.1.b Test Section

A test section 36 feet long was constructed in the wave channel. The determination of the optimum test section length for minimum end wall effects is discussed in Appendix C. The four foot deep, four foot wide section was constructed of 3/4 inch plyboard reinforced with 2 x 4 studs. The side walls were braced to the wave channel walls and the bottom was attached to the channel bottom. Wood to wood connections

were glued and screwed and the entire section was treated with a water sealer. The test section is shown in place in Figure 5.1 before the addition of the soil layers.

The volume between the wave tank walls and the test section was filled with gravel to provide extra stability and prevent deflection of the side walls during the cyclic wave loading. A typical cross section of the test section is shown in Figure 5.2.

A uniform gravel ($D_{50} = 10.5$ mm) was selected as the upper soil layer material. The gravel provides good transmission of the pore pressure to the geotextile while also providing a stable surface under the test wave conditions. A uniform, fine, clean sand ($D_{50} = 0.2$ mm) was selected for the lower layer. Such a material demonstrates a potential for liquefaction [Seed and Idriss (1967)]. Accurate determination of the physical properties of the two soils is important when comparing the analytical model with the experimental observations. These properties are summarized in Table 5.1 and Figures 5.3 and 5.4.

Table 5.1. Test section upper layer soil properties.

$\gamma_{B1} = 58.6$ lb/ft ³
$K_1 = 0.059$ ft/s
$G_1 = 4.0 \times 10^5$ lb/ft ²
$\nu_1 = 0.35$
$n_1 = 0.465$

The two soil layers were separated by a geotextile. Four geotextile conditions were tested; woven, impermeable, semi-rigid and no geotextile. Typical geotextiles are shown in Figures 5.5, 5.6, 5.7 and 5.8.

Important geotextile physical properties for the analytical model include: tension, elasticity, permeability and thickness. The perme-

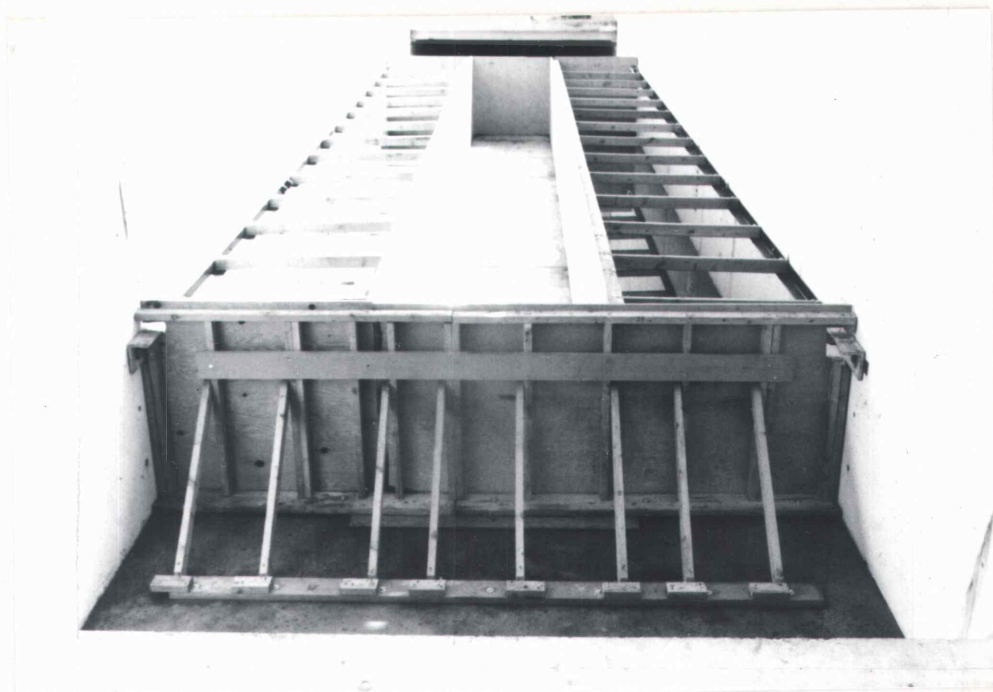


Figure 5.1. In place photograph of the test section before the addition of the soil layers.

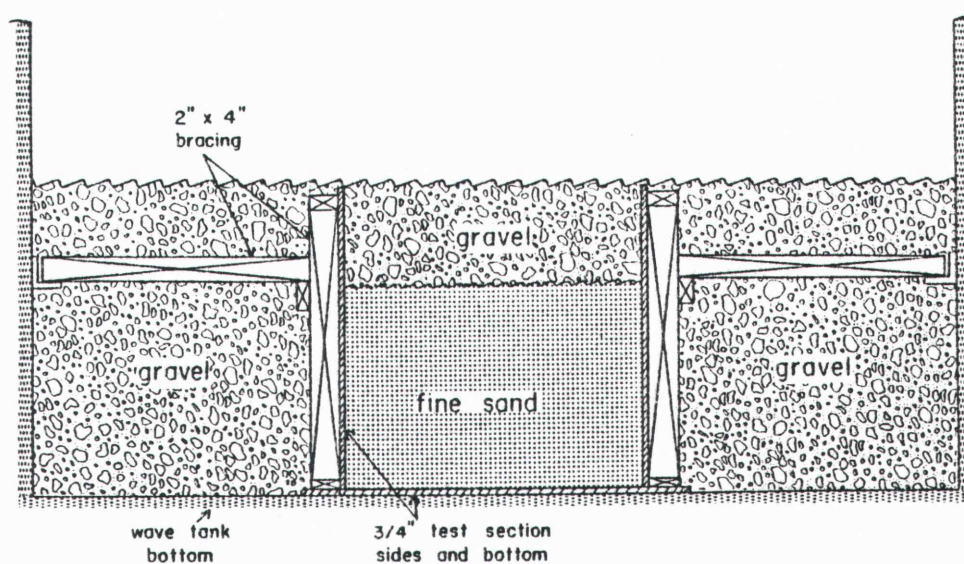


Figure 5.2. Typical cross-section of the test section.

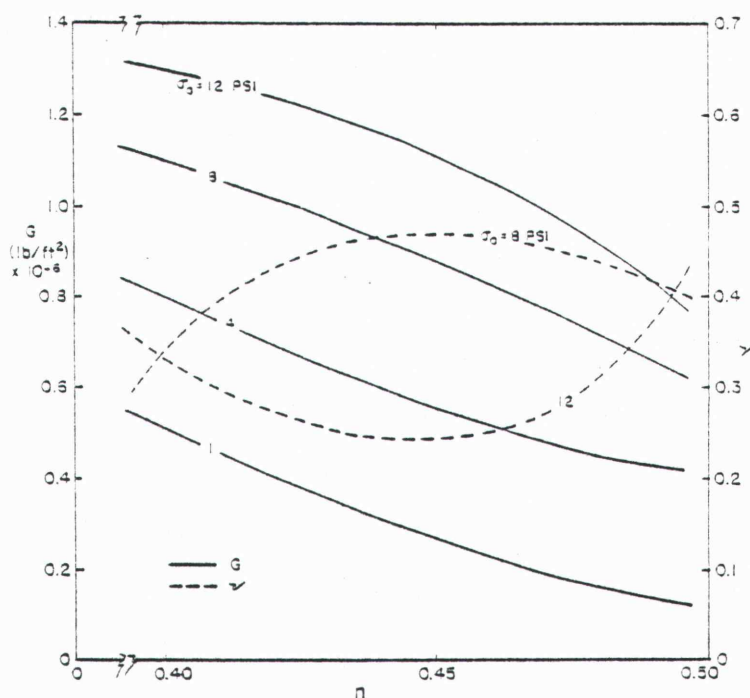


Figure 5.3. Shear modulus and Poisson's ratio in the lower soil layer as a function of porosity for different confining pressures.

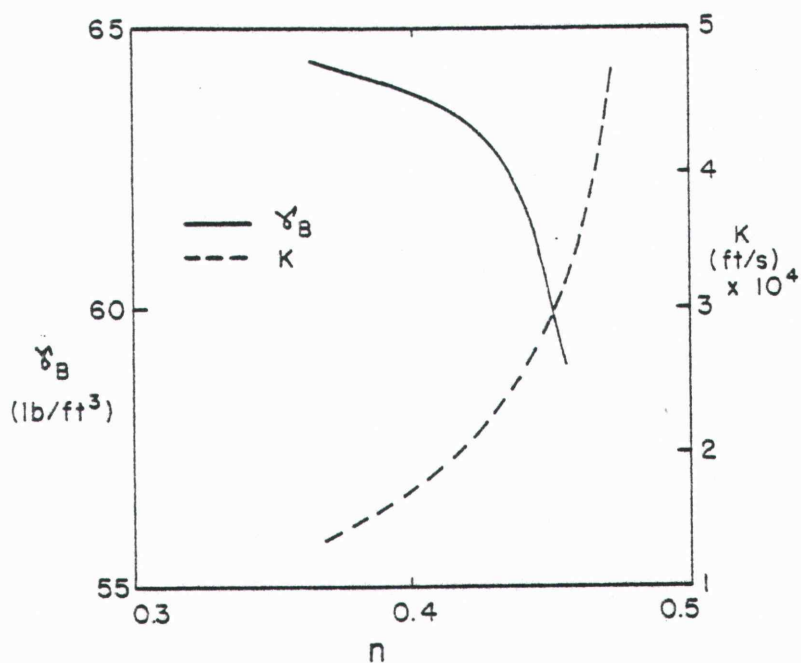


Figure 5.4. Bouyant weight and permeability of the lower soil layer as a function of porosity.

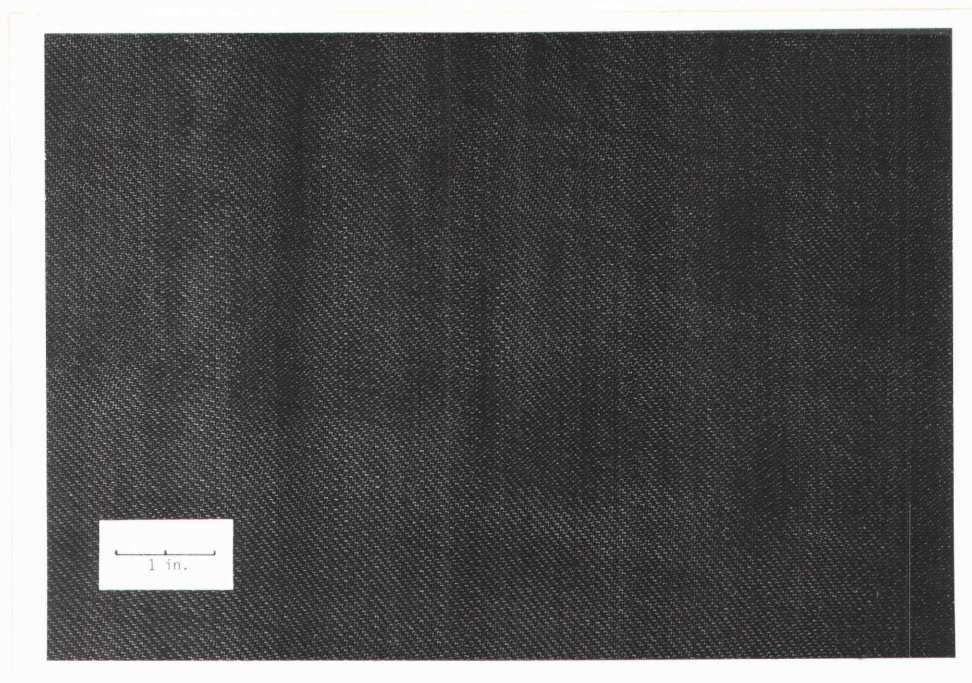


Figure 5.5. Monofilament woven geotextile (Polyfilter GB, Carthage Mills).

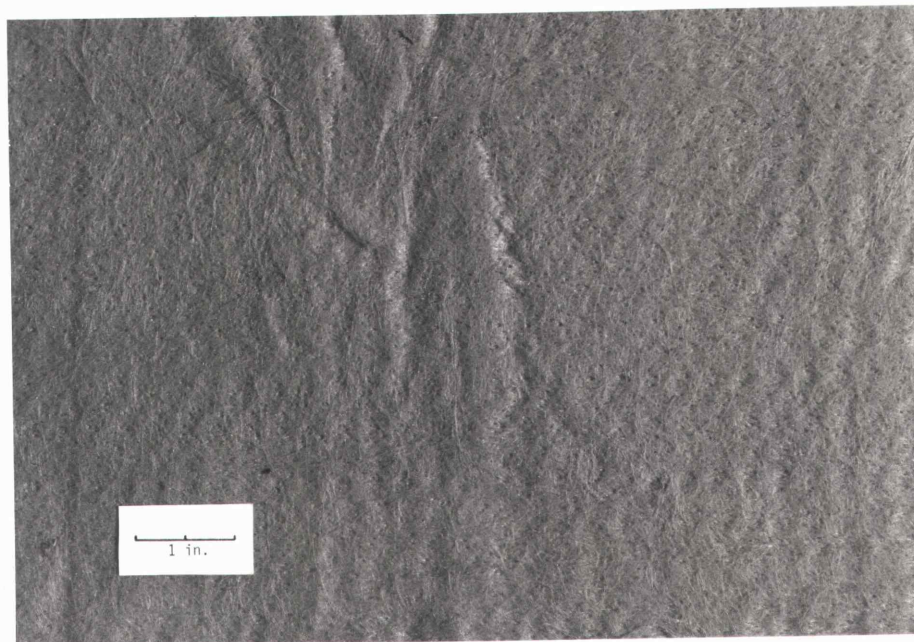


Figure 5.6. Needle punch nonwoven geotextile (Bidim C42, Monsanto).

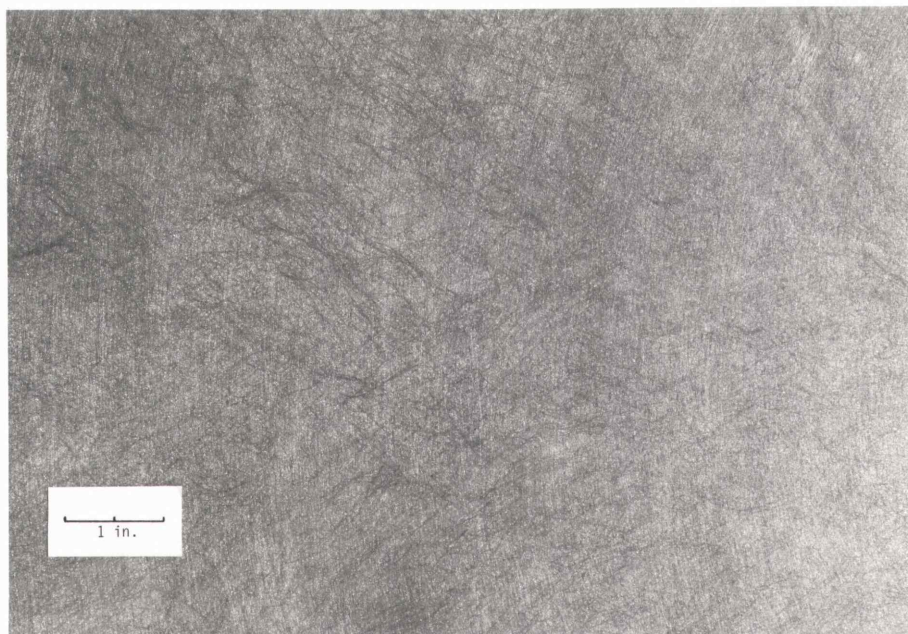


Figure 5.7. Heat bonded nonwoven geotextile (Typar, Dupont).

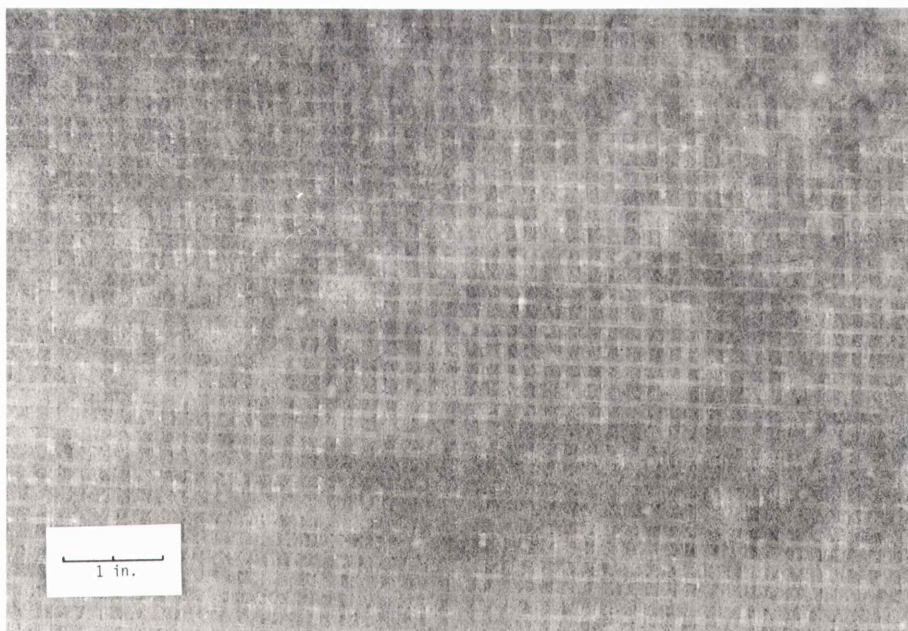


Figure 5.8. Combination woven/nonwoven geotextile (Terrafix 500N, Terrafix)

ability and thickness may be combined into a single term, the permissibility. Properties for several fabrics are listed in Table 5.2. The values for elasticity are only approximate values because the stress-strain behavior of geotextiles is very non-linear.

Table 5.2 Geotextile properties.

Geotextile	Permeability (ft/s)	Thickness (in)	Elasticity (lb/ft ²)
Polyfilter GB	0.059	0.025	2040
Bidim C42	0.130	0.180	5280
Typar	0.004	0.015	12000
Terrafix 500 N	0.118	0.175	12000

The uniform preparation of the lower soil is an important aspect of the experiments to insure repeatability. The soil was first completely fluidized by injecting a high pressure water jet into the sand. The "fluidizer", an inverted tee shaped manifold [see Nath et al. (1977)] was moved through the soil at one foot intervals. In the 1980 experiments the soil was reconsolidated by moving a hinged metal flap activated by a concrete vibrator through the bed at one foot intervals. This left the soil in a relatively dense state. The following year the soil was slightly consolidated by manually vibrating vertical rods at a specific number of locations. This left the soil in a uniform condition very near liquefaction. A gravel overburden of approximately 60 lb/ft² was then added and the soil was allowed to consolidate for 24 hours. During this period the soil consolidated from $n = 0.460$ to a more stable value of $n = 0.425$. This second consolidation technique was more consistent from test to test than the hinged flap concrete vibrator method. Thielen (1981) provides a detailed description of the bed preparation techniques.

The lower soil layer porosities for the 1980 tests are summarized in Table 5.3. The 1981 tests showed little variation.

Table 5.3. Lower soil layer porosities for the 1980 tests.

<u>Geotextile</u>	<u>n</u>	<u>σ</u>
woven	0.430	0.000
semi-rigid	0.480	0.000
impermeable	0.418	0.005
no fabric	0.457	0.015

The average porosity for all tests was 0.442 with a standard deviation of 0.023 or about 5% of the mean. Because of this small variation, a single set of soil parameters is used to describe the lower soil for all tests. These properties are summarized in Table 5.4.

Table 5.4. Mean lower soil layer properties.

$$\gamma_{B2} = 61.7 \text{ lb/ft}$$

$$K_2 = 2.6 \times 10^{-4} \text{ ft/s}$$

$$G_2 = 3.0 \times 10^5 \text{ lb/ft}^2$$

$$\nu_2 = 0.374$$

$$n_2 = 0.442$$

In both series of experiments the pore water pressure was monitored to reveal the dynamic response of the soil-geotextile system to ocean waves. The 1980 tests were designed to examine the periodic pore water responses only, while in the 1981 tests both the periodic response and mean accumulation of pore pressure was monitored. The periodic responses were used to verify the Biot model and the accumula-

tion measurements were compared with the earthquake consolidation equation predictions [Thielen (1981)]. Thielen (1981) also includes an analysis of the random waves and more information on the laboratory experiments.

5.1.c Pressure Transducers

The response of the soil-geotextile system was examined by measuring the dynamic pore pressure response in the soil. Nine pressure transducers (Druck model PDCR10) were mounted in the side wall of the test section in the 1980 experiments and 14 in the 1981 experiments. Carborundum filter stones were placed between the soil and transducers in flush mounting aluminum brackets. This prevented soil from clogging the pressure transducers. The stones were boiled for 20 minutes to remove air and were always kept underwater. A small amount of air in the stones significantly changes the dynamic response of the transducers due to the compressibility of air.

Most of the transducers were placed to measure the vertical profile of the pressure. However, two transducers in the 1980 experiments and four in the 1981 experiments were placed off this vertical profile to insure that the central location of the test section was homogeneous and free from end effects. The locations of the pressure transducers are summarized in Table 5.5.

The transducers were calibrated by raising the still water level in the wave channel and the response was nearly linear at one volt per psi of static pressure. The calibrations were checked before and after each sequence of runs. No DC drift was observed as a function of time.

5.2 Laboratory Measurements

The free surface profiles and the pore pressure response were recorded for different wave and geotextile conditions. The simple periodic waves tested corresponded to Dean's stream function cases [Dean (1974)]. These waves are summarized in Tables 5.6 and 5.7 for the two water depths examined, four and eight feet, respectively.

Table 5.5. Pressure transducer locations

<u>Transducer</u>	<u>1980</u>		<u>1981</u>	
	<u>x(ft)</u>	<u>z(ft)</u>	<u>x(ft)</u>	<u>z(ft)</u>
1	0.00	4.00	0.00	3.44
2	0.00	3.76	0.00	2.77
3	0.00	2.21	0.00	1.85
4	0.00	1.45	0.00	1.60
5	0.00	1.17	0.00	1.35
6	0.00	0.54	0.00	1.10
7	0.00	0.00	0.00	0.85
8	-6.00	2.21	0.00	0.62
9	6.00	2.21	0.00	0.36
10	--	--	0.00	0.00
11	--	--	-10.00	1.60
12	--	--	-4.67	1.60
13	--	--	4.67	1.60
14	--	--	10.00	1.60

Table 5.6. Simple periodic waves tested for a water depth of four feet.

<u>Wave Case</u>	<u>T (sec)</u>	<u>H (ft)</u>
7A	1.98	0.64
7B	1.98	1.26
7C	1.98	1.88
6A	2.80	0.74
6B	2.80	1.46
5A	3.95	0.78
5B	3.95	1.54
4A	6.25	0.78
4B	6.25	1.58

Table 5.7. Simple periodic waves tested for a water depth of eight feet.

<u>Wave Case</u>	<u>T (sec)</u>	<u>H (ft)</u>
8A	1.77	0.68
8B	1.77	1.36
8C	1.77	2.03
7A	2.80	1.28
7B	2.80	2.52
7C	2.80	3.76
6A	3.95	1.47
6B	3.95	2.92
6C	3.95	4.40
5A	5.59	1.55
5B	5.59	3.07
4A	8.84	1.56

The physical significance of the Dean's stream function wave cases is shown in Figure 5.9. In the stream function wave case designation the number indicates the relative depth and the letter, the percent of the breaking wave height. The waves utilized in the tests span the range of intermediate waves.

The free surface elevation and pressure transducer outputs were recorded on magnetic analog tape as a function of time. The 1980 results were transcribed on strip charts and visually read. The 1981 results were digitally recorded and analyzed by the computer. Both sets of measurements are summarized in Appendix D.

The dynamic wave-induced pressure at the mudline drives the soil-geotextile system. Therefore, an accurate measurement of this value is important. It is also the amplitude of the dynamic pressure at the mudline which is used to nondimensionalize the analytic solutions. There is some scatter in this measurement which is propagated through the nondimensionalizing. These errors vary from 2% to 8% of the mean

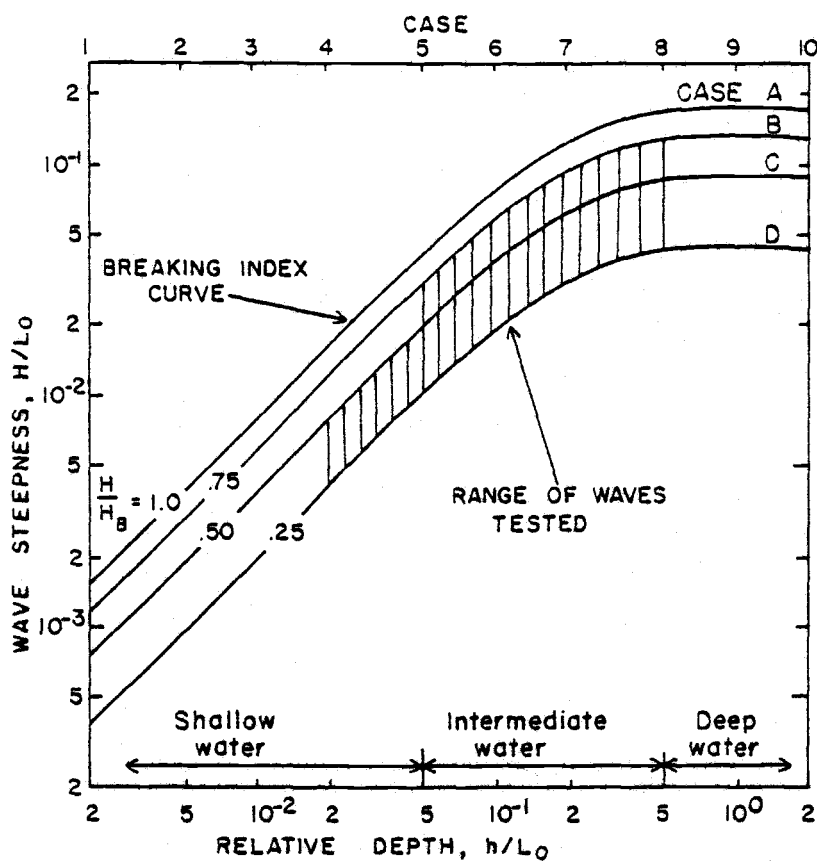


Figure 5.9. Definition diagram for Dean's stream function wave cases [from Dean (1974)].

mudline pressure amplitudes for the various wave cases. This error primarily results from small variations in the simulation of test waves for a given stream function case. However, the nondimensional pressure is not very sensitive to the magnitude of the mudline pressure and the theoretical solution to the pressure ratio is amplitude independent.

5.3 Comparison of Theory and Observations

The soil-geotextile system is driven by the wave-induced pressure at the mudline. (The wave-induced fluid shear stress at the mudline also drives the soil system but this stress is approximately five orders of magnitude less than the pressure and is negligible.) The pore pressure response in the soil is therefore linear in the pressure amplitude at the mudline. Pressure profiles scaled by the mudline pressure amplitude would then be expected to be independent of wave steepness. This result was confirmed by the laboratory measurements. Figure 5.10 shows the dimensionless measured soil pressure response for wave cases 8A, 8B and 8C. Each case is the average of the four no geotextile runs for the 1980 experiments.

A surprising observation is that the geotextile properties have very little influence on the cyclic pore water response. This lack of dependency on the geotextile properties is shown in Figure 5.11. The dimensionless pressure profile is similar for a no geotextile, an impermeable geotextile, a semi-rigid geotextile and a woven geotextile. Each data point is the average of wave cases 8A, 8B and 8C for a given geotextile condition.

Theory and measurements are compared in Figures 5.12 and 5.13 for the no geotextile condition. Theoretical results for both the free slip and no slip bottom conditions are shown. For the smooth laboratory test section, the free slip condition provides the best predicted response. In general the agreement with theory is good suggesting that the soil response is well modeled by Biot consolidation theory and that the soil-geotextile-soil model is valid for layered soils.

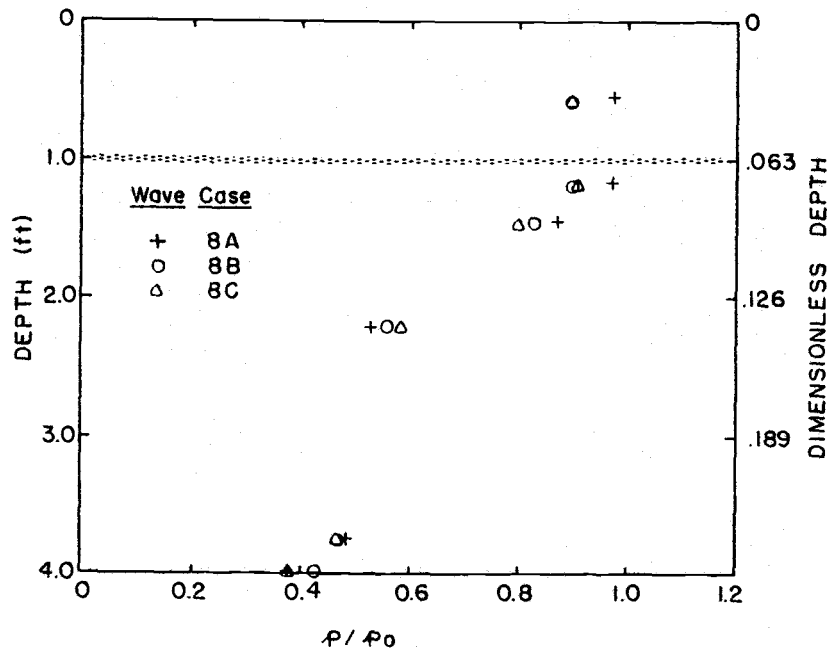


Figure 5.10. Dimensionless measured pore water pressure profiles for stream function wave cases 8A, 8B and 8C.

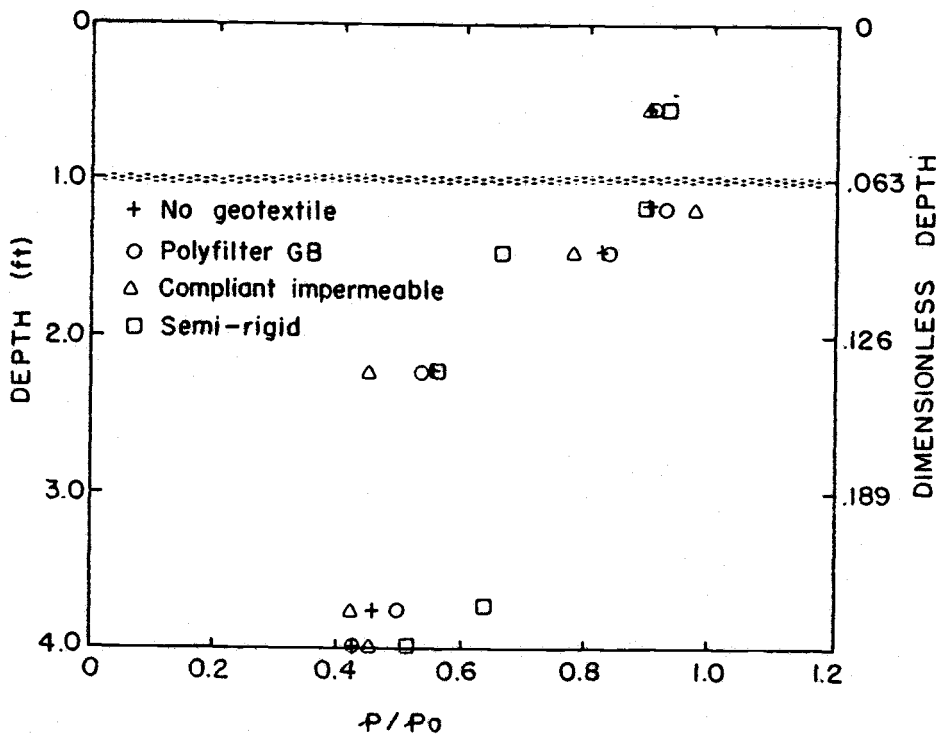


Figure 5.11. Average dimensionless measured pore water pressure profiles for stream function wave cases 8A, 8B and 8C as a function of geotextile conditions.

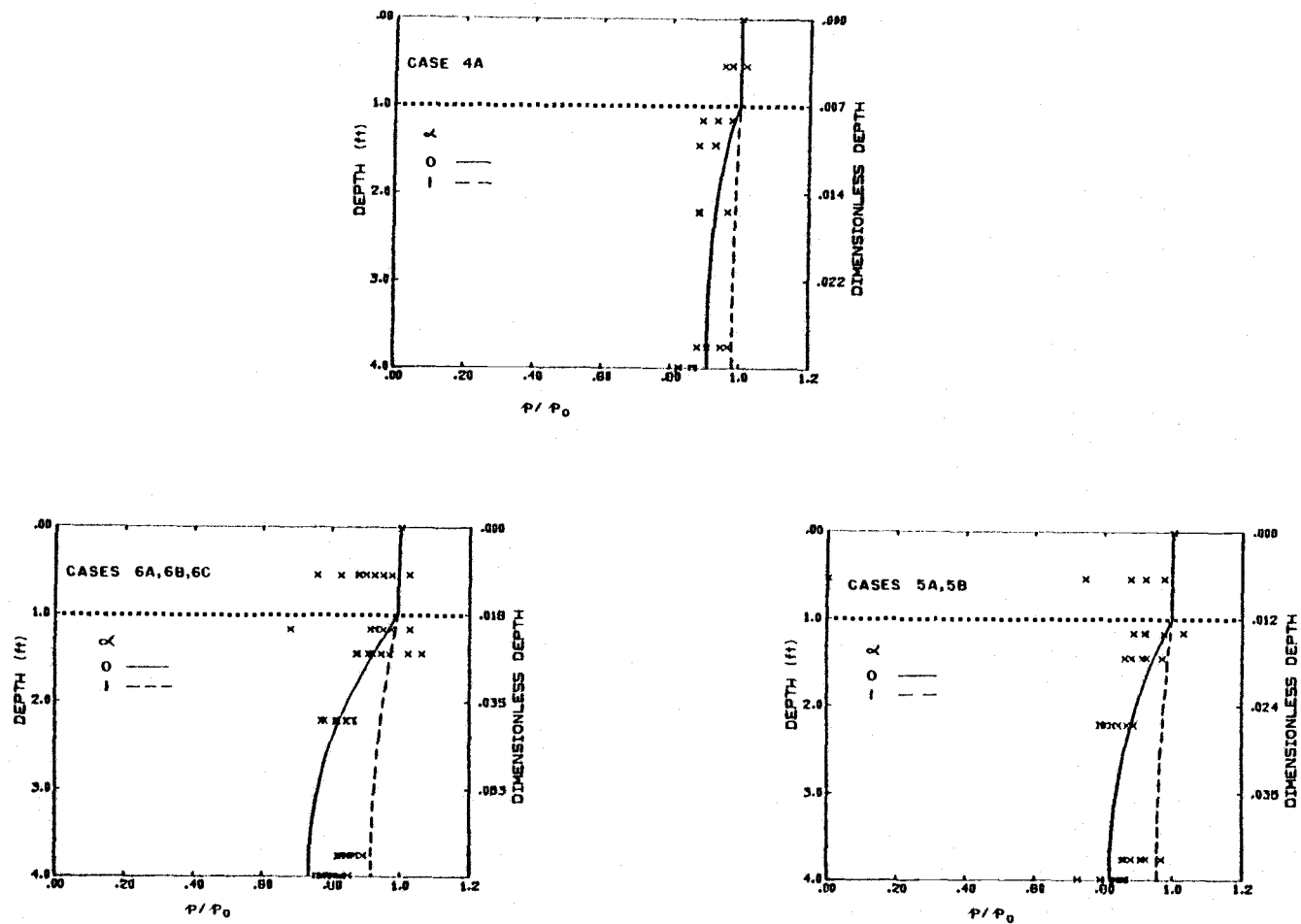


Figure 5.12. Comparison of theory and measurements for the no geotextile condition.

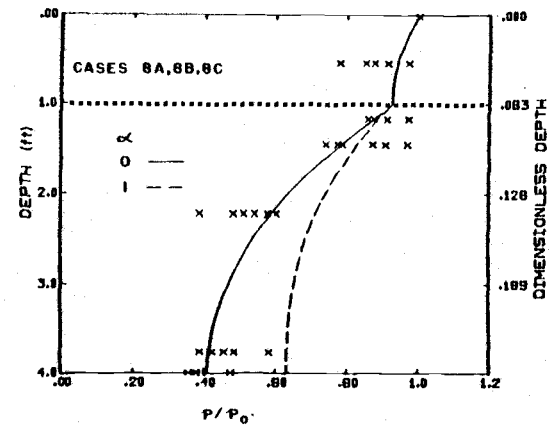
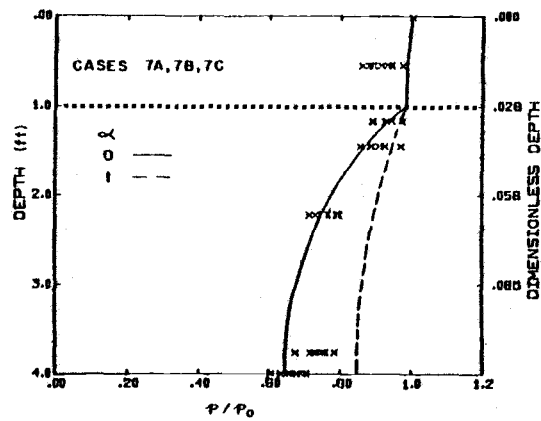


Figure 5.13. Comparison of theory and measurements for the no geotextile condition.

Theory and measurements are compared in Figures 5.14 and 5.15 for the Polyfilter GB geotextile. Again the agreement is good. The lack of dependency of the pore water pressure profiles on the geotextile properties (see Figure 5.11) is also revealed by the analytic solution. Most commercially available geotextiles are relatively permeable and do not induce a pressure drop. Geotextile elasticity is generally low so little resistance to displacement is developed. Finally, fabrics are usually placed rather loosely so that there is no tension. This leads to the conclusion that most geotextiles will appear to be transparent having little or no influence on the cyclic soil response, other than maintaining the interface between the soil layers.

The permittivity of a geotextile may be measured in the laboratory by inducing a cyclic pressure differential across the fabric and measuring the gradients and head loss. Such a test for the compliant impermeable geotextile indicated a permittivity much more transparent to the transmission of pressure than would have been anticipated based on the permeability. The apparent permeability is due to the dynamic deflection of the loose membrane and is approximately equal to 10^{-4} ft/s. Employing this result, the theory and measurements are compared in Figures 5.16 and 5.17 for the impermeable geotextile.

The fourth geotextile tested was an impermeable semi-rigid condition imposed by sandwiching a plastic sheet between two layers of quarter-inch plyboard. Theory and measurements are compared in Figures 5.18 and 5.19. As anticipated from the discussion of geotextile mechanical properties in Chapter 4, the geotextile stiffness has little influence on the pore water pressure profiles. The elasticity and effective permeability were taken as 10^4 lb/ft² and 10^{-4} ft/s, respectively.

The preceding comparisons of theory and measurements are based on the 1980 experiments. The pore pressure responses in the 1981 experiments were very similar, except that the gravel upper layer was only five inches thick rather than one foot as in the 1980 experiments. The influence of a reduced armor layer overburden is shown in Figure 5.20 for approximately the experimental conditions and a case 7B wave. The maximum displacements and shear stress are also a function of the armor

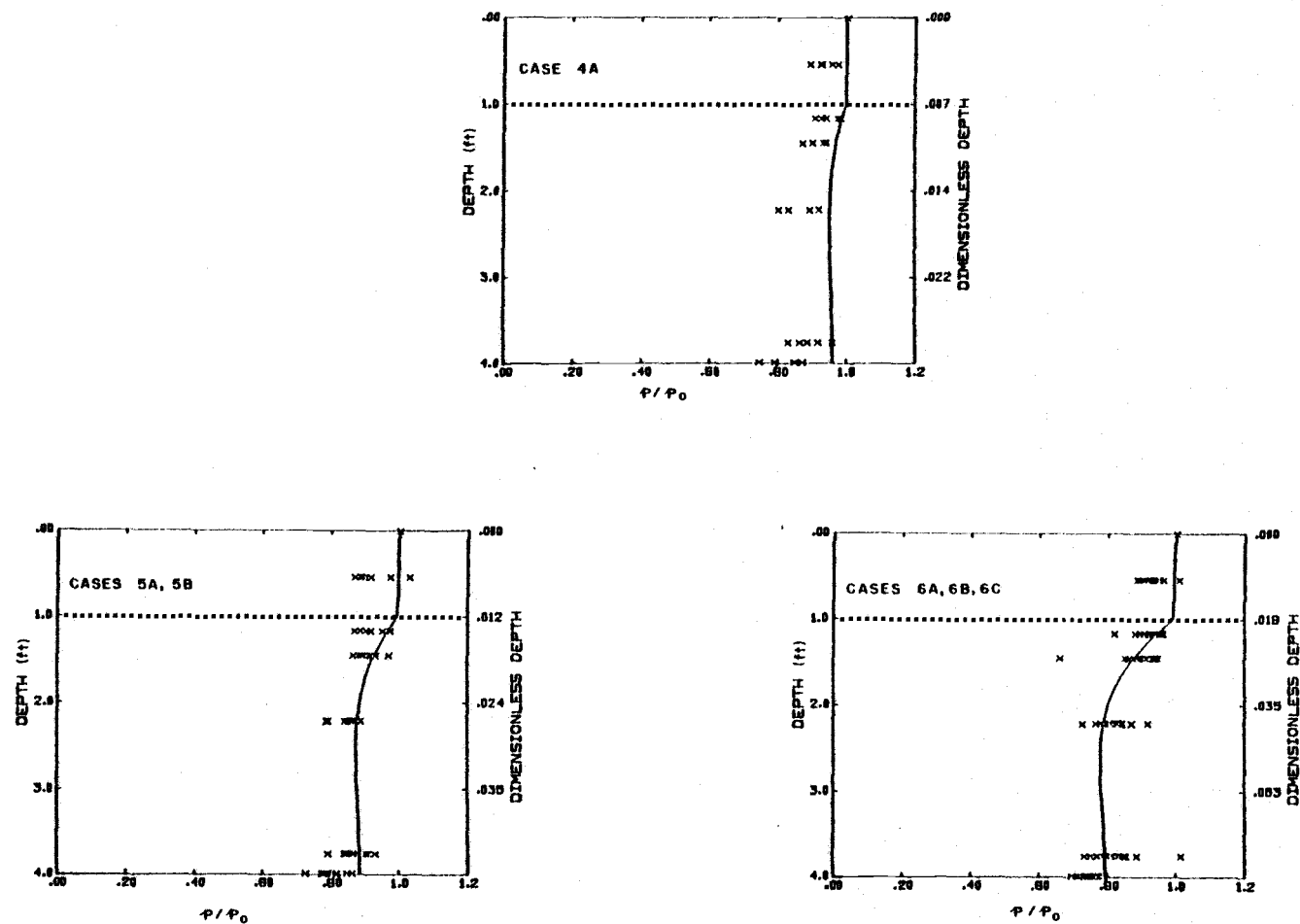


Figure 5.14. Comparison of theory and measurements for Polyfilter GB geotextile.

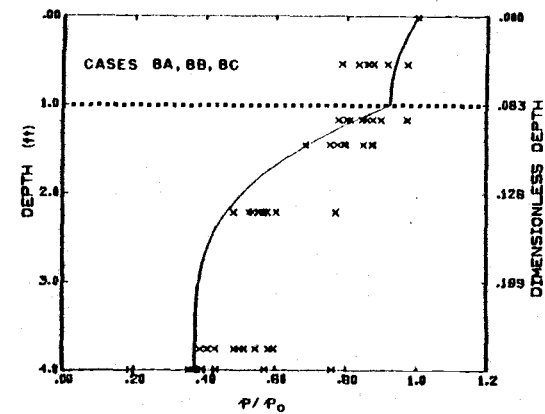
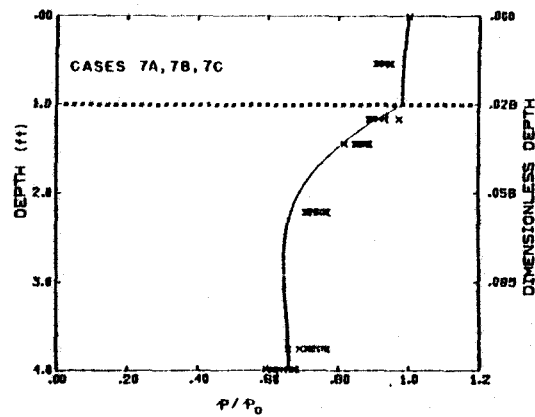


Figure 5.15. Comparison of theory and measurements for Polyfilter GB geotextile.

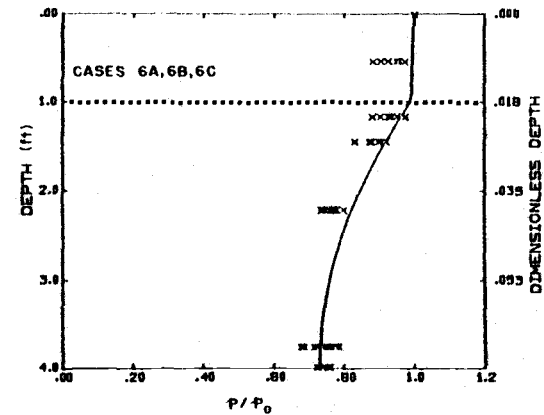
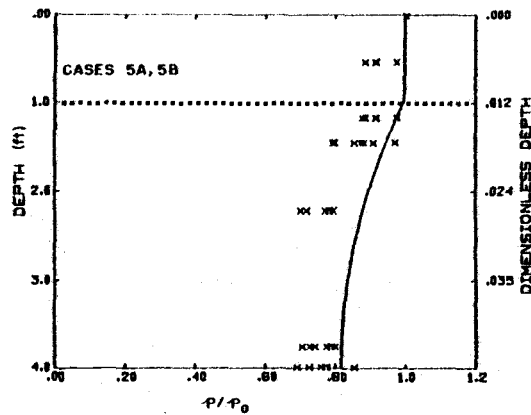
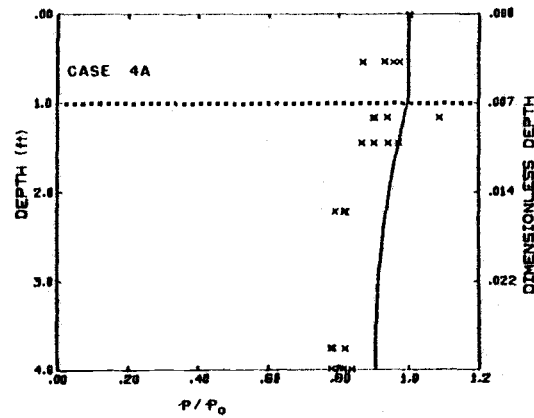


Figure 5.16. Comparison of theory and measurements for the compliant impermeable geotextile.

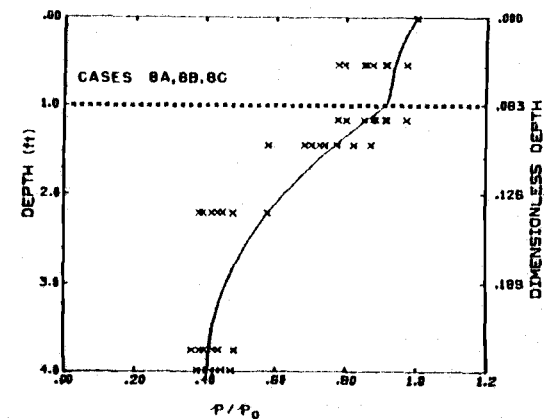
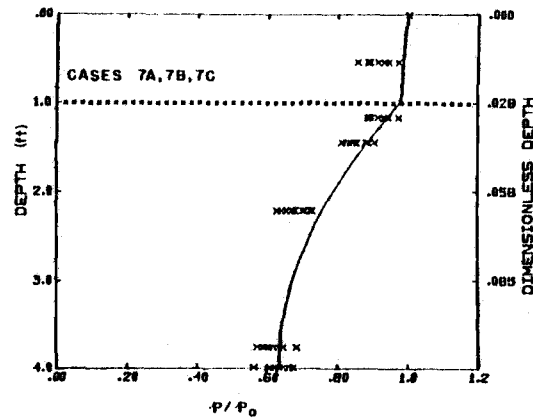


Figure 5.17. Comparison of theory and measurements for the compliant impermeable geotextile.

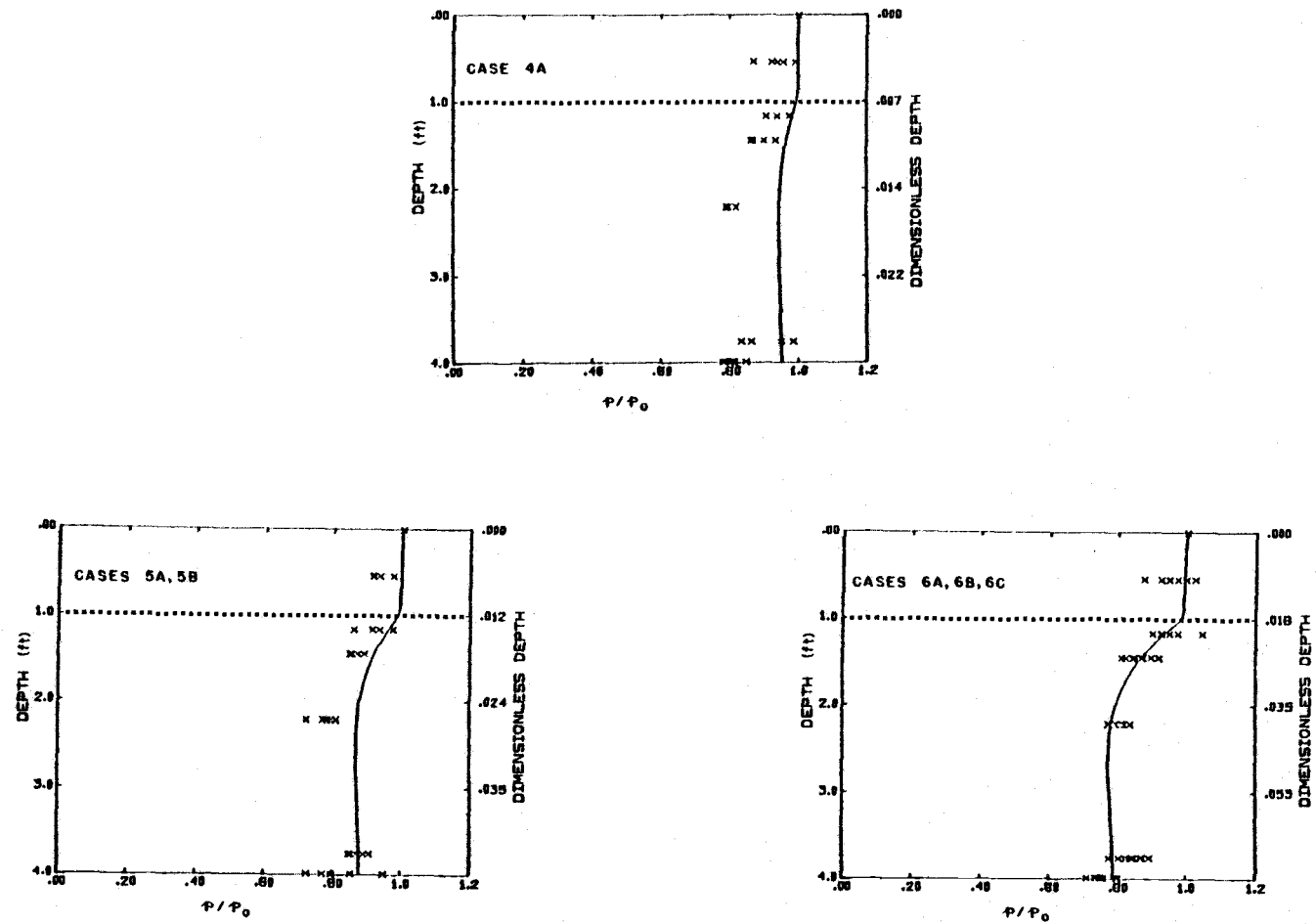


Figure 5.18. Comparison of theory and measurements for the semi-rigid geotextile.

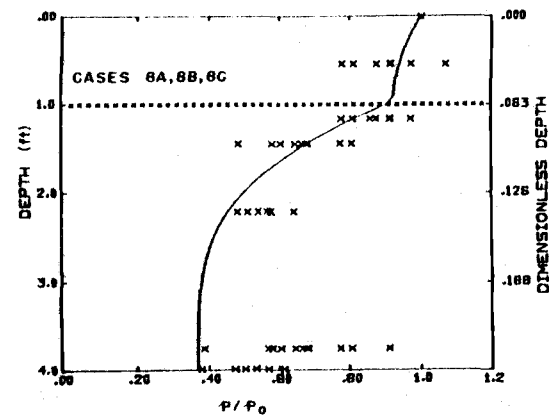
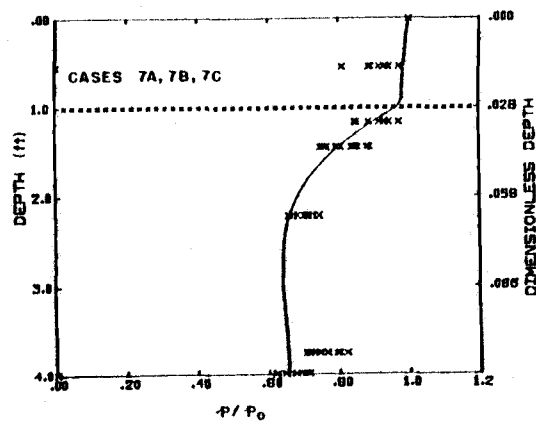


Figure 5.19. Comparison of theory and measurements for the semi-rigid geotextile.

thickness as shown in Figure 4.21. For these wave and soil conditions a maximum failure potential (as discussed in Chapter 4 and depicted in Figure 4.3) occurs at an armor thickness of approximately two feet.

5.4 Wave-Induced Failure

There were two potential modes of soil failure: momentary failure associated with the cyclic stresses and complete failure associated with the accumulation of pore water pressure. In the 1980 series of experiments neither type of failure was observed. In this series of experiments the change in pressure amplitude in one hour of testing was less than 0.1% of the initial values for eight time series measurements. This change is less than the experimental error. The 1981 experiments were designed to monitor both the mean accumulation of pressure and the dynamic response. There was a general tendency for both the cyclic pore pressure amplitude and the mean pressure to decrease with time. Decreases in amplitude ranged from 0.2% to 4.5% of the initial value in 100 waves for the different tests. The mean pore water pressure decreased from 0.0% to 1.7%. Again, this represents a relatively small change but suggests that cyclic stressing associated with waves may slowly consolidate the soil and increase the stability. An exception to this general trend was observed for an impermeable geotextile. In this run complete failure occurred. The mean pore pressure rapidly accumulated during the first several stress cycles until the effective stress went to zero (see Figure 5.22). The response of the liquefied soil was similar to a dense viscous liquid. This response continued until there was a structural failure associated with the geotextile and the excess pore pressure was released. The geotextile is shown in place before and after this run in Figures 5.23 and 5.24. The settlement at the geotextile boundaries was approximately eight inches and occurred immediately upon the release of the pore water pressure.

Although this type of failure was observed only once, it does document wave-induced liquefaction. Complete soil failure due to liquefaction should therefore be anticipated in the field, but is like-

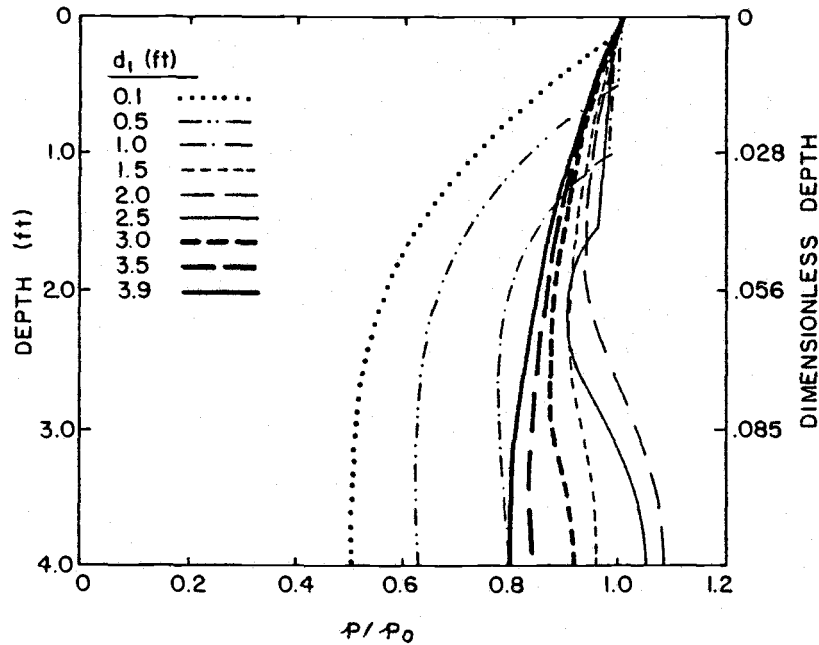


Figure 5.20. Pore water pressure profiles as a function of the armor layer thickness for approximately the experimental conditions and wave case 7B.

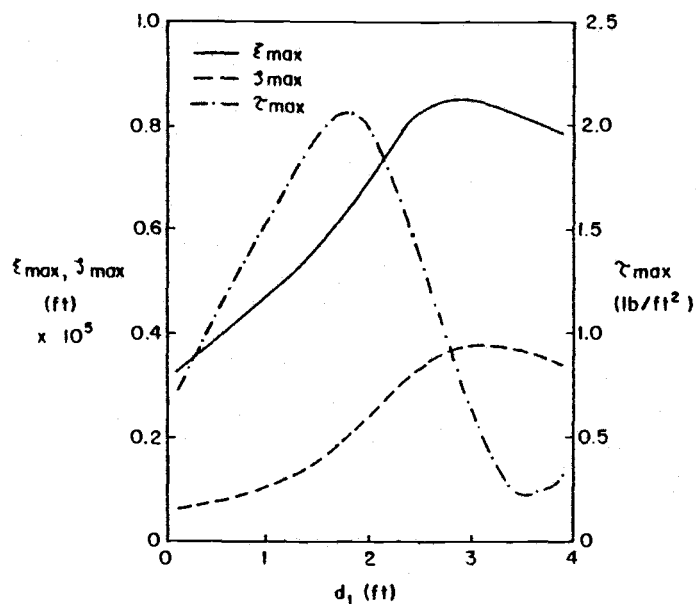


Figure 5.21. Maximum displacements and shear stress as a function of the armor layer thickness for approximately the experimental conditions and wave case 7B.

ly to occur infrequently. A more common failure is associated with the presence of a structure. For such foundation failures, the soil does not need to completely liquefy, only experience a decrease in strength. Several failures of this type were identified in Chapter 1.

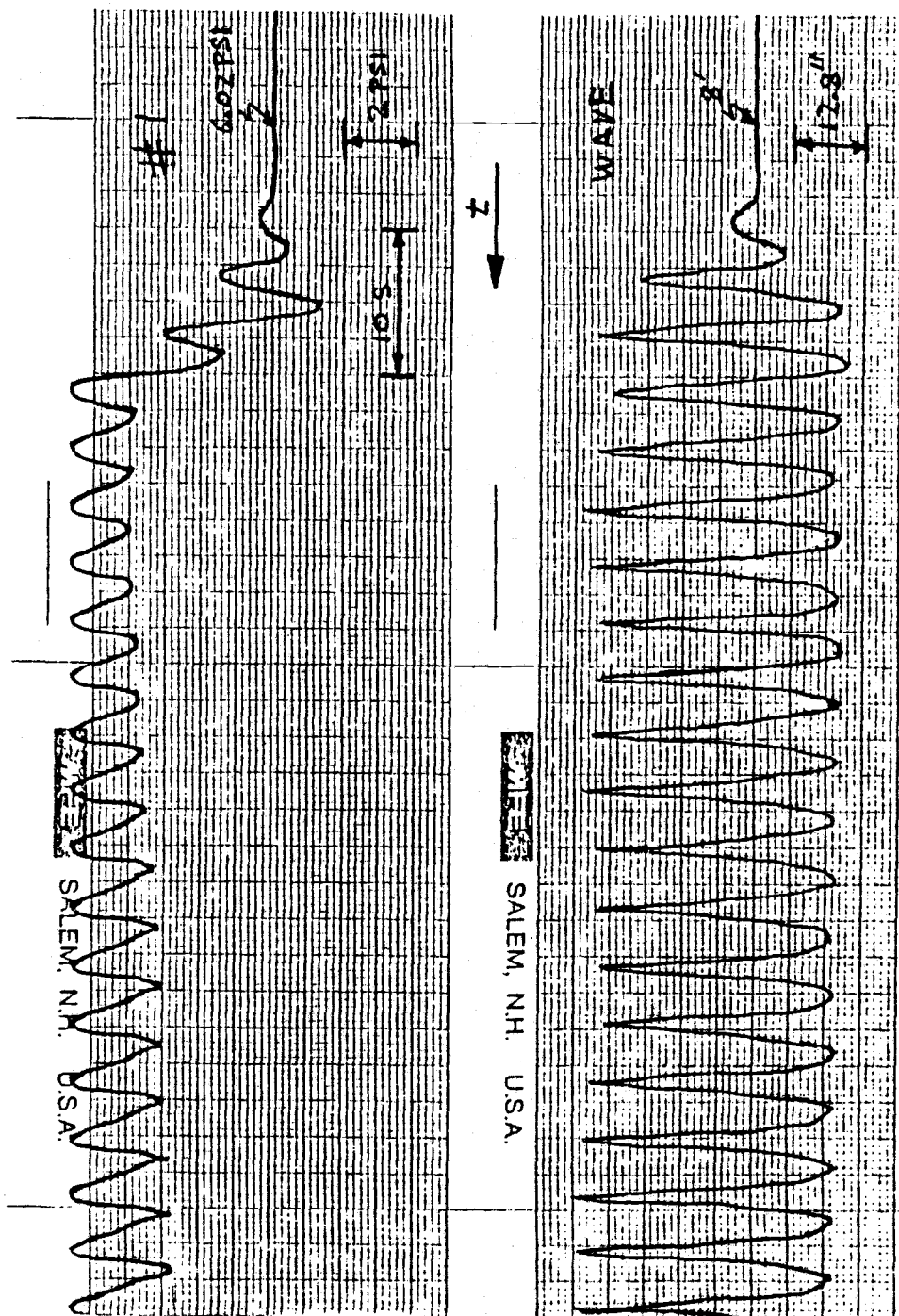


Figure 5.22 Laboratory measurements of wave-induced liquefaction.



Figure 5.23. Geotextile before failure.



Figure 5.24. Geotextile after failure.

6.0 CONCLUSIONS

6.1 Summary

An analytical model is developed to quantify the response of a horizontal, three-layered soil-geotextile-soil system to wave excitation. The theory is based on the Biot consolidation equations in which each soil layer is modeled as a homogeneous, isotropic, linearly elastic medium. The fluid flow in the interstices of the soil is described by an unsteady, compressible fluid form of Darcy's equation. The two soils are coupled through the geotextile which acts as an elastic permeable membrane. A general solution is obtained to the differential equations by seeking solutions with a simple harmonic dependence in time and in the direction of surface wave propagation. The solution is given as a 12×12 complex matrix which is solved numerically.

It is also shown that two other common methods for modeling wave-soil interaction, the potential pressure model and the earthquake consolidation equation, are simplifications of the Biot model. These models provide insight into the response of marine soils to ocean waves. The earthquake consolidation equation yields information on the mean accumulation of pore water pressure not revealed by the periodic Biot equation solution.

An examination of the Biot solution behavior indicates that:

- 1) the most important soil property is the permeability,
- 2) the pore water pressure profiles are very sensitive to the degree of saturation,
- 3) the soil response is frequency selective,
- 4) soil stability may be slightly increased by pretensioning the geotextile.

Two series of laboratory experiments were conducted at the Oregon State University Wave Research Facility. In both cases the pore water

pressure was monitored in the soil and recorded as a function of time. These data, which are among the first to be taken in a large wave facility, are used to verify the theoretical model. A second result of the experiments is the documentation of a wave-induced liquefaction failure. Some investigators have expressed doubt about the actual occurrence of such failures.

6.2 Applications

The theoretical description of the combined soil-geotextile response to waves provides the basis for rational design procedures and geotextile selection. A fundamental consideration in the selection of a geotextile is the influence of the fabric hydraulic and mechanical properties on the dynamic response of the soil. In general, for commercially available geotextiles, this influence is very small. The fabric appears to be transparent; its main function being separation of the two soil layers. Exceptions to this are:

- 1) When the geotextile becomes clogged with soil particles and the permeability is significantly reduced. This results in an undrained boundary condition which is much more susceptible to a liquefaction type failure due to the mean accumulation of pore water pressure.
- 2) When the geotextile is pretensioned. For the wave and soil conditions examined in Chapter 4, a pretensioning of approximately 100 lb/ft resulted in a 30% reduction in maximum shear stresses.

The theoretical model also predicts the dynamic response as a function of the soil properties. Results indicate that the relative permeability of the two soil layers is important. For a given design condition, a worst combination of geologic materials exists in terms of potential soil failure. The model may be used to select the optimum armor layer thickness for a given set of material properties. The soil-geotextile model may be used to model the response of a single homogeneous soil layer or a vertically inhomogeneous deposit, the vertical

inhomogeneities being approximated by homogeneous horizontal layers.

6.3 Future Research

The development and verification of the wave-soil-geotextile interaction model provides the theoretical foundation for the analysis of a number of other wave-soil interaction problems. Among these are:

- 1) The response of marine soils to random waves. The Biot consolidation equations are linear. Therefore, the solutions for the soil response at each frequency in the wave spectrum may be superimposed to yield the total response.
- 2) Soil stability on sloping beaches or structures. The down slope component of the weight tends to reduce the stability of the soil or armor. Mathematically, this is a difficult physical system to analyze because the coordinate system is not separable. However, several options are available. A solution may be sought by expanding the equations in terms of a small slope parameter or slope dependent soil parameters may be developed (e.g., a reduced sediment density).
- 3) Influence of standing waves. Standing waves frequently occur near large structures such as breakwaters and jetties, near beaches and in a wave tank. For a perfect standing wave, stationary regions with large soil responses would be associated with the antinodes of the standing waves. These areas may require additional protection due to the locally large erosive and soil destabilizing forces. Again, because the Biot equations are linear, superposition of two progressive waves may be used to model a standing wave.
- 4) Mean accumulation of pore water pressure. The solution developed to the Biot equations is strictly periodic in time while the solution to the earthquake consolidation equation provides no information on the dynamic response. A coupling of these two models would provide a more complete description of the wave-soil interaction process.

The periodic solution oscillates around the mean drift solution. The coupling is accomplished in the evaluation of the failure indicators, the shear stress ratio and the shear stress angle.

- 5) Buried pipe stability. Buoyant buried pipe lines may float to the surface during periods of reduced soil strength associated with periods of high wave activity. For small diameter pipes, the presence of the pipe may have a minor influence on the stress field. However, for larger diameter pipes, soil-structure interaction must be considered. A geotextile may reduce the failure potential by acting as a membrane in tension holding the pipeline down.
- 6) Wave-soil-structure interaction. The presence of a structure changes the wave field, possibly producing a standing wave as discussed above. A more accurate description of the fluid motion and resulting pressure distribution on the bottom may be obtained by solving the wave-structure interaction problem. The resulting bottom pressure is periodic in time but not space. Again, because the Biot equations are linear, the pressure distribution may be represented as a Fourier series, a solution obtained for each spatial frequency component and the complete solution obtained through superposition.

REFERENCES

- Agerschon, H.A., (1961), Synthetic material filters in coastal protection, J. Water and Harb. Div., ASCE, 87:111-123.
- Al-Hussaini, M.M. and L.D. Johnson, (1977), Finite Element Analysis of a Reinforced Earth Wall, Tech. Rept. S-77-6, U.S. Army Engineer Waterways Experiment Station, Vicksburg, Miss., 127 pp.
- Barrett, R.J., (1963), The Benefits of Flexible Protection in the Prevention of Beach Erosion and the Encouragement of Possible Land Restoration, Erosion Control Division, Carthage Mills, Cincinnati, Ohio, 15 pp.
- Barrett, R.J., (1966), Use of plastic filters in coastal structures, Proc. Coastal Engr. Conf., 1048-1068.
- Barvashov, V.A. and V.G. Fedorovsky, (1977), Analysis of stress and strain in multi-layered soil foundations reinforced with synthetic fabrics or films, Proc. Intr. Conf. Use Fabrics in Geotechnics, 1:95-98.
- Bea, R.G., S.G. Wright, P. Sincar and A.W. Niedoroda, (1980), Wave-induced slides in South Pass Block 70, Mississippi Delta, ASCE Spring Convention, preprint, 23 pp.
- Bell, J.R., D.R. Greenway and W. Vischer, (1977), Construction and analysis of a fabric reinforced low embankment, Proc. Intr. Conf. Use Fabrics in Geotechnics, 1:71-76.
- Bell, J.R. and R.G. Hicks, (1980), Evaluation of Test Methods and Use Criteria for Geotechnical Fabrics in Highway Applications, Federal Highway Administration Rept. No. FHWA/RD-80/021, 190 pp.
- Bennet, R. and J. Faris, (1979), Ambient and dynamic pore pressures in fine-grained submarine sediments in Mississippi Delta, Appl. Ocean Res., 1:115-123.
- Biot, M.A., (1941), General theory of three-dimensional consolidation, J. Appl. Phys., 12:155-165.
- Biot, M.A., (1956a), Theory of propagation of elastic waves in a fluid-saturated solid, part I, low-frequency range, J. Acoust. Soc. Am., 28:168-178.
- Biot, M.A., (1956b), Theory of propagation of elastic waves in a fluid-saturated solid, part II, higher frequency range, J. Acoust. Soc. Am., 28:179-191.

- Broms, B.B., (1977), Polyester fabric as reinforcement in soil, Proc. Intr. Conf. Use Fabrics in Geotechnics, 3:129-133.
- Case, K.M. and W.C. Parkinson, (1957), Damping of surface waves in an incompressible liquid, J. Fluid Mech., 2:172-184.
- Creager, W.P., J.D. Justin and J. Hinds, (1955), Engineering for Dams, John Wiley and Sons, Inc., New York, 929 pp.
- Crowell, W.C., (1963), Checkerboard seawall saves beaches, Public Works, 94:110-111.
- Dalrymple, R.A., (1974), Damping of water waves over porous bed, discussion, J. Hyd. Div., ASCE, 100:1725-1728.
- Dalrymple, R.A. and P. L-F Liu, (1978), Waves over soft muds: a two layer fluid model, J. of Phys. Ocean., 8:1121-1131.
- Dalrymple, R.A. and P. L-F Liu (1979), Gravity waves over a poroelastic seabed. In review.
- Dawson, T.H., (1978), Wave propagation over a deformable sea floor, Ocean Engr., 5:227-234.
- Dawson, T.H., J.N. Shuyada and J.M. Coleman, (1981), Correlation of field measurements with elastic theory of sea floor response to surface waves, Proc. Offshore Tech. Conf., 201-210.
- Dean, R.G., (1974), Evaluation and Development of Water Wave Theories for Engineering Application, Vol. I Special Rept. No. 1, U.S. Army Corps of Engineers, Coastal Engineering Research Center, 121 pp.
- DeAlba, P., H.B. Seed and C.K. Chan, (1976), Sand liquefaction in large-scale simple shear tests, J. of the Geotech. Div., ASCE, 102:909-928.
- DeMent, L.E., (1978), Two New Methods of Erosion Protection for Louisiana, U.S. Army District, New Orleans, 11 pp.
- Dunham, J.W. and R.J. Barrett, (1974), Woven plastic cloth filters for stone seawalls, J. WHCE Div., ASCE, 100:13-22.
- Finn, W.D.L., P.L. Bransby and D.J. Pickering (1970), Effects of strain history on liquefaction of sand, J. of the Soil Mech. and Found. Div., ASCE, 96:1917-1934.
- Finn, W.D.L., K.W. Lee and G.R. Martin, (1977), An effective stress model for liquefaction, J. of the Geotech. Div., ASCE, 103:517-533.
- Finn, W.D.L., R. Siddharthan and G.R. Martin, (1980), Wave induced instability in ocean floor sands, ASCE Fall Convention, preprint, 15 pp.

- Gade, H.G., (1958), Effects of a non-rigid, impermeable bottom on plane surface waves in shallow water, J. of Marine Res., 16:61-82.
- Hannoura, A.A. and J.A. McCorquadale, (1978), Virtual mass of coarse granular media, J. of WPCO Div., ASCE, 104:191-200.
- Heerten, G., (1981), Long-term experience with the use of synthetic filter fabrics in coastal engineering, Proc. Offshore Tech. Conf., 2174-2193.
- Henkel, D.J., (1970), The role of waves in causing submarine landslides, Geotechnique, 20:75-80.
- Hildebrand, F.B., 1962, Advanced Calculus for Applications, Prentice Hall, New Jersey, 646 pp.
- Hunt, J.N., (1952), Viscous damping of waves over an inclined bed in a channel of finite width, Houille Blanche, 6:836-842.
- Hunt, J.N., (1959), On the damping of gravity waves propagated over a permeable surface, J. Marine Res., 16:61-82.
- Hunt, J.N., (1964), The viscous damping of gravity waves in shallow water, Houille Blanche, 6:685-691.
- Hsiao, S.V. and O.H. Shemdin, (1980), Interaction of ocean waves with a soft bottom, J. of Phys. Ocean, 10:605-610.
- Ippen, A.T., (1966), Estuary and Coastline Hydrodynamics, McGraw-Hill, New York, 744 pp.
- Isaacson, M.Q., (1977), Second approximation to gravity wave attenuation, J. WHCE Div., ASCE, 103:43-55.
- Jessberger, H.L., (1977), Load-bearing behavior of a gravel subbase-nonwoven fabric - soft subgrade system, Proc. Intr. Conf. Use Fabrics in Geotechnics, 1:9-14.
- Johns, B., (1968), A boundary layer method for the determination of the viscous damping of small amplitude gravity waves, Quart. J. Mech. Appl. Math., 21:93-103.
- Jumikis, A.R., (1969), Theoretical Soil Mechanics, Van Nostrand Reinhold Co., N.Y., 432 pp.
- Kamphuis, J.W., (1978), Attenuation of gravity waves by bottom friction, Coastal Engng., 2:111-118.
- Lamb, J., (1932), Hydrodynamics, Dover Publications, New York, 738 pp.
- Lee, T.T., (1972), Design of filter system for rubble mound structures, Proc. Ocean Engr. Conf., 1917-1924.

- Liu, P. L-F, (1973), Damping of water waves over a porous bed, J. Hyd. Div., ASCE, 99:2263-2271.
- Lorentz, H.A., (1926), Report of the State Committee Zuidersee, 1918-1926, (Dutch Text), Den Haag, La Houille Blanche, 148-179.
- McClain, C.R., N.E. Huang and L.J. Pietrafesa (1977), Application of a radiation-type boundary condition to the wave, porous bed problem, J. Phys. Ocean., 7:823-835.
- MacPherson, H., (1980), The attenuation of waves over a non-rigid bed, J. Fluid Mech., 97:721-742.
- Madsen, O.S., (1978), Wave-induced pore pressures and effective stresses in a porous bed, Geotechnique, 28:377-393.
- Mallard, W.W. and R.A. Dalrymple, (1977), Water waves propagating over a deformable bottom, Proc. Offshore Tech. Conf., 141-146.
- Massel, S.R., (1976), Gravity waves propagated over a permeable bottom, J. WHCE Div., ASCE, 102:111-121.
- Mei, C.C. and M.A. Foda, (1979), Wave-induced responses in a fluid-filled poro-elastic solid with a free surface - a boundary layer theory. In review.
- Mei, C.C. and P. L-F Liu, (1973), The damping of surface gravity waves in a bounded liquid, J. Fluid Mech., 59:239-256.
- Moshagen, H. and A. Torum, (1975), Wave induced wave pressures in seabeds, J. WHCE Div., ASCE, 101:49-57.
- Murray, J.D., (1965), Viscous damping of gravity waves over a permeable bed, J. Geophys. Res., 70:2325-2331.
- Nakamura, H., R. Onishi and H. Minamide, (1973), On the seepage in the seabed due to waves, Proc. Coastal Engr. Conf., 421-428.
- Nath, J.H., J.L. Washburn, T. Dibble, R.T. Hudspeth, M. Hoening, D. Ladd, C.K. Sollitt, W.L. Schroeder, T. Yamamoto and L.S. Slotta, (1977), Pressure in Sand from Waves and Caisson Motion, Wave Res. Fac., T.R. 1, Oregon State Univ., 266 pp.
- Nieuwenhuis, J.D., (1977), Membranes and the bearing capacity of road bases, Proc. Intr. Conf. Use Fabrics in Geotechnics, 1:3-8.
- Prevost, J.H., O. Eide and K.H. Anderson, (1975), Discussion on wave induced pressures in permeable seabeds, by Moshagen and Torum, (1975), J. WHCE Div. ASCE, 101:464-465.

- Puri, K.K., (1980), Damping of gravity waves over a porous bed, J. Hyd. Div., ASCE, 106:303-312.
- Putnam, J.A., (1949), Loss of wave energy due to percolation in a permeable sea bottom, Trans. Am. Geophys. Un., 30:349-356.
- Putnam, J.A. and J.W. Johnson, (1949), The dissipation of wave energy by bottom friction, Trans. Am. Geophys. Un., 30:67-74.
- Rahman, M.S., H.B. Seed and J.R. Booker, (1977), Pore pressure development under offshore gravity structures, J. Geotech. Div., ASCE, 103:1419-1436.
- Reid, R.D. and K. Kajiura, (1957), On the damping of gravity waves over a permeable sea bed, Trans. Am. Geophys. Un., 38:662-666.
- Rousseau, D.P., (1981), Wave damping Over Poro-Elastic Ocean Beds, Masters Project, Dept. of Civil Engr., Oregon State Univ., 72 pp.
- Seed, H.B. and K.L. Lee, (1966), Liquefaction of saturated sands during cyclic loading, J. of the Soil Mech. and Found. Div., ASCE, 92:105-134.
- Seed, H.B. and I.M. Idriss (1967), Analysis of soil liquefaction: Nigata earthquake, J. of Soil Mech. and Found. Div., ASCE, 93:83-108.
- Seed, H.B., P.P. Martin and J. Lysmer, (1975), The Generation and Dissipation of Pore Water Pressures During Soil Liquefaction. Rept. No. EERC 75-26, College of Engr., Univ. of Calif., Berkeley, 27 pp.
- Seed, H.B., P.P. Martin and J. Lysmer, (1976), Porewater pressure changes during soil liquefaction, J. Geotech. Div., ASCE, 102:323-346.
- Seed, H.B., R.M. Pyke and G.R. Martin, (1978), Effect of multi-directional shaking on pore pressure development in sands, J. of the Geotech. Div., ASCE, 104:27-44.
- Seed, H.B. and M.S. Rahman, (1978), Wave-induced pore pressure in relation to ocean floor stability of cohesionless soils, Marine Geotech., 3:123-150.
- Sleath, F.A., (1970), Wave-induced pressures in beds of sand, J. Hyd. Div., ASCE, 96:367-378.
- Sollitt, C.K. and R.H. Cross, (1972), Wave transmission through permeable breakwaters, Proc. of 13th ICCE, ASCE, 1827-1846.

- Terzaghi, K. and R.B. Peck, (1967), Soil Mechanics in Engineering Practice, John Wiley and Sons, Inc., New York, 729 pp.
- Thielen, D.L., (1981), Masters Thesis, Oregon State Univ. In progress.
- Transportation Research Circular, (1978), Engineering Fabrics, a Literature Review (1978), Transportation Research Circular, No. 204, 15 pp.
- Treloar, P.D. and A. Brebner, (1970), Energy losses under wave action, Proc. Coastal Engr. Conf., 257-267.
- Van Dorn, W.G., (1966), Boundary dissipation of oscillatory waves, J. Fluid Mech., 24:769-779.
- Verruijt, A., (1969), Elastic storage of aquifers in Flow Through Porous Media, J.M. DeWiest, ed., Academic Press, New York, 331-376.
- Welsh, J.P. and R.M. Koerner, (1979), Innovative uses of synthetic fabrics in coastal construction, Proc. ASCE Spec. Conf., Coastal Structures, 364-372.
- Wylie, C.R., (1975), Advanced Engineering Mathematics, McGraw-Hill, Inc., New York, 937 pp.
- Yamamoto, T., (1977), Wave-induced instability is seabed, Proc. ASCE Spec. Conf., Coastal Sediments, 898-913.
- Yamamoto, T., (1978), Sea bed instability form waves, Proc. Offshore Tech. Conf., 1819-1828.
- Yamamoto, T. and Y. Suzuki, (1980), Stability analysis of seafloor foundations, Proc. Coastal Engr. Conf., 1799-1818.
- Yamamoto, T., (1981a), Wave-induced pore pressures and effective stresses in inhomogeneous seabed foundations, Ocean Engng., 8:1-16.
- Yamamoto, T., (1981b), Ocean wave spectrum transformations due to sea-seabed interactions, Proc. Offshore Tech. Conf., 249-258.
- Yamamoto, T., H. Koning, H. Sellmeijer and E. Van Hijum, (1978), On the response of a poroelastic bed to water waves, J. Fluid Mech., 78:193-206.

APPENDIX A

List of Notations

$a_n; n=1,12$	horizontal displacement integration constants
$A1, A2, A3$	Biot solution constants in soil layer 1
$b_n; n=1,12$	vertical displacement integration constants
$B1, B2, B3$	Biot solution constants in soil layer 2
c	coefficient of consolidation
$c_n; n=1,12$	pressure integration constants
C_D	drag coefficient
C_f	friction coefficient
C_ϵ	permittivity
C_m	inertial coefficient
d, d_1, d_2	soil layer thicknesses
\bar{d}	total thickness of both layers
e_x, e_y, e_z	normal strains
E	Young's modulus
g	acceleration due to gravity
G	shear modulus
h	water depth
H	wave height
i	square root of -1
K	unsteady permeability
K_f	geotextile permeability
K_s	geotextile elasticity
K_w	bulk modulus of pure water

Appendix A (continued)

\hat{K}	steady permeability
ℓ	length of test section
L	wave length
n	porosity
N	number of cyclic loadings
N_L	number of cyclic loadings to liquefaction
p	excess pore water pressure
p_g	reference pressure
\overline{p}_g	pore water pressure generation term
p_0	amplitude of dynamic wave-induced mudline pressure
p_s	hydrostatic pressure
\hat{p}	dimensionless time-averaged pressure in earthquake equation
\vec{q}	vector discharge velocity
\vec{Q}	vertical dependency of vector discharge velocity
r	shear stress ratio
r_e	relative error due to end conditions
R_1, R_2, R_3	constants in potential pressure solution
s	pressure source term
S	degree of saturation
t	time
\hat{t}	dimensionless time in earthquake equation
T	wave period
\hat{T}	geotextile tension
T	potential pressure model transfer function

Appendix A (continued)

u	horizontal discharge velocity (relative to soil)
u_0	amplitude of near bottom fluid velocity
$\vec{v}_A, \vec{v}_B, \vec{v}_C$	vector velocities of solids, liquid and gas
w	vertical discharge velocity (relative to soil)
x	coordinate in direction of wave propagation
y	coordinate along wave crest
z	vertical coordinate down from mudline
\hat{z}	dimensionless depth in earthquake equation
α	bottom slip parameter
α	pore pressure accumulation shape factor
β	liquid compressibility
β'	combined liquid-gas compressibility
γ	weight density of fluid
γ_B	buoyant weight density of soil
$\gamma_x, \gamma_y, \gamma_z$	shear strains
Δp	pressure drop across geotextile
Δz_f	geotextile thickness
ϵ	volume strain
ζ	vertical displacement of soil
κ_n	eigenvalue in potential pressure model
$\hat{\kappa}_n$	dimensionless eigenvalue in potential pressure model
λ	radian wave number
λ'	eigenvalue in Biot model
μ	geotextile displacement
ν	Poisson's ratio

Appendix A (continued)

ξ	horizontal displacement of soil
π	numerical constant (3.14159)
ρ	fluid density
ρ_A, ρ_B, ρ_C	densities of solids, liquid and gas
ρ_0, ρ_g	reference densities
$\sigma_x, \sigma_y, \sigma_z$	effective normal stresses
$\bar{\sigma}_x, \bar{\sigma}_y, \bar{\sigma}_z$	total normal stresses
σ_0'	effective overburden stress
τ	shear stress
$\bar{\tau}_{ij}$	total shear stress
τ_m	maximum shear stress
ϕ	shear stress angle
$\bar{\phi}$	geotextile mechanical property coefficient
χ	lateral displacement of soil
ψ_A, ψ_B, ψ_C	relative mass of solids, liquid and gas
ω	radian wave frequency
$D(\cdot)$	vertical gradient operator
$\nabla(\cdot)$	gradient operator
$\nabla \cdot (\cdot)$	divergence operator
∇^2	La Placian operator
$\overline{(\cdot)}$	time-averaged
$\overrightarrow{(\cdot)}$	vector
$(\cdot)_1$	soil layer 1
$(\cdot)_2$	soil layer 2
$(\cdot)_{\max}$	maximum value in vertical profile

APPENDIX B

Computer ProgramsB.1 Program GEOTEX

```

PROGRAM GEOTEX(INPUT,TAPE5=INPUT,OUTPUT,TAPE6=OUTPUT,
.DAT4,TAPE7=DATA,CPRINT,TAPE8=CPRINT,CPLOT,TAPE9=CPLOT)
C*
REAL NU1,NU2,N1,N2,K1,K2,KF,LENGTH
COMPLEX C1,C2,XLP1,XLP2,XP,XKP1,XKP2,I1,I2
COMPLEX HLL,STRECH,XDIM,DUM1,DUM2,DUM3
COMPLEX ZERO,A,E3,E4,E7,E8,E9,E10
DIMENSION IDENT(15),Z(42),F1(42),F2(42)
COMPLEX Q(12,12),F1(12),F2(12),Q3(12)
COMPLEX S(12),CHECK(12),WK(12),WA(153)
COMPLEX U(42),W(42),P(42),SIGX(42),SIGZ(42),TAU(42)
COMPLEX FVX(42),FVZ(42),STR(42),PHI(42)
COMPLEX DUDX(42),DUDZ(42),DWDY(42),DWDZ(42)
COMPLEX DPOX(42),DPOZ(42),TAUMAX(42)
COMPLEX SS(42),VS(42),FF(42)
C*
C* .....
C*
C* INPUT VARIABLES
C*
C* HEADER CARD
C*   FORMAT(15A4)
C*   IDENT(I)      - DATA FILE IDENTIFICATION
C*
C* WAVE PARAMETERS
C*   FORMAT(8G10.4)
C*   LENGTH        - WAVE LENGTH
C*   PERIOD        - WAVE PERIOD
C*   DEPTH         - WATER DEPTH
C*   HEIGHT        - WAVE HEIGHT
C*   P0            - WAVE PRESSURE AMPLITUDE
C*   R0W          - FLUID DENSITY
C*   G             - ACCELERATION DUE TO GRAVITY
C*   CF           - BOTTOM FRICTION COEFFICIENT
C*
C* SOIL PARAMETERS (1 CARD PER LAYER)
C*   FORMAT(8G10.4)
C*   C1,C2        - SHEAR MODULUS
C*   NU1,NU2      - POISSON'S RATIO
C*   N1,N2        - POROSITY
C*   SAT1,SAT2    - DEGREE OF SATURATION
C*   GAMMA1,GAMMA2 - BUCYANT WEIGHT
C*   D1,D2        - SOIL LAYER THICKNESS
C*   K1,K2        - PERMEABILITY
C*   CM1,CM2      - ADDED MASS COEFFICIENT
C*
C* GEOTEXTILE PARAMETERS
C*   FORMAT(4G10.4)
C*   GC          - GEOTEXTILE ELASTICITY
C*   TEN         - GEOTEXTILE TENSION
C*   DZF         - GEOTEXTILE THICKNESS
C*   KF          - GEOTEXTILE PERMEABILITY
C*
C* INTERNAL PARAMETERS
C*   FORMAT(1X,I1.5X,F10.7)
C*   NONDIM      - DIMENSIONAL/DIMENSIONLESS PLAT PARAMETER
C*               NONDIM=0  DIMENSIONLESS PLATE
C*               NONDIM=1  DIMENSIONAL PLATE
C*   ALP         - BOTTOM SLIP PARAMETER
C*               ALP=0     FREE SLIP

```

Appendix B (continued)

```

C*                                0<ALP<1    INTERMEDIATE
C*                                ALP=1      NO SLIP
C*
C*.....
C*
C*    INPUT DATA
C*
C*    HEADDEF CARD
C*    READ(7,50) (IDENT(I),I=1,15)
50  FORMAT(1X,15A4)
C*
C*    WAVE PARAMETERS
C*    READ(7,100) LENGTH,PERIOD,DEPTH,HEIGHT,P0,POW,G,CF
100 FORMAT(4G10.4)
C*
C*    SOIL PARAMETERS
C*    READ(7,200) G1,NU1,N1,SAT1,GAMMA1,D1,K1,CM1
200 FORMAT(4G10.4)
C*    READ(7,200) G2,NU2,N2,SAT2,GAMMA2,D2,K2,CM2
C*
C*    GEOTEXTILE PARAMETERS
C*    READ(7,400) GF,TEN,DZF,KF
400 FORMAT(4G10.4)
C*
C*    INTERNAL PARAMETERS
C*    READ(7,450) NONDIR,ALP
450 FORMAT(1X,I1,5X,F10.7)
C*
C*.....
C*
C*    PRINT INPUT DATA
C*
C*    WRITE(8,480)
480  FORMAT(1H1///)
C*    WRITE(8,520)
C*    WRITE(8,510)
C*    WRITE(8,500)
500  FORMAT(10X,"* SOIL-GEOTEXTILE INTERACTION MODEL *")
C*    WRITE(8,510)
510  FORMAT(10X,"*-",35X,"*")
C*    WRITE(8,520)
520  FORMAT(10X,37(" "))
C*    WRITE(8,550) (IDENT(I),I=1,15)
550  FORMAT(/5X,"IDENTIFICATION: ",15A4//)
C*    WRITE(8,600)
600  FORMAT(5X,"WAVE PARAMETERS"/)
C*    WRITE(8,700) LENGTH,PERIOD,DEPTH,HEIGHT,P0,POW,G,CF
700  FORMAT(10X,"LENGTH",16X,G15.4/10X,"PERIOD",16X,G15.4/
.10X,"WAVE DEPTH",11X,G15.4/10X,"WAVE HEIGHT",11X,G15.4/
.10X,"PRESSURE AMPLITUDE",4X,G15.4/
.10X,"FLUID DENSITY",9X,G15.4/10X,"GRAVITY",
.15X,G15.4/10X,"BOTTOM FRICTION",7X,G15.4//)
C*    WRITE(8,800)
800  FORMAT(5X,"SOIL PARAMETERS")
C*    WRITE(8,900)
900  FORMAT(40X,"LAYER 1",17X,"LAYER 2"/)
C*    WRITE(8,1000) G1,G2,NU1,NU2,N1,N2
1000 FORMAT(10X,"SHEAR MODULUS",3X,G15.4,5X,G15.4/
.10X,"POISSON'S RATIO",7X,G15.4,5X,G15.4/
.10X,"POROSITY",14X,G15.4,5X,G15.4)
C*    WRITE(8,1100) SAT1,SAT2,GAMMA1,GAMMA2
1100 FORMAT(10X,"DEGREE OF SATURATION",2X,G15.4,5X,G15.4/
.10X,"BUOYANT WEIGHT",4X,G15.4,5X,G15.4)
C*    WRITE(8,1200) D1,D2,K1,K2,CM1,CM2
1200 FORMAT(10X,"THICKNESSES",13X,G15.4,5X,G15.4/
.10X,"PERMEABILITY",10X,G15.4,5X,G15.4/

```

Appendix B (continued)

```

      .10X,"ADDED MASS",12X,G15.4,5X,G15.4//)
      WRITE(8,1300)
1300  FORMAT(5X,"GEOTEXTILE PARAMETERS"/)
      WRITE(8,1400)GE,TEN,DZF,KF
1400  FORMAT(10X,"ELASTICITY",12X,G15.4/
      .10X,"TENSION",15X,G15.4/
      .10X,"THICKNESS",17X,G15.4/
      .10X,"PERMEABILITY",10X,G15.4/)

C*
C* .....
C*
C*  PROGRAM VARIABLES
C*
C*      ZERO          - COMPLEX 0.0
C*      A              - SQRT(-1.0)
C*      F              - RADIAN WAVE FREQUENCY
C*      BETA1,BETA2    - FLUID COMPRESSIBILITY
C*      XKP1,XKP2      - UNSTEADY PERMEABILITY
C*      XL             - FIRST EIGENVALUE (SAME IN BOTH LAYERS
C*                      AND IS EQUAL TO THE WAVE NUMBER)
C*      XLP1,XLP2      - SECOND EIGENVALUES FOR LAYERS 1 AND 2
C*      Q(I,J)         - COEFFICIENT MATRIX
C*      S(I)           - FORCING VECTOR
C*      R1(I)          - HORIZONTAL DISPLACEMENT CONSTANTS
C*      R2(I)          - VERTICAL DISPLACEMENT CONSTANTS
C*      R3(I)          - PRESSURE CONSTANTS
C*      U(I)           - HORIZONTAL DISPLACEMENT
C*      W(I)           - VERTICAL DISPLACEMENT
C*      P(I)           - PRESSURE
C*      FVX(I)         - HORIZONTAL FLUID VELOCITY
C*      FVZ(I)         - VERTICAL FLUID VELOCITY
C*      STRECH         - MECHANICAL GEOTEXTILE PROPERTY
C*      HLL            - HEAD LOSS(DIMENSIONS OF LENGTH)
C*      U0             - NEAR BOTTOM WATER PARTICLE VELOCITY
C*
C*      PRESSURE, STRESS AND SHEAR ARE NON-
C*      DIMENSIONALIZED BY P0.
C*      DISPLACEMENTS ARE NON-DIMENSIONALIZED
C*      BY P0*LENGTH/G1.
C*      FLUID VELOCITIES ARE NON-DIMENSIONALIZED
C*      BY XKP1*P0/(LENGTH*P0W*G)
C*
C* .....
C*
C*  CONSTANTS
C*      PI=3.14159
C*      A=(0.0,1.0)
C*      ZERO=(0.0,0.0)
C*      F=2.0*PI/PERIOD
C*      U0=0.5*HEIGHT*PERIOD/(LENGTH*COSH(2.0*PI*DEPTH/LENGTH))
C*      COMP=2.1879
C*      IF(G.GT.12.0)COMP=4.55E7
C*      PATH=101330.0
C*      IF(G.GT.12.0)PATH=2116.8
C*      BETA1=1.0/COMP+(1.0-SAT1)/(P0W*G*(DEPTH*0.5*01)+PATH)
C*      BETA2=1.0/COMP+(1.0-SAT2)/(P0W*G*(DEPTH*01+0.5*02)+PATH)
C*      XKP1=1.0/(1.0/Y1-(A*F)/(G*N1)-(A*F*CM1)/(G*N1))
C*      XKP2=1.0/(1.0/Y2-(A*F)/(G*N2)-(A*F*CM2)/(G*N2))
C*
C*
C*  EIGENVALUES
C*      XL=2.0*PI/LENGTH
C*      AX=N1*BETA1*G1

```

Appendix B (continued)

```

      9X=N2*BETA2*G2
      C1=(A*ROW*G*F)/(XKP1*G1)*(AX+(1.0-2.0*NU1)/
      .(2.0-2.0*NU1))
      C2=(A*ROW*G*F)/(XKP2*G2)*(9X+(1.0-2.0*NU2)/
      .(2.0-2.0*NU2))
      XLP1=CSQRT(XL*XL-C1)
      XLP2=CSQRT(XL*XL-C2)
C*
C*  MORE CONSTANTS
      C3=1.0-NU1
      C4=1.0-2.0*NU1
      C5=1.0-NU2
      C6=1.0-2.0*NU2
      DB=D1+D2
      STRECH=-TEN*XL*XL+A*XL*GF
      IF(KF.EQ.0.0)KF=1.0E-50
      HLL=QZF*XKP2/KF
      E1=COSH(XL*D1)
      E2=TANH(XL*D1)
      E3=0.5*(CEXP(XLP1*D1)+CEXP(-XLP1*D1))
      E4=0.5*(CEXP(XLP1*D1)-CEXP(-XLP1*D1))
      E5=COSH(XL*DB)
      E6=TANH(XL*DB)
      E7=0.5*(CEXP(XLP2*D1)+CEXP(-XLP2*D1))
      E8=0.5*(CEXP(XLP2*D1)-CEXP(-XLP2*D1))
      E9=0.5*(CEXP(XLP2*DB)+CEXP(-XLP2*DB))
      E10=0.5*(CEXP(XLP2*DB)-CEXP(-XLP2*DB))
      A1=(1.0/XL)*(1.0+AX*(3.0-4.0*NU1)/C4)/(1.0+AX/C4)
      B1=(1.0/XL)*(1.0+BX*(3.0-4.0*NU2)/C6)/(1.0+BX/C6)
      A2=(2.0*G1)/(1.0+AX/C4)
      B2=(2.0*G2)/(1.0+BX/C6)
      A3=(ROW*G*F)/(XL*XKP1)*(AX+1.0)
      B3=(ROW*G*F)/(XL*XKP2)*(9X+1.0)
C*
C* .....
C*
C*  COEFFICIENT MATRIX
C*
      Q(1,1) = ZERO
      Q(1,2) = ZERO
      Q(1,3) = ZERO
      Q(1,4) = -A*A2
      Q(1,5) = -A3
      Q(1,6) = ZERO
      Q(1,7) = ZERO
      Q(1,8) = ZERO
      Q(1,9) = ZERO
      Q(1,10) = ZERO
      Q(1,11) = ZERO
      Q(1,12) = ZERO
C*
      Q(2,1) = 1.0
      Q(2,2) = ZERO
      Q(2,3) = ZERO
      Q(2,4) = C3/C4*(1.0-XL*A1)/XL
      Q(2,5) = (C3*XLP1*XLP1-NU1*XL*XL)/(XL*XL*C4)
      Q(2,6) = ZERO
      Q(2,7) = ZERO
      Q(2,8) = ZERO
      Q(2,9) = ZERO
      Q(2,10) = ZERO
      Q(2,11) = ZERO
      Q(2,12) = ZERO

```


Appendix B (continued)

```

C*
Q(3,1) = ZERO
Q(3,2) = 2.0*XL
Q(3,3) = -(XL*A1-1.0)
Q(3,4) = ZERO
Q(3,5) = ZERO
Q(3,6) = 2.0*XL*P1
Q(3,7) = ZERO
Q(3,8) = ZERO
Q(3,9) = ZERO
Q(3,10) = ZERO
Q(3,11) = ZERO
Q(3,12) = ZERO

C*
Q(4,1) = 1.0
Q(4,2) = E2
Q(4,3) = D1
Q(4,4) = D1*E2
Q(4,5) = E3/E1
Q(4,6) = E4/E1
Q(4,7) = -1.0
Q(4,8) = -E2
Q(4,9) = -D1
Q(4,10) = -D1*E2
Q(4,11) = -E7/E1
Q(4,12) = -E8/E1

C*
Q(5,1) = E2
Q(5,2) = 1.0
Q(5,3) = D1*E2-A1
Q(5,4) = -A1*E2+D1
Q(5,5) = (XLP1/XL)*E4/E1
Q(5,6) = (XLP1/XL)*E3/E1
Q(5,7) = -E2
Q(5,8) = -1.0
Q(5,9) = -D1*E2+A1
Q(5,10) = B1*E2-D1
Q(5,11) = -(XLP2/XL)*E8/E1
Q(5,12) = -(XLP2/XL)*E7/E1

C*
Q(6,1) = E2
Q(6,2) = 1.0
Q(6,3) = 1.0/(2.0*XL)-A1/2.0+D1*E2
Q(6,4) = (1.0-XL*A1)/(2.0*XL)*E2+D1
Q(6,5) = (XLP1/XL)*E4/E1
Q(6,6) = (XLP1/XL)*E3/E1
Q(6,7) = -G2/G1*E2*(1.0+XL*GE/G2)
Q(6,8) = -G2/G1*(1.0+XL*GE/G2)
Q(6,9) = -G2/G1*(1.0/(2.0*XL)-B1/2.0+D1*E2
+GE/G2*(1.0+XL*D1*E2))
Q(6,10) = -G2/G1*((1.0-XL*D1)/(2.0*XL)*E2+D1
+GE/G2*(E2+XL*D1))
Q(6,11) = -G2/G1*(XLP2/XL+XLP2*GE/G2)*E8/E1
Q(6,12) = -G2/G1*(XLP2/XL+XLP2*GE/G2)*E7/E1

C*
RT1=(1.0-N2)*G2/((1.0-N1)*G1)
RT2=2.0*XL*G1*(1.0-N1)
Q(7,1) = 1.0
Q(7,2) = E2
Q(7,3) = D1+(1.0-XL*A1)*C3/(C4*XL)*E2+N1*A2*E2/RT2
Q(7,4) = D1*E2+(1.0-XL*A1)*C3/(C4*XL)*N1*A2/RT2
Q(7,5) = ((C3*XLP1*XLP1-NU1*XL*XL)/(XL*XL*C4)*N1*A2/(A*E2))*
E3/E1

```

Appendix B (continued)

```

Q(7,6) = Q(7,5)*E4/E3
Q(7,7) = -(RT1*STRECH*E2)
Q(7,8) = -(RT1*E2+STRECH)
Q(7,9) = (RT1*(C5/(XL*C6)*(XL*B1-1.0)*E2-Q1)
      -N2*B2*E2/RT2+STRECH*(Q1-Q1*E2))
Q(7,10) = RT1*(C5/(XL*C6)*(XL*B1-1.0)-Q1*E2)
      -N2*B2/RT2+STRECH*(Q1*E2-Q1)
Q(7,11) = (RT1*NU2*XL*XL-C5*XL*P2*XL*P2)/(XL*XL*C6)
      -N2*B3/(A*RT2)*E7/E1-STRECH*XL*P2/XL*E8/E1
Q(7,12) = (RT1*(NU2*XL*XL-C5*XL*P2*XL*P2)/(XL*XL*C6)
      -N2*B3/(A*RT2))*E8/E1-STRECH*XL*P2/XL*E7/E1
C*
Q(8,1) = ZERO
Q(8,2) = ZERO
Q(8,3) = A*E2
Q(8,4) = A
Q(8,5) = A3/A2*E3/E1
Q(8,6) = A3/A2*E4/E1
Q(8,7) = ZERO
Q(8,8) = ZERO
Q(8,9) = -A*B2/A2*(E2*XL*(-HLL))
Q(8,10) = -A*B2/A2*(1.0+XL*(-HLL)*E2)
Q(8,11) = -B3/A2*(E7/E1+XL*P2*(-HLL)*E8/E1)
Q(8,12) = -B3/A2*(E8/E1+XL*P2*(-HLL)*E7/E1)
C*
Q(9,1) = ZERO
Q(9,2) = ZERO
Q(9,3) = -A
Q(9,4) = -A*E2
Q(9,5) = -A3/A2*(XLP1/XL)*E4/E1
Q(9,6) = -A3/A2*(XLP1/XL)*E3/E1
Q(9,7) = ZERO
Q(9,8) = ZERO
Q(9,9) = XKP2/XKP1*A*B2/A2
Q(9,10) = XKP2/XKP1*A*B2/A2*E2
Q(9,11) = XKP2/XKP1*B3/A2*(XLP2/XL)*E8/E1
Q(9,12) = XKP2/XKP1*B3/A2*(XLP2/XL)*E7/E1
C*
Q(10,1) = ZERO
Q(10,2) = ZERO
Q(10,3) = ZERO
Q(10,4) = ZERO
Q(10,5) = ZERO
Q(10,6) = ZERO
Q(10,7) = ALP*(1.0-ALP)*XL*Q8*E6
Q(10,8) = ALP*E6+(1.0-ALP)*XL*Q8
Q(10,9) = ALP*Q8+(1.0-ALP)*Q8*(1.0+XL*Q8*E6)
Q(10,10) = ALP*Q8*E6+(1.0-ALP)*Q8*(E6+XL*Q8)
Q(10,11) = ALP*E9/E5+(1.0-ALP)*XLP2*Q8*E10/E5
Q(10,12) = ALP*E10/E5+(1.0-ALP)*XLP2*Q8*E9/E5
C*
Q(11,1) = ZERO
Q(11,2) = ZERO
Q(11,3) = ZERO
Q(11,4) = ZERO
Q(11,5) = ZERO
Q(11,6) = ZERO
Q(11,7) = -E6
Q(11,8) = -1.0
Q(11,9) = B1-Q8*E6
Q(11,10) = B1*E6-Q8
Q(11,11) = -(XLP2/XL)*E10/E5
Q(11,12) = -(XLP2/XL)*E9/E5

```

Appendix B (continued)

```

C*
      Q(12,1) = ZERO
      Q(12,2) = ZERO
      Q(12,3) = ZERO
      Q(12,4) = ZERO
      Q(12,5) = ZERO
      Q(12,6) = ZERO
      Q(12,7) = ZERO
      Q(12,8) = ZERO
      Q(12,9) = -A
      Q(12,10) = -4*E6
      Q(12,11) = -(XLP2/XL)*B3/P2*E10/E5
      Q(12,12) = -(XLP2/XL)*B3/P2*E9/E5
C*
C* .....
C*
C*
C*
C*   WRITE COEFFICIENT MATRIX
C*
      WRITE(8,400)
      WRITE(8,1500)
1500  FORMAT(/20X,"COEFFICIENT MATRIX"//)
      DO 1600 I=1,12
      WRITE(8,1700) (REAL(Q(I,J)),J=1,12)
1600  WRITE(8,1900) (AIMAG(Q(I,J)),J=1,12)
1700  FORMAT(2X,12E10.3)
1800  FORMAT(2X,12F10.3/)
C*
C* .....
C*
C*
C*   FORCING VECTOR
C*
      S(1) = CMPLX(P3,0.0)
      S(2) = ZERO
      XX=(1.0/G1)*(A.0/(3.0*PI)*ROW*CF*U0*U0)
      S(3) = CMPLX(XX,0.0)
      S(4) = ZERO
      S(5) = ZERO
      S(6) = ZERO
      S(7) = ZERO
      S(8) = ZERO
      S(9) = ZERO
      S(10) = ZERO
      S(11) = ZERO
      S(12) = ZERO
C*
C*   WRITE FORCING VECTOR
      WRITE(8,400)
      WRITE(8,1900)
1900  FORMAT(///10X,"FORCING VECTOR"//)
      DO 2000 I=1,12
2000  WRITE(8,2100) REAL(S(I)),AIMAG(S(I))
2100  FORMAT(2X,2E15.5)
C*   WRITE CONSTANTS
      WRITE(8,2102)
2102  FORMAT(///10X,"CONSTANTS"//)
      WRITE(8,2104) XL,REAL(XLP1),REAL(XLP2),AIMAG(XLP1),AIMAG(XLP2)
2104  FORMAT(5X,"XL",8X,E15.8/5X,"XLP1",8X,E15.8,5X,"XLP2",8X,E15.8/
      .15X,E15.8,15X,E15.8)
      WRITE(8,2106) A1,E1,12,P2,REAL(A2),REAL(A3),AIMAG(A3),AIMAG(A3)
2106  FORMAT(5X,"A1",8X,E15.8,5X,"P1",8X,E15.8/5X,"A2",8X,E15.8,
      .5X,"P2",8X,E15.8/5X,"A1",8X,E15.8,5X,"A3",8X,E15.8/
      .15X,E15.8,15X,E15.8)

```

Appendix B (continued)

```

      WRITE(8,2109)HLL
2108 FORMAT(5X,"HLL",7X,E15.4,15X,E15.4)
C*
C*
C*
      IER=0
      CALL LEQ2C(0,12,12,S,1,12,0,WA,WK,IER)
C*
C*
C*
C*   CHECK COEFFICIENT MATRIX
C*
      DO 2109I=1,12
2109  R1(I)=S(I)
      DO 2112I=1,12
      SUM=ZERO
      DO 2110J=1,12
2110  SUM=SUM+Q(I,J)*R1(J)
2112  CHECK(I)=SUM
      WRITE(8,2114)
2114  FORMAT(///10X,"COEFFICIENT MATRIX CHECK"//)
      DO 2116I=1,12
2116  WRITE(8,2118)CHECK(I)
2118  FORMAT(2X,2E15.5)
C*
C*   VERTICAL DISPLACEMENT INTEGRATION CONSTANTS
      R2(1) = -A*R1(2)+A*A1*R1(3)
      R2(2) = -A*R1(1)+A*A1*R1(4)
      R2(3) = -A*R1(4)
      R2(4) = -A*R1(3)
      R2(5) = -A*XLP1/XL*R1(6)
      R2(6) = -A*XLP1/XL*R1(5)
      R2(7) = -A*R1(8)+A*B1*R1(9)
      R2(8) = -A*R1(7)+A*B1*R1(10)
      R2(9) = -A*R1(10)
      R2(10) = -A*R1(9)
      R2(11) = -A*XLP2/XL*R1(12)
      R2(12) = -A*XLP2/XL*R1(11)
C*
C*   PRESSURE INTEGRATION CONSTANTS
      R3(1) = -A*A2*R1(4)
      R3(2) = -A*A2*R1(3)
      R3(3) = ZERO
      R3(4) = ZERO
      R3(5) = -A*A3*R1(5)
      R3(6) = -A*A3*R1(6)
      R3(7) = -A*B2*R1(10)
      R3(8) = -A*B2*R1(9)
      R3(9) = ZERO
      R3(10) = ZERO
      R3(11) = -B3*R1(11)
      R3(12) = -B3*R1(12)
C*
C*   WRITE INTEGRATION CONSTANTS
C*
      WRITE(8,4A0)
      WRITE(8,2120)
2120  FORMAT(20X,"INTEGRATION CONSTANTS"//)
      WRITE(8,2130)
2130  FORMAT(6X,"HORIZONTAL DISPLACEMENT",3X,"VERTICAL DISPLACEMENT",
.1X,"PRESSURE"//)
      WRITE(8,2140)
2140  FORMAT(2X,3(7X,"REAL",5X,"IMAGINARY"//))

```

Appendix B (continued)

```

      DO 2150 I=1,12
2150  WRITE(8,2150) REAL(R1(I)), AIMAG(P1(I)), REAL(P2(I)), AIMAG(P2(I)),
      .REAL(R3(I)), AIMAG(P3(I))
2160  FORMAT(2X,3(2X,2E12.5)/)
C*
C*    COMPUTATION DEPTHS
C*
      NZ=40
      DZ=08/NZ
      NZF=01/08*NZ+1.5
      NZP=NZ+2
      L=1
      DO 2200 I=1,NZP
      IF(I.GT.NZF) L=2
2200  Z(I)=DZ*(I-L)
C*
C*    HORIZONTAL DISPLACEMENT
C*
      CALL FUNC(XL,XLP1,XLP2,Z,P1,NZF,NZP,U)
      XDIM=LENGTH*P0/G1
      WRITE(8,400)
      WRITE(8,2600)
2600  FORMAT(/2X,"HORIZONTAL DISPLACEMENTS"/)
      CALL OUT1(Z,U,NZP,XDIM)
C*
C*    VERTICAL DISPLACEMENT
C*
      CALL FUNC(XL,XLP1,XLP2,Z,R2,NZF,NZP,W)
      WRITE(8,400)
      WRITE(8,2800)
2800  FORMAT(/2X,"VERTICAL DISPLACEMENTS"/)
      CALL OUT1(Z,W,NZF,XDIM)
C*
C*    PRESSURE
C*
      CALL FUNC(XL,XLP1,XLP2,Z,R3,NZF,NZP,P)
      XDIM=P0
      WRITE(8,400)
      WRITE(8,3000)
3000  FORMAT(/2X,"PRESSURE"/)
      CALL OUT1(Z,P,NZF,XDIM)
C*
C*    HORIZONTAL AND VERTICAL GRADIENTS
C*
      L=0
      XP=XLP1
      DO 3010 I=1,NZP
      DPOX(I)=A*XL*P(I)
      DUOX(I)=A*XL*U(I)
      DWOX(I)=A*XL*W(I)
      IF(I.GT.NZF) L=6
      IF(I.GT.NZF) XP=XLP2
      D=Z(I)
      DPO7(I)=XL*(P3(L+1)*SINH(XL*D)+P3(L+2)*COSH(XL*D))+
      .XP*(0.5*(CEXP(XP*D)-CEXP(-XP*D))*P3(L+5)+
      .0.5*(CEXP(XP*D)+CEXP(-XP*D))*P3(L+6))
      DUO7(I)=XL*(P1(L+1)*SINH(XL*D)+P1(L+2)*COSH(XL*D)+
      .P1(L+3)*(COSH(XL*D)/XL+D*SINH(XL*D))+
      .P1(L+4)*(SINH(XL*D)/XL+D*COSH(XL*D)))+
      .XP*(R1(L+5)*0.5*(CEXP(XP*D)-CEXP(-XP*D))+
      .P1(L+6)*0.5*(CEXP(XP*D)+CEXP(-XP*D)))
      DWO7(I)=XL*(P2(L+1)*SINH(XL*D)+P2(L+2)*COSH(XL*D)+
      .P2(L+3)*(COSH(XL*D)/XL+D*SINH(XL*D))+

```

Appendix B (continued)

```

      .R2(L+4)*(SINH(XL*D)/XL*D*COSH(XL*D)))+
      .XP*(R2(L+5)*0.5*(CEXP(XP*D)-CEXP(-XP*D))+
      .R2(L+6)*0.5*(CEXP(XP*D)+CEXP(-XP*D)))
C*
C*   FLUID VELOCITY
C*
C*   DISCHARGE VELOCITY
C*
      DO 3100 I=1,NZF
      XY=XKP1
      IF(I.GT.NZF)XY=XKP2
      FVX(I)=-XY/(PCW*G)*DPDX(I)
      FVZ(I)=-XY/(PCW*G)*DPDZ(I)
3100  CONTINUE
      XDIM=(XKP1*P0/LENGTH)
      WRITE(8,480)
      WRITE(8,3200)
3200  FORMAT(/2X,"HORIZONTAL DISCHARGE VELOCITY"/
      .2X,"(RELATIVE TO THE SOIL MATRIX)"/)
      XDIM=P0*XKP1/(LENGTH*PCW*G)
      CALL OUT1(Z,FVX,NZF,XDIM)
      WRITE(8,480)
      WRITE(8,3300)
3300  FORMAT(/2X,"VERTICAL DISCHARGE VELOCITY"/
      .2X,"(RELATIVE TO THE SOIL MATRIX)"/)
      CALL OUT1(Z,FVZ,NZF,XDIM)
C*
C*   STRAINS
C*
C*   VOLUME STRAIN
      DO 3552 I=1,NZF
3552  VS(I)=DUDX(I)+DWDZ(I)
      XDIM=P0/G1
      WRITE(8,480)
      WRITE(8,3554)
3554  FORMAT(/2X,"VOLUME STRAIN"/)
      CALL OUT1(Z,VS,NZF,XDIM)
C*
C*
C*
      DO 3556 I=1,NZF
3556  SS(I)=DUDZ(I)+DWDY(I)
      WRITE(8,480)
      WRITE(8,3558)
3558  FORMAT(/2X,"SHEAR STRAIN"/)
      CALL OUT1(Z,SS,NZF,XDIM)
C*
C*   SEEPAGE VELOCITY
C*
      DO 3400 I=1,NZF
      XN=N1
      IF(I.GT.NZF)XN=N2
      FVX(I)=(1.0/XN)*FVX(I)
3400  FVZ(I)=(1.0/XN)*FVZ(I)
      WRITE(8,480)
      WRITE(8,3500)
3500  FORMAT(/2X,"HORIZONTAL SEEPAGE VELOCITY"/
      .2X,"(RELATIVE TO THE SOIL MATRIX)"/)
      XDIM=P0*XKP1/(LENGTH*PCW*G)
      CALL OUT1(Z,FVX,NZF,XDIM)
      WRITE(8,480)
      WRITE(8,3550)
3550  FORMAT(/2X,"VERTICAL SEEPAGE VELOCITY"/

```

Appendix B (continued)

```

      .2X,"(RELATIVE TO THE SOIL MATRICE)"/)
      CALL OUT1(Z,FVZ,N7P,XDIM)
      XN=N1
      DO 3560 I=1,N7P
      IF(I.GT.N7F)XN=N2
      FVX(I)=FVX(I)*XN
3560 FVZ(I)=FVZ(I)*XN
C*
C*   STRESS AND SHEAR
C*
      XDIM=P0
      G=G1
      XNU=NU1
      DO 3600 I=1,N7P
      IF(I.GT.NZF)G=G2
      IF(I.GT.NZF)XNU=NU2
      SIGX(I)=2.0*G/(1.0-2.0*XNU)*((1.0-XNU)*DUDX(I)+
      .XNU*ODWD(I))
      SIGZ(I)=2.0*G/(1.0-2.0*XNU)*((1.0-XNU)*ODWD(I)+
      .XNU*ODUX(I))
3600 TAU(I)=G*(ODUD(I)+ODUX(I))
      XDIM=P0
      WRITE(8,480)
      WRITE(8,3700)
3700 FORMAT(/2X,"HORIZONTAL EFFECTIVE STRESS"/)
      CALL OUT1(Z,SIGX,N7P,XDIM)
      WRITE(8,480)
      WRITE(8,3800)
3800 FORMAT(/2X,"VERTICAL EFFECTIVE STRESS"/)
      CALL OUT1(Z,SIGZ,N7P,XDIM)
      WRITE(8,480)
      WRITE(8,3900)
3900 FORMAT(/2X,"SHEAR"/)
      CALL OUT1(Z,TAU,N7P,XDIM)
C*
C*   SHEAR STRESS ANGLE
C*
      WRITE(8,480)
      WRITE(8,3902)
3902 FORMAT(/2X,"SHEAR STRESS ANGLE"/)
      DO 3904 I=1,N7P
      TAUMAX(I)=CSQRT(((SIGZ(I)-SIGX(I))*0.5)**2+TAU(I)**2)
      DUM1=(SIGX(I)+SIGZ(I))*0.5
      DUM2=TAUMAX(I)/((DUM1+TAUMAX(I))*(DUM1-TAUMAX(I)))
      DUM3=(1+DUM2)/(1-DUM2)
      DUM4=CABS(DUM3)
      DUM5=REAL(DUM3)
      DUM6=AIMAG(DUM3)
      IF(DUM5.EQ.0.0 .AND. DUM6.GT.0.0)DUM7=90.0
      IF(DUM5.EQ.0.0 .AND. DUM6.LT.0.0)DUM7=-90.0
      IF(DUM5.EQ.0.0 .AND. DUM6.EQ.0.0)DUM7=0.0
      IF(DUM5.EQ.0.0)GO TO 3903
      DUM7=ATAN2(DUM6,DUM5)
3903 CONTINUE
3904 PHI(I)=(ALOG(DUM4)+A*ODU7)*0.5*A*(180./PI)
      XDIM=(1.0,0.0)
      CALL OUT1(Z,PHI,N7P,XDIM)
C*
C*   SHEAR STRESS RATIO
C*
      WRITE(8,480)
      WRITE(8,3910)
3910 FORMAT(/2X,"SHEAR STRESS RATIO"/)

```

Appendix B (continued)

```

DO 3920 I=2, N7P
  IF (I.LE.NZF) SSP(I)=TAUMAX(I)/(7(I)*GAMMA1)
  IF (I.GT.NZF) SSP(I)=TAUMAX(I)/(7(NZF)*GAMMA1+(7(I)-7(NZF))*
    .GAMMA2)
3920 CONTINUE
  SSP(1)=ZERO
  CALL OUT1(7,SSP,N7P,XDIM)

C*
C*   OUTPUT TO GRAPHICS
C*
C*

  IIDPTH=0
  XDIM=CMPLX(1.0,0.0)
  IF (NONDIM.EQ.0) XDIM=LENGTH*P0/G1
  CALL SCALE(U,FF,XDIM,N7P)
  CALL ARGMOD(FF,F1,F2,N7P)
  CALL OUTPLT(LENGTH,IDENT,NZF,N7P,XDIM,1,IIDPTH,7,F1,F2)
  CALL SCALE(W,FF,XDIM,N7P)
  CALL ARGMOD(FF,F1,F2,N7P)
  CALL OUTPLT(LENGTH,IDENT,NZF,N7P,XDIM,2,IIDPTH,7,F1,F2)
  IF (NONDIM.EQ.0) XDIM=P0
  CALL SCALE(P,FF,XDIM,N7P)
  CALL ARGMOD(FF,F1,F2,N7P)
  CALL OUTPLT(LENGTH,IDENT,NZF,N7P,XDIM,3,IIDPTH,7,F1,F2)
  CALL SCALE(SIGX,FF,XDIM,N7P)
  CALL ARGMOD(FF,F1,F2,N7P)
  CALL OUTPLT(LENGTH,IDENT,NZF,N7P,XDIM,4,IIDPTH,7,F1,F2)
  CALL SCALE(SIGZ,FF,XDIM,N7P)
  CALL ARGMOD(FF,F1,F2,N7P)
  CALL OUTPLT(LENGTH,IDENT,NZF,N7P,XDIM,5,IIDPTH,7,F1,F2)
  CALL SCALE(TAU,FF,XDIM,N7P)
  CALL ARGMOD(FF,F1,F2,N7P)
  CALL OUTPLT(LENGTH,IDENT,NZF,N7P,XDIM,6,IIDPTH,7,F1,F2)
  IF (NONDIM.EQ.0) XDIM=P0/G1
  CALL SCALE(VS,FF,XDIM,N7P)
  CALL ARGMOD(FF,F1,F2,N7P)
  CALL OUTPLT(LENGTH,IDENT,NZF,N7P,XDIM,7,IIDPTH,7,F1,F2)
  CALL SCALE(SS,FF,XDIM,N7P)
  CALL ARGMOD(FF,F1,F2,N7P)
  CALL OUTPLT(LENGTH,IDENT,NZF,N7P,XDIM,8,IIDPTH,7,F1,F2)
  IF (NONDIM.EQ.0) XDIM=XKF1*P0/(LENGTH*ROW*G)
  CALL SCALE(FVX,FF,XDIM,N7P)
  CALL ARGMOD(FF,F1,F2,N7P)
  CALL OUTPLT(LENGTH,IDENT,NZF,N7P,XDIM,9,IIDPTH,7,F1,F2)
  CALL SCALE(FVZ,FF,XDIM,N7P)
  CALL ARGMOD(FF,F1,F2,N7P)
  CALL OUTPLT(LENGTH,IDENT,NZF,N7P,XDIM,10,IIDPTH,7,F1,F1)
DO 3970 I=1, N7P
  XN=N1
  IF (I.GT.NZF) XN=N2
  FVX(I)=FVX(I)/XN
3970 FVZ(I)=FVZ(I)/XN
  CALL SCALE(FVX,FF,XDIM,N7P)
  CALL ARGMOD(FF,F1,F2,N7P)
  CALL OUTPLT(LENGTH,IDENT,NZF,N7P,XDIM,11,IIDPTH,7,F1,F2)
  CALL SCALE(FVZ,FF,XDIM,N7P)
  CALL ARGMOD(FF,F1,F2,N7P)
  CALL OUTPLT(LENGTH,IDENT,NZF,N7P,XDIM,12,IIDPTH,7,F1,F2)
  XDIM=(1.0,0.0)
  CALL SCALE(SSP,FF,XDIM,N7P)
  CALL ARGMOD(FF,F1,F2,N7P)
  CALL OUTPLT(LENGTH,IDENT,NZF,N7P,XDIM,13,IIDPTH,7,F1,F2)
  CALL SCALE(PHI,FF,XDIM,N7P)

```


Appendix B (continued)

```

      CALL ARGMOD(FF,F1,F2,NZF)
      CALL OUTPLT(LENGTH,IDENT,NZF,NZF,XDIM,14,IIDPTH,7,F1,F2)
C*
C*
      4000 CONTINUE
      END
C*
C*.....
C*
      SUBROUTINE FUNC(XL,XLP1,XLP2,7,R,NZF,NZF,X)
      COMPLEX R(42),X(42)
      DIMENSION Z(42)
      COMPLEX XP,XLP1,XLP2
      L=0
      XP=XLP1
      DO 100 I=1,NZF
      IF(1.GT.NZF)L=6
      IF(1.GT.NZF)XP=XLP2
      Z(I)
100 X(I)=R(L+1)*COSH(XL*D)+R(L+2)*SINH(XL*D)+P(L+3)*D*CCSH(XL*D)+
      .R(L+4)*D*SINH(XL*D)+R(L+5)*D*.5*(CEXP(XP*D)+CEXP(-XP*D))+
      .R(L+6)*D*.5*(CEXP(XP*D)-CEXP(-XP*D))
      RETURN
      END
C*
C*.....
C*
      SUBROUTINE OUT1(Z,X,NZF,XDIM)
      COMPLEX X(42),XDIM,FF(42)
      DIMENSION Z(42),XMOD(42),XARG(42),FFMOD(42),FFARG(42)
      WRITE(8,50)XDIM
50  FORMAT(4X,"NON-DIMENSIONALIZED BY",2E15.5/)
      WRITE(8,100)
100  FORMAT(10X,"7",12X,"REAL",9X,"IMAGINARY",7X,"MODULUS",
      .9X,"PHASE",6X,"DIMENSIONLESS",2X,"DIMENSIONLESS"/)
      CALL ARGMOD(X,XMOD,XARG,NZF)
      CALL SCALE(X,FF,XDIM,NZF)
      CALL ARGMOD(FF,FFMOD,FFARG,NZF)
      DO 200 I=1,NZF
      H=Z(I)
      F1=REAL(X(I))
      F2=AIMAG(X(I))
      F3=XMOD(I)
      F4=XARG(I)
      F5=FFMOD(I)
      F6=FFARG(I)
200  WRITE(8,300)H,F1,F2,F3,F4,F5,F6
300  FORMAT(F15.5,3F15.5,F15.5,E15.5,F15.5)
      RETURN
      END
C*
C*.....
C*
      SUBROUTINE OUTPLT(XL,IDENT,NZF,NZF,XDIM,IFUNCT,IIDPTH,7,F1,F2)
      DIMENSION IF(14,4),IDENT(15),F1(42),F2(42),Z(42)
      COMPLEX XDIM
C*
      DATA (IF(1,I),I=1,4)/4H      ,4HNOF1,4H7ONT,4HAL D,
      .4HISPL,4HACEM,4HENT ,4H      /
      DATA (IF(2,I),I=1,4)/4H      ,4H VEP,4HTICA,4HLD OF,
      .4HSPLA,4HCEME,4HNT ,4H      /
      DATA (IF(3,I),I=1,4)/4H      ,4H PD,4HIE W,4HATER,
      .4H PRE,4HSUR,4HE ,4H      /
      DATA (IF(4,I),I=1,4)/4H      ,4HPIZO,4HNTAL,4H EFF,

```

Appendix B (continued)

```

.4HECTI,4HVE S,4HTRES,4HS /
DATA(IF(5,I),I=1,8)/4H V,4HERTI,4HCAL ,4HEFFE.
.4HCTIV,4HE ST,4HEFFS,4H /
DATA(IF(6,I),I=1,8)/4H ,4H ,4H SH,4HEAR ,
.4HSTRE,4HSS ,4H ,4H /
DATA(IF(7,I),I=1,8)/4H ,4H ,4H VOL,4HUMF ,
.4HSTRA,4HIN ,4H ,4H /
DATA (IF(8,I),I=1,8)/4H ,4H ,4H SH,4HEAR ,
.4HSTRA,4HIN ,4H ,4H /
DATA (IF(9,I),I=1,8)/4H HOR,4HIZON,4HTAL ,4HDISC.
.4HHARG,4HE VE,4HLOCI,4HTY /
DATA (IF(10,I),I=1,8)/4H VE,4HRTIC,4HAL D,4HISCH.
.4HARGE,4H VEL,4HCCIT,4HY /
DATA (IF(11,I),I=1,8)/4H HQ,4HRIZO,4HPNTAL,4H SEP.
.4HPAGE,4H VEL,4HCCIT,4HY /
DATA (IF(12,I),I=1,8)/4H V,4HEFTI,4HCAL ,4HSEEP.
.4HAGE ,4HVELO,4HCITY,4H /
DATA (IF(13,I),I=1,8)/4H ,4H S,4HHEAR,4H STR.
.4HESS ,4HRTI,4HCC ,4H /
DATA(IF(14,I),I=1,8)/4H ,4H S,4HHEAR,4H STR.
.4HESS ,4HANGL,4HE ,4H /
DATA DEPTH /5HDEPTH/
DATA IMOD /4HMOD /
DATA IARG /4HARG /

```

```

C*
IF(IIDPTH.EQ.1)GO TO 450
IIDPTH=1
WRITE(9,100)(IDENT(I),I=1,15)
100 FORMAT(1X,15A4)
WRITE(9,200)N7F,N7P
200 FORMAT(2X,12,6X,12)
WRITE(9,300)DEPTH,XL
300 FORMAT(1X,A5,2F12.5)
WRITE(9,400)(Z(I),I=1,N7P)
400 FORMAT(1X,612.5)
450 CONTINUE
WRITE(9,500)(IF(IFUNCT,I),I=1,8).XDIM
500 FORMAT(1X,8A4/1X,2G15.5)
WRITE(9,600)IMOD,IARG
600 FORMAT(7X,A4,12X,A4)
DO 700I=1,N7P
700 WRITE(9,800)F1(I),F2(I)
800 FORMAT(1X,2G15.5)
RETURN
END

```

```

C*
C*****
C*

```

```

SUBROUTINE ARGMOD(F,FMOD,FARG,N7P)
DIMENSION F(42),FMOD(42),FARG(42)
COMPLEX F
DO 100I=1,N7P
A1=REAL(F(I))
A2=AIMAG(F(I))
FMOD(I)=SQRT(A1**2+A2**2)
IF(A1.EQ.0.0 .AND. A2.GT.0.0)TEST=90.0
IF(A1.EQ.0.0 .AND. A2.LT.0.0)TEST=-90.0
IF(A1.EQ.0.0 .AND. A2.EQ.0.0)TEST=0.0
IF(A1.EQ.0.0)GO TO 50
TEST=ATAN2(A2,A1)*57.296
50 CONTINUE
100 FARG(I)=TEST
RETURN

```

Appendix B (continued)

```
      END  
C*  
C* .....  
C*  
      SUBROUTINE SCALE(X,F,XDIM,NZP)  
      COMPLEX X,F,XDIM  
      DIMENSION X(42),F(42)  
      DO 100 I=1,NZP  
100  F(I)=X(I)/XDIM  
      RETURN  
      END
```

B.2 Program PLOTT

```

PROGRAM PLOTT (INPLT,TAPE5=INPUT,OUTPUT,TAPE6=OUTPUT,
.SOILIN,TAPE7=SOILIN,TAPE10=0)
DIMENSION IF(8),IDENT(15),IPLOTS(24),Z(42),F1(42),F2(42)
DIMENSION ZD(41),FD(41),FF1(42),FF2(42)
COMPLEX XOIM
READ(7,100)(IDENT(I),I=1,15)
100 FORMAT(1X,15A4)
READ(7,200)NZF,NZP
200 FORMAT(2X,I2,6X,I2)
READ(7,230)DEPTH,XL
230 FORMAT(1X,A5,G12.5)
READ(7,250)(Z(I),I=1,NZP)
250 FORMAT(1X,G12.5)
NZPM1=NZP-1
DO 260I=1,NZPM1
II=I
IF(I.GT.NZF)II=I+1
260 F1(II)=Z(II)
F1(NZP)=Z(NZP)
DO 270I=1,NZP
II=NZP+1-I
270 Z(I)=F1(II)
300 FORMAT(1X,#ENTER TOTAL NUMBER OF PLOTS DESIRED#)
400 FORMAT(1X,#ENTER CODES FOR DESIRED PLOTS#//
.1X,#HORIZONTAL DISPLACEMENT 1 #/
.1X,#VERTICAL DISPLACEMENT 2 #/
.1X,#PORE WATER PRESSURE 3 #/
500 FORMAT(1X,#HORIZONTAL EFFECTIVE STRESS 4 #/
.1X,#VERTICAL EFFECTIVE STRESS 5 #/
.1X,#SHEAR STRESS 6 #/
.1X,#VOLUME STRAIN 7 #/
.1X,#SHEAR STRAIN 8 #/
600 FORMAT(1X,#HORIZONTAL DISCHARGE VELOCITY 9 #/
.1X,#VERTICAL DISCHARGE VELOCITY 10 #/
.1X,#HORIZONTAL SEEPAGE VELOCITY 11 #/
.1X,#VERTICAL SEEPAGE VELOCITY 12 #/
.1X,#SHEAR STRESS RATIO 13 #/
.1X,#SHEAR STRESS ANGLE 14 #/
620 FORMAT(1X,#PHASE PLOTS* (YES=1,NO=0)*)
WRITE(6,300)
READ *,NPLOTS
WRITE(6,400)
WRITE(6,500)
WRITE(6,600)
READ *,(IPLOTS(I),I=1,NPLOTS)
WRITE(6,620)
READ *,IPHASE
WRITE(6,640)
640 FORMAT(1X,#FABRIC LOCATION SHOWN* (YES=1,NO=0)*)
READ *,LINE1
NN=1
DO 1100N=1,14
READ(7,700)(IF(I),I=1,8),XOIM
700 FORMAT(1X,8A4/1X,2G15.5)
READ(7,750)IMOD,IARG
750 FORMAT(7X,A4,12X,A4)
DO 800I=1,NZP
800 READ(7,900)FF1(I),FF2(I)
900 FORMAT(1X,2G15.5)
IF(IPLOTS(NN) .NE. N)GO TO 1000

```

Appendix B (continued)

```

      NN=NN+1
      DO 920 I=1,NZP
        II=I+1
        IF (I.GT.NZF) II=I
        F1(II)=FF1(I)
920    F2(II)=FF2(I)
        F1(1)=FF1(1)
        F2(1)=FF2(1)
        WRITE(6,950) IDENT,XDIM
950    FORMAT(1X,15A4/,1X,2G15.5)
        CALL PLTMOD(RUN,CASE,NZF,NZP,IF,DEPTH,
        .Z,F1,F2,IPHASE,LINE1,N,XL)
1000   CONTINUE
1100   CONTINUE
      END
      SUBROUTINE PLTMOD(RUN,CASE,NZF,NZP,IF,DEPTH,Z,F1,F2,
        .IPHASE,LINE1,NSSF,XL)
      DIMENSION F02(39),Z02(39),F01(40),Z01(40),F0(41),Z0(41)
      DIMENSION DOT1(49),DOT2(49)
      DIMENSION IF(8),Z(42),F1(42),F2(42),XLABZ(5),XLABF(10)
      DIMENSION XLABZ0(10)
      WIDTH=5.5
      HEIGHT=4.5
      CALL PLOTTYPE(1)
      CALL TKTYPE(4010)
      CALL BAUD(1200)
      CALL SIZE(WIDTH+2.0,HEIGHT+2.0)
      FMIN=0.0
      FMAX=F1(1)
      DO 100 I=1,NZP
100    IF (F1(I).GT.FMAX) FMAX=F1(I)
      DO 120 I=1,50
        IEXPN=I-1
        IF (FMAX.LT.1.0) IEXPN=-IEXPN
        TEST=10.0**IEXPN
        IF (IEXPN.LT.0 .AND. TEST.LE.FMAX) GO TO 130
        IF (IEXPN.GT.0 .AND. TEST.GE.FMAX) GO TO 130
        IF (FMAX.GE.1.0 .AND. FMAX.LE.10.0) GO TO 130
120    CONTINUE
130    CONTINUE
      DO 140 I=1,NZP
140    F1(I)=F1(I)/10.0**IEXPN
        FMAX=FMAX/10.0**IEXPN
        EXPN=-IEXPN
        CALL RANGE(FMIN,FMAX,5,FLOW,FHIGH,DIST)
        CALL RANGE(0.0,Z(1),4,ZLOW,ZHIGH,ZDIST)
        FFACT=WIDTH/FHIGH
        ZFACT=HEIGHT/Z(1)
        CALL SCALE(FFACT,ZFACT,0.6,1.0,FLOW,Z(NZP))
      DO 150 IBOX=1,3
        CALL PLOT(FLOW,Z(NZP),0,0)
        CALL PLCT(FLOW,Z(1),1,0)
        CALL PLOT(FHIGH,Z(1),1,0)
        CALL PLOT(FHIGH,Z(NZP),1,0)
        CALL PLCT(FLOW,Z(NZP),1,0)
150    CONTINUE
C*    DL - HASH MARK LENGTH
        DL=0.04
        NF=FHIGH/DIST-0.5
        OZ=Z(NZP)+DL
        DO 200 I=1,NF
          CALL PLOT(FLOW+I*DIST,Z(NZP),0,0)
          CALL PLOT(FLOW+I*DIST,OZ,1,0)
200    CONTINUE
        OZ=Z(1)-DL
        DIST2=DIST

```

Appendix B (continued)

```

      IF(IPHASE.EQ.1)DIST2=FWHIGH/4.0
      IF(IPHASE.EQ.1)NF=3
      DO 300I=1,NF
      CALL PLOT(FLOW+I*DIST2,Z(1),0,0)
300  CALL PLOT(FLOW+DIST2*I,OZ,1,0)
      OZ=Z(1)/4.0
      OL=OL*FWHIGH/Z(1)
      OF=FLOW+OL
      DO 400I=1,3
      CALL PLOT(FLOW,Z(NZP)+I*OZ,0,0)
400  CALL PLOT(OF,Z(NZP)+I*OZ,1,0)
      OF=FWHIGH-OL
      NR=Z(1)/ZOIST-0.5
      DO 500I=1,NR
      CALL PLOT(FHIGH,Z(NZP)+I*ZOIST,0,0)
500  CALL PLOT(OF,Z(NZP)+I*ZOIST,1,0)
      DO 600I=1,5
600  XLABZ(I)=Z(1)-(I-1)*OZ
      NF=FWHIGH/DIST+1.5
      DO 700I=1,NF
700  XLABF(I)=(I-1)*DIST
C*  DS = LABEL CHARACTER SIZE
      DS=0.0125*FWHIGH
      OSF=0.0375*Z(1)
      DO 800I=1,5
800  CALL NUMBER(FLOW-6.0*DS,Z(NZP)+(I-1)*OZ-OSF/4.,0.0,0.1,4,XLABZ(I))
      NRP1=NR+1
      DO 820I=1,NRP1
820  XLABZD(I)=(I-1)*ZOIST/XL
      DO 840I=1,NRP1
840  CALL NUMBER(FHIGH+OS/2.0,Z(1)-(I-1)*ZOIST-OSF/4.0,
      .0,0.0,1.5,XLABZD(I))
      DO 900I=1,NF
900  CALL NUMBER(FLOW-3.0*DS+(I-1)*DIST,Z(NZP)-OSF,0.0,0.1,4,XLABF(I))
      ENCODE(25,920,LABLE1)
920  FORMAT(*MODULUS X10 (SOLID LINE)*)
      CALL SYMBOL(FHIGH/2.0-23.0*DS,Z(NZP)-2.5*OSF,0.0,0.12,25,LABLE1)
      ENCODE(19,930,LABLE3)
930  FORMAT(*DIMENSIONLESS DEPTH*)
      CALL SYMBOL(FHIGH+10.5*DS,Z(1)/2.0-7.5*OSF,90.0,0.12,19,LABLE3)
      IF(EXPN.GE.0.0)ISP=-1
      IF(EXPN.GE.10.0)ISP=-2
      IF(EXPN.LT.0.0)ISP=-2
      IF(EXPN.LE.-10.0)ISP=-3
      CALL NUMBER(FHIGH/2.0-2.2*DS,Z(NZP)-2.0*OSF,0.0,0.10,ISP,EXPN)
      ENCODE(21,940,LABLE2)
940  FORMAT(*ARGUMENT(DASHED LINE)*)
      CALL SYMBOL(FLOW-6.0*DS,Z(1)/2.0-1.8*OSF,90.0,0.12,5,DEPTH)
      IF(IPHASE.EQ.1)CALL SYMBOL(FHIGH/2.0-18.0*DS,Z(1)+2.1*OSF,0.0,
      .0,12,21,LABLE2)
      IF(NSSR.NE.13)GO TO 960
      NZPM2=NZP-2
      DO 950I=1,NZPM2
      II=I+2
      ZD1(I)=Z(II)
950  F01(I)=F1(II)
      CALL LINE(F01,ZD1,0,NZPM2)
      GO TO 970
960  CONTINUE
      CALL LINE(F1,Z,0,NZP)
970  CONTINUE
      IF(IPHASE.EQ.0) GO TO 1500
      XP=FLOW-0.2*DS

```

Appendix B (continued)

```

      YP=Z(1)*DSF/2.0
      CALL SYMBEL(XP,YP,0.0,0.14,3,3H^>P)
      CALL SYMBEL(XP-1.85*OS,YP,0.0,0.1,3,3H<v-)
      XP=FHIGH-OS
      CALL SYMBEL(XP,YP,0.0,0.14,3,3H^>P)
      XP=FHIGH/2.0-OS
      CALL SYMBEL(XP,YP,0.0,0.12,3,3H^>0)
C*
      DO 1400 I=1,NZP
1400  F2(I)=(F2(I)+180.0)/360.0*FHIGH
C*
      IF(NSSR.NE.13)GO TO 1480
      NZPM3=NZP-3
      CALL DASHES
      DO1460 I=1,NZPM3
      II=I+2
      F02(I)=F2(II)
1460  Z02(I)=Z(II)
      CALL LINE(F02,Z02,0,NZPM3)
      GO TO 1490
1480  CONTINUE
      NZPM1=NZP-1
      DO 1490 I=1,NZPM1
      Z0(I)=Z(I)
1490  F0(I)=F2(I)
      CALL DASHES
      CALL LINE(F0,Z0,0,NZPM1)
1490  CONTINUE
1500  CONTINUE
      IF(LINE1.EQ.0)GO TO 1560
      DO 1550 I=1,49
      XZ=(FLOAT(NZP)-FLCAT(NZF)+0.5)/FLCAT(NZF)*Z(1)
      DOT1(I)=(FHIGH-FLOW)*(I)/50.0
1550  DOT2(I)=XZ
      CALL PLOT(FLOW,XZ,0,0)
      CALL POINTS
      CALL LINE(DOT1,DOT2,1,49)
1560  CONTINUE
      DS=1.5*OS
      DO 1600 II=1,8
      CALL SYMBOL(FHIGH/2.0-25.0*OS+(II-1)*6.38*OS,Z(NZP)-5.0*
        .DSF,0.0,0.15,4,IF(II))
1600  CONTINUE
      CALL BELL
      CALL PLOTEND
      RETURN
      END

```

APPENDIX C

Determination of Test Section Length

The ends of the test section are no flow boundaries which are not included in the formulation of the Biot model. It is therefore necessary to examine the region of influence of this boundary. Laboratory measurements are only valid outside of this region. The longer the test section, the less the influence on the measurements made near the centerline. However, each increase in the length of the test section of three feet results in an additional four cubic yards of soil. It is therefore desirable to estimate an optimum test section length which minimizes both the volume of soil and the end effects.

To estimate the region of influence two, one-layer potential pressure models were developed; one for a test section of infinite length and the other for a test section of finite length. The boundary value problem for the infinite length test section is

$$\nabla^2 p = 0 \quad (C.1a)$$

$$p(x, z, t) = p^*(z) \cos(\lambda x - \omega t) \quad (C.1b)$$

$$p^*(0) = p_0 \quad (C.1c)$$

$$\frac{d}{dz} p^*(d) = 0 \quad (C.1d)$$

A solution to this problem is

$$p = p_0 \frac{\text{ch}[\lambda(d-z)]}{\text{ch}(\lambda d)} \cos(\lambda x - \omega t) \quad (C.2)$$

The boundary value problem for the finite length test section is given by

$$\nabla^2 p = 0 \quad (C.2a)$$

$$p(x, z, t) = p^*(x, z) \cos(\omega t) \quad (C.2b)$$

Appendix C (continued)

$$\frac{\partial}{\partial x} p^*(0, z) = 0 \quad (C.2c)$$

$$\frac{\partial}{\partial x} p^*(\ell, z) = 0 \quad (C.2d)$$

$$p^*(x, 0) = p_0 \cos(\lambda x) \quad (C.2e)$$

$$\frac{\partial}{\partial z} p^*(x, d) = 0 \quad (C.2f)$$

in which ℓ is the length of the test section. A solution to this problem is

$$p = p_0 \sum_{n=0}^{\infty} \alpha_n \operatorname{ch}[\kappa_n (d-z)] \cos(\kappa_n x) \cos(\omega t) \quad (C.3)$$

in which

$$\alpha_n = \frac{(-1)^n \lambda \kappa_n \sin(\kappa_n \ell)}{2\pi \operatorname{ch}(\kappa_n d) (\lambda^2 - \kappa_n^2)} \quad ; \quad \lambda^2 \neq \kappa_n^2 \quad (C.4)$$

and

$$\kappa_n = \frac{n \pi}{\ell} \quad (C.5)$$

The relative error due to the end conditions, r_e , is

$$r_e = 1 - \sum_{n=0}^{\infty} \frac{(-1)^n \lambda \kappa_n \sin(\lambda \ell)}{\pi (\lambda^2 - \kappa_n^2)} \frac{\operatorname{ch}(\lambda d)}{\operatorname{ch}(\kappa_n d)} \frac{\operatorname{ch}[\kappa_n (d-z)]}{\operatorname{ch}[\lambda (d-z)]} \frac{\cos(\kappa_n x)}{\cos(\lambda x)} \quad (C.6)$$

The portion of the test section in which the error is less than 5% is shown in Figure C.1 for different wave and test section lengths. The false bottom concrete plates are 12 feet long. Therefore, the

Appendix C (continued)

test section is most easily constructed at a multiple of 12 feet. A 36 foot test section provided an optimum between end effects and volume of soil.

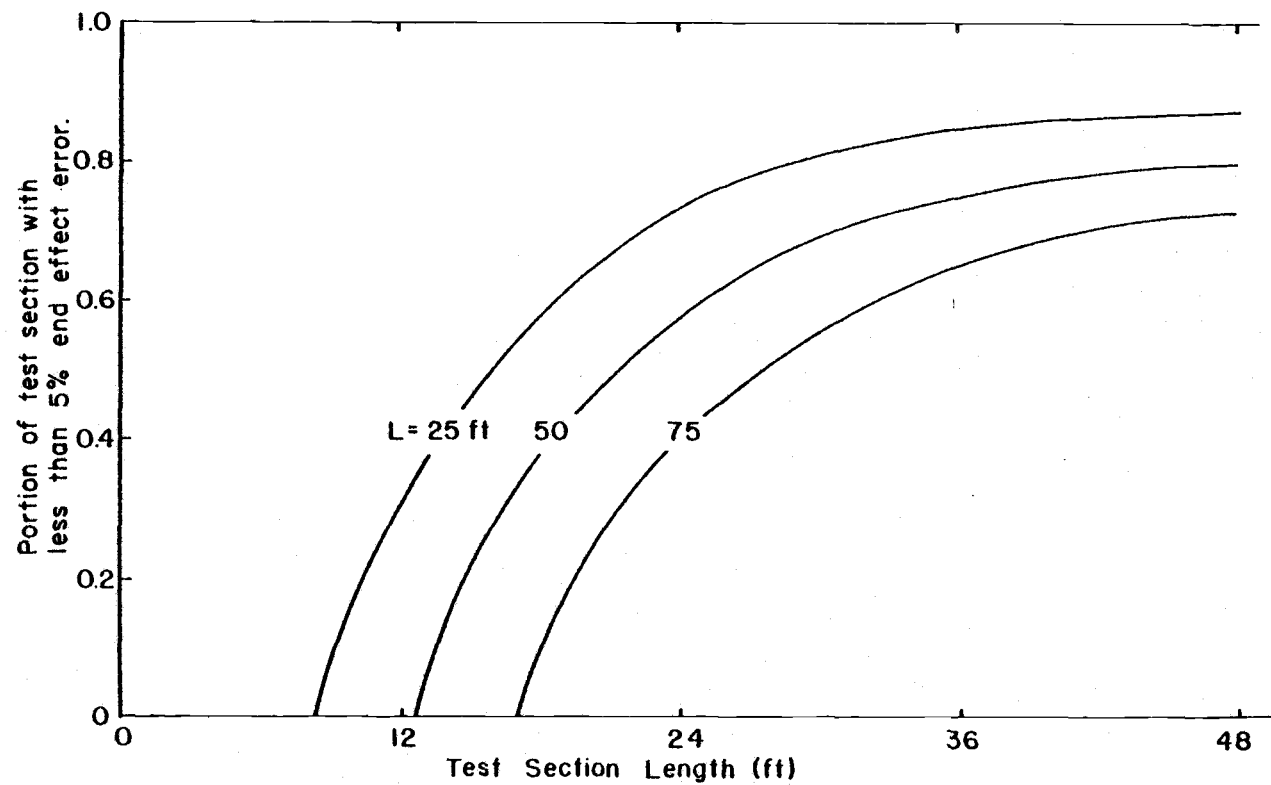


Figure C.1. Portion of the test section with less than 5% error due to the end effects as a function of different wave and test section lengths.

Laboratory Measurements

APPENDIX D

Run	Case	Height	Period	Depth	P1	P2	P3	P4	P5	P6	P7	P8	P9	Fabric	Remarks
001	68	2.95	3.93	8.00	49.566	61.573	54.564	0.000	61.195	60.035	66.132	54.280	54.835	FAB	0 MIN
002	68	2.92	3.95	8.00	49.992	59.759	54.220	0.000	61.416	59.367	61.330	51.713	55.206	FAB	2 MIN
003	68	2.92	3.95	8.00	49.708	58.673	53.499	0.000	61.486	59.063	60.955	50.979	54.835	FA3	4 MIN
004	68	2.92	3.95	8.00	49.708	59.035	54.476	0.000	61.923	59.731	62.078	54.260	55.576	FA3	8 MIN
005	68	2.92	3.95	8.00	49.140	58.673	53.643	0.000	61.135	59.003	59.834	52.446	53.724	FAB	15 MIN
006	68	2.92	3.95	8.00	49.704	60.846	54.503	0.000	61.486	59.367	64.322	53.547	54.465	FA3	30 MIN
007	68	2.92	3.95	8.00	48.998	59.397	53.355	59.455	61.195	65.419	64.770	53.180	54.094	FAB	60 MIN
008	8A	0.68	1.77	8.00	.710	1.159	1.082	1.704	1.748	1.530	1.945	1.650	1.112	FAB	
009	80	1.36	1.77	8.00	1.775	1.992	2.163	3.263	3.533	3.533	4.114	2.567	2.223	FA3	
010	8C	2.03	1.77	8.00	2.556	3.260	3.605	5.075	5.537	5.463	6.544	4.218	3.779	FA3	
011	7A	1.28	2.80	8.00	11.362	12.894	13.050	15.661	16.173	16.335	17.950	15.991	13.857	FA3	
012	79	2.52	2.80	8.00	23.008	26.222	25.956	32.193	34.240	34.819	36.648	34.035	28.159	FAB	
013	7C	3.76	2.80	8.00	31.955	33.755	36.771	42.054	45.896	46.620	51.308	46.945	37.051	FA3	
014	6A	1.44	3.95	8.00	23.576	25.352	25.235	27.987	29.869	29.137	32.909	33.008	25.936	FA3	
015	68	2.92	3.95	8.00	48.208	53.079	52.490	57.280	60.175	51.274	62.452	62.349	54.094	FAB	
016	8C	4.48	5.59	8.00	30.745	35.554	34.172	39.202	43.572	45.155	52.272	52.252	50.656	FA3	
017	5A	1.55	5.59	8.00	31.955	34.763	34.688	36.611	37.154	36.786	41.136	45.478	35.569	FAB	
018	58	3.07	5.59	8.00	52.904	54.327	55.474	59.455	61.559	53.362	64.696	67.117	57.635	FA3	
019	4A	1.56	8.84	8.00	36.216	39.839	38.214	39.153	40.796	40.428	41.510	48.050	38.533	FAB	
020	68	2.92	3.95	8.00	47.578	58.705	51.624	57.135	58.135	57.546	62.826	62.349	53.724	FA3	0 MIN
021	68	2.92	3.95	8.00	47.152	51.423	52.922	58.805	59.446	58.639	63.574	62.349	54.094	FA3	2 MIN
022	68	2.92	3.95	8.00	48.572	51.791	53.499	58.875	59.883	58.639	63.574	64.181	54.465	FAB	4 MIN
023	68	2.92	3.95	8.00	48.572	51.791	53.643	58.875	60.029	58.274	63.574	64.916	54.094	FAB	8 MIN
024	68	2.92	3.95	8.00	48.438	52.516	53.643	59.745	60.466	58.639	63.574	64.183	54.094	FAB	15 MIN
025	68	2.92	3.95	8.00	48.288	51.429	53.355	58.738	60.466	58.639	63.208	64.183	52.612	FAB	30 MIN
026	68	2.92	3.95	8.00	48.714	53.240	53.355	59.330	60.758	59.367	63.574	63.449	52.612	FAB	60 MIN
27 RUN MISSING															
028	8A	0.68	1.77	8.00	1.420	1.087	1.442	1.450	1.457	1.821	1.878	1.834	1.112	FAB	
029	88	1.36	1.77	8.00	2.130	1.811	2.163	3.263	3.643	3.278	3.740	2.934	2.594	FA3	
030	8C	2.03	1.77	8.00	2.485	2.897	3.605	5.075	5.464	5.827	6.731	4.461	3.335	FAB	
031	7A	1.28	2.80	8.00	18.652	11.590	11.536	13.776	15.299	14.569	15.706	16.871	14.820	FA3	
032	78	2.52	2.80	8.00	22.724	26.077	27.358	30.453	33.511	33.508	35.904	35.269	26.677	FAB	
033	7C	3.76	2.80	8.00	31.245	36.218	37.493	44.954	46.625	48.097	52.355	46.945	38.533	FA3	
034	6A	1.47	3.95	8.00	22.724	31.872	27.358	27.552	27.683	29.137	31.413	30.808	25.195	FAB	
035	68	2.92	3.95	8.00	46.157	58.705	46.866	58.754	58.281	58.274	62.272	58.681	51.871	FAB	
036	6C	4.48	3.95	8.00	60.368	65.192	64.891	72.586	72.851	72.843	78.532	80.687	66.692	FAB	
037	5A	1.55	5.59	8.00	31.955	32.596	32.445	36.253	36.425	36.422	41.136	44.811	37.051	FA3	
038	58	3.07	5.59	8.00	46.157	54.327	54.076	58.005	58.281	58.274	63.574	66.016	59.281	FAB	
039	4A	1.56	8.84	8.00	36.926	39.839	36.050	39.153	40.796	40.064	43.380	47.679	40.756	FAB	
040	68	2.92	3.95	8.00	46.869	58.705	49.829	58.005	61.195	61.917	67.376	62.349	55.576	FA3	0 MIN
041	68	2.92	3.95	8.00	48.208	58.705	51.913	58.005	58.281	58.274	64.322	62.349	51.871	FAB	2 MIN
042	68	2.92	3.95	8.00	48.208	58.705	51.913	58.005	59.728	58.274	64.322	58.681	51.871	FA3	4 MIN
043	68	2.92	3.95	8.00	46.868	47.083	51.903	58.005	59.728	58.274	62.826	62.349	51.871	FAB	8 MIN
044	68	2.92	3.95	8.00	49.708	47.093	51.903	59.445	58.281	58.274	64.322	62.349	51.871	FAB	15 MIN
045	68	2.92	3.95	8.00	48.288	47.083	51.903	58.005	58.281	58.274	64.322	62.349	51.871	FAB	30 MIN
046	68	2.92	3.95	8.00	47.854	58.705	59.113	58.005	59.728	58.274	64.322	58.681	55.576	FA3	60 MIN
047	8A	0.68	1.77	8.00	.355	.765	1.082	1.450	1.457	1.821	1.878	1.100	1.112	FAB	
048	88	1.36	1.77	8.00	1.420	1.811	1.803	3.263	3.643	3.642	3.740	2.934	3.705	FAB	
049	8C	2.03	1.77	8.00	2.485	3.260	3.605	5.075	5.464	5.463	6.357	4.834	3.705	FAB	
050	78	2.52	2.80	8.00	24.144	26.801	29.843	31.903	33.511	34.965	37.396	34.475	28.988	FAB	
051	7A	1.28	2.80	8.00	18.652	13.038	12.978	15.226	16.027	16.025	17.282	16.137	14.820	FA3	
052	7C	3.76	2.80	8.00	34.086	36.218	38.935	44.954	46.625	48.076	50.859	46.945	40.815	FA3	
053	6A	1.47	3.95	8.00	22.724	26.077	25.956	29.002	29.140	29.137	31.413	33.742	26.677	FAB	
054	69	2.92	3.95	8.00	39.482	41.777	43.261	47.854	49.539	48.076	53.851	52.813	44.461	FAB	
055	6C	4.48	3.95	8.00	56.809	61.570	61.286	72.586	72.851	72.843	78.532	77.019	66.692	FAB	
056	5A	1.55	5.59	8.00	31.245	36.218	34.608	36.253	37.082	40.064	38.892	48.343	37.051	FAB	
057	58	3.07	5.59	8.00	49.708	57.943	54.076	58.005	58.281	61.917	63.574	69.684	55.576	FA3	
058	4A	1.56	8.84	8.00	35.506	36.218	37.493	39.153	40.796	40.064	41.884	47.679	37.051	FAB	
059	68	2.92	3.95	8.00	49.708	58.705	58.471	58.005	58.281	58.274	64.322	58.681	55.576	FA3	0 MIN
060	68	2.92	3.95	8.00	49.708	58.705	51.913	58.005	59.738	58.274	64.322	62.349	55.576	FA3	2 MIN
061	68	2.92	3.95	8.00	49.708	58.705	51.903	58.005	59.728	61.917	64.322	62.349	51.871	FAB	4 MIN

062	68	2.92	3.95	8.00	44.288	50.705	53.355	59.445	59.728	59.274	64.322	62.349	55.576	FA3	8 MIN
063	68	2.92	3.95	8.00	48.288	54.327	53.355	43.504	53.910	59.274	65.818	62.349	55.576	FA3	15 MIN
064	68	2.92	3.95	8.00	48.288	54.327	53.355	56.555	56.824	58.274	61.320	62.349	51.871	FA1	30 MIN
065	68	2.92	3.95	8.00	49.708	54.327	51.901	59.445	59.723	61.317	64.322	62.349	51.871	FA1	60 MIN
66 RANDOM WAVE															
067	8A	0.68	1.77	8.00	.710	.724	1.002	1.450	1.021	1.921	1.870	1.160	1.112	FAH	
068	8B	1.36	1.77	8.00	1.420	1.811	2.163	3.263	3.643	3.642	3.740	2.567	2.223	FAR	
069	8C	2.03	1.77	8.00	2.130	3.260	3.665	5.075	5.829	5.827	5.981	4.334	3.335	FAH	
070	7B	2.52	2.00	8.00	24.144	26.801	27.394	31.903	33.511	34.236	37.396	34.475	29.641	FAB	
071	7A	1.28	2.00	8.00	106.517	13.038	122.572	10.372	15.293	16.025	17.950	16.137	14.820	FA1	
072	7C	3.76	2.00	8.00	32.665	37.666	17.493	44.944	46.625	48.076	50.359	46.945	40.015	FAB	
73 RANDOM WAVE															
074	6A	1.47	3.95	8.00	22.724	241.934	27.358	29.002	29.140	29.137	31.413	30.808	28.159	FAB	
075	6B	2.92	3.95	8.00	45.447	47.083	50.471	58.005	58.281	61.917	61.320	62.349	51.871	FAH	
076	6C	4.40	3.95	8.00	60.360	65.192	68.496	72.506	72.851	72.443	70.532	79.953	67.464	FA3	
077	5A	1.55	5.59	8.00	31.245	36.520	34.688	26.253	36.425	36.422	40.389	44.011	35.198	FAB	
078	5B	3.07	5.59	8.00	49.708	52.536	54.076	58.005	58.281	55.361	63.574	66.016	57.429	FAB	
079	4A	1.56	8.84	8.00	35.506	36.218	36.850	36.253	36.425	36.422	41.884	44.011	37.051	FAB	
080	6B	2.92	3.95	8.00	46.868	52.143	50.471	56.555	58.281	58.274	62.826	63.882	54.835	FA9	0 MIN
081	6B	2.92	3.95	8.00	49.708	52.143	51.903	58.005	61.195	61.188	64.322	66.016	56.317	FAB	30 MIN
082	6B	2.92	3.95	8.00	48.288	53.602	51.901	58.005	59.728	61.188	64.322	66.016	56.317	FAB	60 MIN
083	6B	2.92	3.95	8.00	48.288	53.602	51.901	58.005	59.728	61.188	64.322	66.016	57.799	FAB	30 MIN
084	6B	2.92	3.95	8.00	48.288	53.602	51.901	58.005	58.281	61.188	64.322	66.016	56.317	FA1	120 MIN
085	6B	2.92	3.95	8.00	48.288	53.602	51.901	59.445	61.195	61.188	64.322	66.016	57.799	FAB	150 MIN
086	6B	2.92	3.95	8.00	48.288	53.602	51.901	58.005	59.728	61.188	64.322	63.882	57.799	FA3	180 MIN
087	6B	2.92	3.95	8.00	48.288	53.602	51.901	58.005	58.281	59.721	62.826	64.549	56.317	FAB	210 MIN
088	6B	2.92	3.95	8.00	48.288	52.143	51.903	59.445	61.195	61.188	64.322	64.549	53.343	FA9	240 MIN
089	8A	0.68	1.77	8.00	.710	1.887	.721	1.088	1.821	1.821	1.496	1.467	1.112	FAB	
090	8B	1.36	1.77	8.00	1.420	2.173	1.883	2.900	3.278	3.278	3.740	3.301	1.853	FAB	
091	8C	2.03	1.77	8.00	2.405	3.260	3.605	4.350	5.100	5.827	6.357	4.834	3.705	FA9	
092	7A	1.28	2.00	8.00	11.362	12.314	12.970	15.226	16.027	16.025	17.202	16.137	13.338	FA3	
093	7B	2.52	2.00	8.00	24.144	27.525	27.394	31.903	33.511	33.508	35.908	33.742	28.159	FA9	
094	7C	3.76	2.00	8.00	32.665	36.218	37.493	44.954	46.625	48.076	52.355	48.412	38.533	FAB	
095	6A	1.47	3.95	8.00	22.724	26.077	25.956	27.552	27.683	29.137	31.413	32.275	26.677	FA9	
096	6B	2.92	3.95	8.00	46.868	51.429	57.681	56.555	58.281	58.274	62.826	62.349	48.166	FAB	
097	6C	4.40	3.95	8.00	56.889	61.578	61.286	68.881	69.208	72.843	74.793	77.819	62.987	FA3	
098	5A	1.55	5.59	8.00	35.506	36.218	36.850	39.878	36.425	40.864	41.136	44.811	37.051	FAB	
099	5B	3.07	5.59	8.00	49.708	54.327	50.471	58.005	61.923	61.317	63.574	69.684	59.281	FAB	
100	4A	1.56	8.84	8.00	35.506	39.833	36.850	39.153	40.796	40.864	44.876	44.811	37.051	FA3	
101 RANDOM WAVE															
102	7A	0.64	1.58	4.00	3.551	4.346	5.047	6.526	7.285	7.649	8.965	6.968	5.187	FAB	
103	7B	1.26	1.58	4.00	7.101	7.968	10.094	13.776	15.299	15.297	17.950	12.470	8.151	FAB	
104	7C	1.98	1.58	4.00	9.942	10.965	14.420	20.302	21.855	21.124	25.056	16.871	13.338	FA9	
105	6A	0.74	2.00	4.00	9.231	10.965	12.257	14.501	15.249	14.569	16.454	14.670	12.597	FA9	
106	6B	1.46	2.00	4.00	19.883	22.455	24.514	29.082	30.597	32.051	34.405	28.607	23.713	FA9	
107	5A	0.78	3.95	4.00	15.623	15.936	15.862	8.000	18.941	18.939	20.342	20.538	17.784	FAB	
108	5B	1.54	3.95	4.00	29.825	33.320	33.166	39.153	39.339	39.335	41.884	38.143	32.605	FA9	
109	4A	0.78	6.25	4.00	14.282	15.936	15.862	17.401	18.941	17.482	19.446	23.473	17.784	FAB	
110	4B	1.58	6.25	4.00	26.984	30.423	30.282	33.353	36.425	36.422	38.892	42.544	32.605	FA9	
111	8A	0.64	1.77	8.00	.710	.724	.721	1.450	1.821	1.821	1.870	1.160	1.112	PLS	
112	8B	1.36	1.77	8.00	1.775	1.811	1.863	2.900	3.643	4.006	4.114	2.934	2.223	PLS	
113	8C	2.03	1.77	8.00	2.840	2.535	2.884	4.713	5.828	5.827	6.357	4.461	2.964	PLS	
114	7A	1.28	2.00	8.00	11.362	10.865	10.815	14.501	16.027	16.025	17.202	15.404	13.338	PLS	
115	7B	2.52	2.00	8.00	22.724	23.179	24.514	30.453	33.511	32.051	37.396	30.808	26.677	PLS	
116	7C	3.76	2.00	8.00	32.665	34.763	34.688	42.054	46.625	48.076	50.859	44.811	38.533	PLS	
117	6A	1.47	3.95	8.00	22.724	23.179	23.072	27.552	29.140	29.137	31.413	29.341	25.195	PLS	
118	6B	2.92	3.95	8.00	45.447	46.359	47.587	56.555	58.281	58.274	62.826	61.615	50.389	PLS	
119	6C	4.40	3.95	8.00	56.889	61.578	61.286	68.881	76.493	72.843	78.532	73.352	66.692	PLS	
120	5A	1.55	5.59	8.00	31.955	28.974	29.561	26.253	36.425	36.422	41.136	40.343	33.346	PLS	
121	5B	3.07	5.59	8.00	46.157	50.705	50.471	58.754	58.281	58.274	63.574	58.681	51.871	PLS	
122	4A	1.56	8.84	8.00	39.056	39.833	39.656	47.129	43.710	47.348	48.615	51.346	44.461	PLS	
123	6B	2.92	3.95	8.00	46.868	46.359	47.587	55.185	58.281	58.818	62.826	58.681	51.871	PLS	0 MIN
124	6B	2.92	3.95	8.00	45.447	46.359	47.587	55.185	58.281	58.274	61.320	58.681	51.871	PLS	2 MIN

125	6E	2.92	3.95	8.00	46.460	47.407	47.547	56.555	58.281	58.274	62.426	61.615	51.871	PLS	4	MIN
126	6D	2.92	3.95	8.00	48.288	47.407	49.029	58.005	59.728	61.188	63.917	63.082	51.871	PLS	4	MIN
127	6B	2.92	3.95	8.00	48.841	47.407	49.029	56.555	59.728	59.274	64.322	61.615	51.871	PLS	15	MIN
128	6D	2.92	3.95	8.00	46.868	47.887	49.029	56.555	58.281	56.818	62.826	63.382	50.389	PLS	30	MIN
129	6B	2.92	3.95	8.00	46.868	46.359	47.587	56.555	59.728	56.318	64.322	61.615	50.389	PLS	60	MIN
130	8A	0.68	1.77	8.00	.710	.724	1.082	1.450	1.457	1.821	1.870	1.100	1.112	PLS	60	MIN
131	8D	1.36	1.77	8.00	1.775	1.811	1.803	2.900	3.643	3.278	4.114	2.190	2.223	PLS	60	MIN
132	8C	2.03	1.77	8.00	2.485	2.535	2.884	4.350	5.100	5.899	5.983	3.301	2.594	PLS	60	MIN
133	7A	1.28	2.00	8.00	9.942	13.141	18.815	14.501	14.570	14.569	16.454	14.670	12.597	PLS	60	MIN
134	7B	2.52	2.00	8.00	24.144	21.731	25.956	31.903	32.054	32.051	35.900	32.275	25.195	PLS	60	MIN
135	7C	3.76	2.00	8.00	32.665	31.872	36.050	42.054	45.168	45.163	49.363	42.544	37.051	PLS	60	MIN
136	6A	1.47	3.95	8.00	22.724	21.731	23.072	27.552	29.140	27.600	29.917	29.341	22.211	PLS	60	MIN
137	6B	2.92	3.95	8.00	45.447	44.910	47.587	53.655	58.281	56.818	61.320	60.138	48.937	PLS	60	MIN
138	6C	4.40	3.95	8.00	56.809	57.948	56.279	68.881	72.551	69.201	74.793	73.352	62.987	PLS	60	MIN
139	5A	1.55	5.59	8.00	31.955	28.974	28.840	36.253	36.425	36.422	41.136	40.343	37.051	PLS	60	MIN
140	5B	3.07	5.59	8.00	46.157	47.083	58.471	54.380	58.281	58.274	63.574	62.349	48.166	PLS	60	MIN
141	4A	1.56	0.84	8.00	32.665	32.596	33.166	36.253	37.882	36.422	41.884	40.343	33.346	PLS	120	MIN
142	8A	0.68	1.77	8.00	.710	.724	.721	1.088	1.457	1.821	1.870	.734	.741	PLS	120	MIN
143	8B	1.36	1.77	8.00	1.775	1.449	1.803	3.082	5.100	3.278	3.740	2.934	1.853	PLS	120	MIN
144	8C	2.03	1.77	8.00	2.485	2.535	2.924	4.350	5.100	5.463	6.357	3.668	2.964	PLS	120	MIN
145	7A	1.28	2.00	8.00	10.652	10.141	11.536	15.226	15.299	15.297	17.202	14.670	12.597	PLS	120	MIN
146	7B	2.52	2.00	8.00	22.724	21.731	24.154	31.178	33.511	33.508	34.485	38.808	26.677	PLS	120	MIN
147	7C	3.76	2.00	8.00	31.245	30.423	36.050	43.504	46.625	46.620	49.363	44.811	37.051	PLS	120	MIN
148	6A	1.47	3.95	8.00	22.724	21.731	23.072	26.102	27.683	27.600	29.917	29.341	23.713	PLS	120	MIN
149	6B	2.92	3.95	8.00	45.447	44.910	47.587	55.105	56.824	56.818	62.826	60.138	42.979	PLS	120	MIN
150	6C	4.40	3.95	8.00	56.839	57.948	57.681	65.256	69.208	72.843	78.532	73.352	59.281	PLS	120	MIN
151	5A	1.55	5.59	8.00	28.405	28.974	28.840	32.628	36.425	36.422	41.136	40.343	33.346	PLS	120	MIN
152	5B	3.07	5.54	8.00	46.157	47.083	46.866	54.380	54.632	59.834	58.681	48.166	48.166	PLS	120	MIN
153	4A	1.56	0.84	8.00	34.886	32.596	33.166	37.703	39.339	40.864	41.884	40.343	37.051	PLS	120	MIN
154	8A	0.68	1.77	8.00	.710	.724	.721	1.088	1.457	1.457	1.870	1.100	.741	PLS	240	MIN
155	8B	1.36	1.77	8.00	1.775	1.811	1.483	2.900	3.278	3.278	3.740	2.201	1.853	PLS	240	MIN
156	8C	2.03	1.77	8.00	2.485	2.173	2.524	4.350	5.464	5.463	5.983	3.301	2.964	PLS	240	MIN
157	7A	1.28	2.00	8.00	9.231	9.417	10.815	13.776	14.570	14.569	16.454	14.670	12.597	PLS	240	MIN
158	7B	2.52	2.00	8.00	22.724	21.731	24.514	30.453	34.968	33.508	35.900	35.209	26.677	PLS	240	MIN
159	7C	3.76	2.00	8.00	32.665	30.423	36.050	43.504	46.625	45.163	50.859	44.811	38.533	PLS	240	MIN
160	6A	1.47	3.95	8.00	22.724	20.282	23.072	27.552	29.140	27.600	29.917	24.940	29.641	PLS	240	MIN
161	6B	2.92	3.55	8.00	45.447	42.013	49.029	53.655	56.824	56.818	61.320	58.681	50.389	PLS	240	MIN
162	6C	4.40	3.95	8.00	56.809	54.327	57.681	68.881	69.200	72.843	74.793	73.352	62.987	PLS	240	MIN
163	5A	1.55	5.59	8.00	31.955	28.974	28.840	36.253	32.783	36.422	37.396	40.343	29.641	PLS	240	MIN
164	5B	3.07	5.59	8.00	46.157	43.461	46.866	54.380	58.281	54.632	59.834	62.349	51.871	PLS	240	MIN
165	4A	1.56	0.84	8.00	42.607	39.833	41.819	47.854	55.367	47.348	50.859	55.014	40.756	PLS	240	MIN
166	RANDOM WAVE															
167	8A	0.68	1.77	8.00	.710	.724	.721	1.088	1.457	1.457	1.870	.734	1.112	PLS	480	MIN
168	8B	1.36	1.77	8.00	1.775	1.449	1.442	3.263	3.278	3.642	3.740	1.834	1.853	PLS	480	MIN
169	8C	2.03	1.77	8.00	2.485	2.535	2.884	4.350	5.100	5.463	5.983	2.934	4.076	PLS	480	MIN
170	7A	1.28	2.00	8.00	10.652	10.141	11.536	14.501	16.027	16.025	17.202	12.470	14.820	PLS	480	MIN
171	7B	2.52	2.00	8.00	22.724	21.731	23.872	30.453	33.511	33.508	35.900	27.874	32.685	PLS	480	MIN
172	7C	3.76	2.00	8.00	31.245	28.974	33.166	42.054	45.168	46.620	49.363	36.676	44.461	PLS	480	MIN
173	6A	1.47	3.95	8.00	22.724	21.731	23.072	26.102	27.683	29.137	29.917	24.940	29.641	PLS	480	MIN
174	6B	2.92	3.95	8.00	44.027	43.461	46.145	55.105	55.367	58.274	59.834	48.412	59.281	PLS	480	MIN
175	6C	4.40	3.95	8.00	56.809	58.785	57.681	68.881	72.851	72.843	74.793	62.349	74.102	PLS	480	MIN
176	5A	1.55	5.59	8.00	28.405	28.974	28.840	32.628	32.783	36.422	37.396	36.676	37.051	PLS	480	MIN
177	5B	3.07	5.59	8.00	46.157	43.461	46.866	54.380	54.638	58.274	59.834	51.346	62.987	PLS	480	MIN
178	4A	1.56	0.84	8.00	34.886	32.596	33.166	36.253	39.339	40.864	41.884	37.185	40.756	PLS	480	MIN
179	7A	0.64	1.98	4.00	3.551	2.897	3.685	6.526	7.285	7.284	8.227	3.668	5.187	PLS		
180	7B	1.26	1.98	4.00	6.391	6.519	7.210	12.326	14.570	15.297	17.202	8.069	18.374	PLS		
181	7C	1.88	1.98	4.00	7.811	7.968	8.642	17.401	21.127	21.853	24.682	11.736	15.561	PLS		
182	6A	0.74	2.00	4.00	7.811	8.692	7.931	13.051	14.570	14.569	16.454	11.736	13.338	PLS		
183	6B	1.46	2.00	4.00	17.043	15.936	17.384	29.802	38.597	32.051	35.900	23.473	28.159	PLS		
184	5A	0.78	3.95	4.00	12.782	11.590	12.978	17.401	17.488	18.339	20.942	17.664	19.266	PLS		
185	5B	1.54	3.95	4.00	25.564	23.179	24.514	36.253	37.882	37.878	41.884	33.742	37.051	PLS		
186	4A	0.78	6.25	4.00	12.782	13.038	12.978	17.401	17.488	17.482	19.446	17.684	19.266	PLS		
187	4B	1.58	6.25	4.00	24.144	21.731	24.514	31.903	34.968	34.459	37.396	29.341	34.887	PLS		

188	8A	0.68	1.77	0.00	1.065	1.811	1.442	1.013	1.021	2.105	2.244	1.467	1.453	PLY	
189	8B	1.36	1.77	0.00	1.775	2.897	2.161	2.530	3.270	3.642	3.740	1.834	2.223	PLY	
190	8C	2.03	1.77	0.00	2.940	3.904	3.245	3.900	5.464	5.463	5.903	2.934	3.335	PLY	
191	7A	1.28	2.80	0.00	11.362	13.034	12.257	12.326	15.299	16.025	16.454	11.003	11.856	PLY	
192	7B	2.52	2.80	0.00	24.144	27.525	24.514	27.552	33.511	32.051	35.900	24.940	25.195	PLY	
193	7C	3.76	2.80	0.00	34.036	40.564	36.050	39.153	46.625	46.620	49.363	33.742	37.051	PLY	
194	6A	1.47	3.95	0.00	21.303	24.628	23.072	24.652	27.683	27.680	29.917	22.005	23.713	PLY	
195	6B	2.92	3.95	0.00	45.447	52.143	47.507	52.194	58.281	58.274	59.834	46.945	48.907	PLY	
196	6C	4.40	3.95	0.00	56.809	65.192	61.286	60.724	69.208	69.201	74.793	58.681	59.281	PLY	
197	5A	1.55	5.59	0.00	29.025	33.320	30.282	31.903	34.968	34.965	37.396	30.808	31.123	PLY	
198	5B	3.07	5.59	0.00	46.157	54.327	46.866	50.754	58.281	58.274	59.834	47.679	48.166	PLY	
199	4A	1.56	8.84	0.00	34.086	36.218	33.166	37.703	39.339	39.335	41.884	33.742	35.569	PLY	
200	6B	2.92	3.95	0.00	44.027	49.256	46.145	50.754	55.367	56.818	58.338	52.803	62.246	PLY	0 MIN
201	6B	2.92	3.95	0.00	44.027	49.256	47.587	50.754	56.824	56.818	59.834	54.280	62.246	PLY	2 MIN
202	6B	2.92	3.95	0.00	45.447	50.705	48.668	52.194	58.281	58.274	61.320	54.280	63.728	PLY	4 MIN
203	6B	2.92	3.95	0.00	45.447	49.256	47.587	52.194	64.109	58.274	61.320	52.803	65.210	PLY	8 MIN
204	6B	2.92	3.95	0.00	45.447	50.705	47.587	53.655	56.824	58.274	61.320	52.803	65.210	PLY	15 MIN
205	6B	2.92	3.95	0.00	45.447	50.705	47.587	53.655	56.824	58.274	59.834	52.803	66.692	PLY	30 MIN
206	6B	2.92	3.95	0.00	45.447	50.705	49.829	53.655	58.281	58.274	59.834	46.945	63.728	PLY	60 MIN
207	8A	0.68	1.77	0.00	1.065	1.807	1.002	1.450	1.821	1.457	1.070	1.100	1.402	PLY	60 MIN
208	8B	1.36	1.77	0.00	2.130	2.935	2.163	2.900	3.270	3.270	3.740	2.567	2.994	PLY	60 MIN
209	8C	2.03	1.77	0.00	3.196	3.622	3.605	4.350	5.464	5.827	6.357	3.668	5.187	PLY	60 MIN
210	7A	1.28	2.80	0.00	10.652	12.314	11.536	14.501	14.570	16.025	17.202	13.937	17.043	PLY	60 MIN
211	7B	2.52	2.80	0.00	24.144	27.525	25.956	31.903	33.511	33.508	35.900	27.874	35.569	PLY	60 MIN
212	7C	3.76	2.80	0.00	32.665	37.666	36.050	43.584	46.625	46.620	50.859	42.544	48.907	PLY	60 MIN
213	6A	1.47	3.95	0.00	21.303	24.628	23.072	26.102	27.683	29.137	28.421	24.940	29.641	PLY	60 MIN
214	6B	2.92	3.95	0.00	45.447	50.705	47.587	52.194	55.367	56.818	56.842	52.803	62.246	PLY	60 MIN
215	6C	4.40	3.95	0.00	56.809	57.940	57.681	65.256	69.208	72.843	74.793	62.349	77.807	PLY	60 MIN
216	5A	1.55	5.59	0.00	29.025	32.596	30.282	33.353	34.968	36.422	37.396	33.008	40.756	PLY	60 MIN
217	5B	3.07	5.59	0.00	46.157	50.705	43.261	50.754	54.638	58.274	59.834	51.346	62.987	PLY	60 MIN
218	4A	1.56	8.84	0.00	32.665	39.839	33.166	36.253	39.339	40.864	41.884	36.676	44.461	PLY	60 MIN
219	8A	0.68	1.77	0.00	1.065	1.449	1.002	1.450	1.821	1.821	2.244	1.100	1.402	PLY	120 MIN
220	8B	1.36	1.77	0.00	1.775	2.173	2.163	2.530	3.270	3.270	3.740	2.201	2.964	PLY	120 MIN
221	8C	2.03	1.77	0.00	3.196	4.346	3.245	4.350	5.464	5.827	6.357	3.668	4.446	PLY	120 MIN
222	7A	1.28	2.80	0.00	11.362	11.590	10.815	14.501	15.299	15.297	16.454	13.203	15.561	PLY	120 MIN
223	7B	2.52	2.80	0.00	0.000	26.077	24.514	30.453	30.597	33.508	35.900	27.874	35.569	PLY	120 MIN
224	7C	3.76	2.80	0.00	0.000	36.218	36.050	48.603	46.625	45.161	50.859	38.143	48.907	PLY	120 MIN
225	6A	1.47	3.95	0.00	22.724	24.628	23.072	27.552	27.683	27.680	29.917	24.940	32.605	PLY	120 MIN
226	6B	2.92	3.95	0.00	44.027	49.256	47.587	52.194	53.910	55.361	59.834	51.346	62.246	PLY	120 MIN
227	6C	4.40	3.95	0.00	56.809	65.192	57.681	65.256	69.208	69.201	74.793	62.349	74.102	PLY	120 MIN
228	5A	1.55	5.59	0.00	29.025	32.596	30.282	33.353	34.968	36.422	37.396	33.008	40.756	PLY	120 MIN
229	5B	3.07	5.59	0.00	46.157	54.327	50.471	54.380	54.638	58.274	63.574	51.346	66.692	PLY	120 MIN
230	4A	1.56	8.84	0.00	32.665	39.839	33.166	34.083	39.339	40.864	40.389	36.676	44.461	PLY	120 MIN
231	8A	0.68	1.77	0.00	1.065	1.449	1.002	1.000	1.457	1.821	1.070	1.467	1.402	PLY	240 MIN
232	8B	1.36	1.77	0.00	2.130	2.173	2.163	2.530	3.643	4.086	3.740	2.567	2.964	PLY	240 MIN
233	8C	2.03	1.77	0.00	3.906	5.795	3.605	4.350	5.828	5.827	6.357	4.034	4.817	PLY	240 MIN
234	7A	1.28	2.80	0.00	10.652	12.314	11.536	13.776	16.027	16.025	16.454	13.937	16.302	PLY	240 MIN
235	7B	2.52	2.80	0.00	24.144	27.525	24.514	29.002	32.054	33.508	34.405	27.874	35.569	PLY	240 MIN
236	7C	3.76	2.80	0.00	34.036	37.666	36.050	39.153	46.625	46.620	49.363	39.618	48.907	PLY	240 MIN
237	6A	1.47	3.95	0.00	22.724	24.628	23.072	26.102	27.683	29.137	29.917	24.940	31.123	PLY	240 MIN
238	6B	2.92	3.95	0.00	45.447	49.256	46.145	50.754	56.824	56.818	59.834	52.813	62.246	PLY	240 MIN
239	6C	4.40	3.95	0.00	56.809	61.570	57.681	65.256	69.208	65.559	74.793	62.349	74.102	PLY	240 MIN
240	5A	1.55	5.59	0.00	28.405	32.596	30.282	31.903	34.968	32.779	29.917	33.008	40.756	PLY	240 MIN
241	5B	3.07	5.59	0.00	46.157	50.705	43.261	50.754	54.638	54.632	59.834	47.679	62.987	PLY	240 MIN
242	4A	1.56	8.84	0.00	34.086	36.218	34.600	37.703	39.339	40.864	43.380	.367	48.166	PLY	240 MIN
243	RANDOM HAVE														
244	8A	0.68	1.77	0.00	.710	.724	1.002	1.000	1.821	1.821	1.070	1.100	1.402	PLY	480 MIN
245	8B	1.36	1.77	0.00	1.775	2.173	1.803	1.813	3.270	3.270	3.740	2.201	2.223	PLY	480 MIN
246	8C	2.03	1.77	0.00	3.196	3.622	3.245	3.625	5.828	5.463	5.903	3.301	4.076	PLY	480 MIN
247	7A	1.28	2.80	0.00	11.362	12.314	11.536	13.051	15.299	16.025	17.244	13.937	15.561	PLY	480 MIN
248	7B	2.52	2.80	0.00	25.564	27.525	25.956	29.002	33.511	0.000	35.900	29.341	34.087	PLY	480 MIN
249	7C	3.76	2.80	0.00	24.144	34.769	25.956	29.002	33.511	29.137	35.900	27.874	35.569	PLY	480 MIN
250	6A	1.47	3.95	0.00	22.724	25.131	23.072	26.102	29.140	27.680	29.917	26.223	31.123	PLY	480 MIN

251	68	2.92	3.95	0.00	44.027	50.705	46.145	49.304	55.367	56.318	59.338	51.346	60.753	PLY	480	MIN
252	6C	4.40	3.95	0.00	56.809	61.570	57.681	65.256	69.208	69.201	74.793	62.349	74.102	PLY	480	MIN
253	5A	1.55	5.59	0.00	31.955	32.595	28.440	32.628	36.425	36.422	37.396	33.008	40.756	PLY	480	MIN
254	5B	3.07	5.59	0.00	46.157	50.705	46.066	54.380	58.281	58.274	41.136	51.346	62.987	PLY	480	MIN
255	4A	1.56	0.84	0.00	35.506	36.218	33.166	39.153	39.339	36.422	41.054	40.343	40.756	PLY	480	MIN
256	7A	0.64	1.98	4.00	4.971	5.070	4.687	5.075	0.014	0.013	9.349	6.286	5.187	PLY		
257	7B	1.26	1.98	4.00	9.231	9.417	9.373	11.238	15.663	15.297	17.576	9.536	12.597	PLY		
258	7C	1.88	1.98	4.00	11.362	13.030	12.974	15.226	20.390	21.053	21.914	13.203	16.302	PLY		
259	6A	0.74	2.00	4.00	9.942	10.141	10.094	11.601	14.570	14.569	15.786	11.736	11.056	PLY		
260	6B	1.46	2.00	4.00	21.303	21.731	21.630	24.652	29.140	30.594	32.909	24.940	28.159	PLY		
261	5A	0.70	3.95	4.00	14.202	15.936	14.420	15.351	17.404	15.939	19.446	16.137	17.784	PLY		
262	5B	1.54	3.95	4.00	28.485	30.421	28.840	31.903	37.082	37.078	41.044	33.742	37.051	PLY		
263	4A	0.78	6.28	4.00	15.623	15.936	14.420	15.951	17.404	17.402	17.950	17.604	20.743	PLY		
264	4B	1.58	6.25	4.00	27.044	28.974	28.840	29.002	36.425	31.508	37.396	30.068	37.051	PLY		
265	8A	0.68	1.77	0.00	.710	1.007	1.002	1.450	1.021	1.021	1.070	1.100	1.482	NON		
266	0B	1.36	1.77	0.00	1.420	1.011	1.003	2.908	3.643	2.914	3.740	1.034	2.964	NON		
267	0C	2.03	1.77	0.00	2.130	2.097	3.245	4.713	5.464	5.099	5.983	3.361	4.076	NON		
268	7A	1.28	2.00	0.00	11.362	12.314	12.257	15.226	15.299	16.025	16.454	13.203	16.302	NON		
269	7B	2.52	2.00	0.00	22.724	26.077	25.956	33.353	33.511	33.508	34.405	27.074	34.087	NON		
270	7C	3.76	2.00	0.00	34.086	36.218	36.050	44.954	46.625	45.163	49.363	39.610	51.071	NON		
271	6A	1.47	3.95	0.00	24.144	24.628	24.514	27.552	27.693	26.223	29.917	27.074	31.123	NON		
272	6B	2.92	3.95	0.00	46.060	50.705	50.471	59.105	56.824	53.904	58.338	54.200	63.728	NON		
273	6C	4.40	3.95	0.00	60.368	65.192	61.206	68.081	72.051	69.201	78.532	66.016	77.807	NON		
274	5A	1.55	5.59	0.00	31.955	36.218	32.445	36.253	36.425	36.422	37.396	29.341	44.461	NON		
275	5B	3.07	5.59	0.00	49.708	54.327	50.471	58.005	58.281	58.274	59.934	55.014	78.397	NON		
276	4A	1.56	0.84	0.00	35.506	36.218	36.050	36.253	40.068	40.064	41.136	40.343	48.166	NON		
277	6B	2.92	3.95	0.00	48.288	52.143	50.471	56.555	56.824	55.361	58.338	52.003	65.210	NON	0	MIN
278	6B	2.92	3.95	0.00	48.288	52.143	50.471	58.005	58.281	58.018	59.834	54.200	65.210	NON	2	MIN
279	6B	2.92	3.95	0.00	48.288	52.143	51.903	58.005	58.281	56.818	61.320	52.003	68.174	NON	4	MIN
280	6B	2.92	3.95	0.00	48.288	52.143	51.903	58.005	58.281	56.818	61.320	52.003	68.174	NON	8	MIN
281	6B	2.92	3.95	0.00	48.288	52.143	51.903	58.005	58.281	56.818	61.320	54.200	66.692	NON	15	MIN
282	6B	2.92	3.95	0.00	48.288	52.143	51.903	65.256	58.281	56.818	61.320	54.200	68.174	NON	30	MIN
283	6B	2.92	3.95	0.00	48.288	52.143	50.471	56.555	58.281	56.818	59.834	52.003	68.174	NON	60	MIN
284	8A	0.68	1.77	0.00	.710	.724	1.002	1.013	1.021	1.021	1.070	1.100	1.053	NON	60	MIN
285	0B	1.36	1.77	0.00	1.775	1.011	2.163	3.263	3.270	3.642	3.740	1.034	3.335	NON	60	MIN
286	0C	2.03	1.77	0.00	2.040	2.535	3.605	5.430	5.464	5.463	5.993	2.934	4.446	NON	60	MIN
287	7A	1.28	2.00	0.00	10.652	12.314	12.417	14.501	14.570	13.840	15.786	13.263	16.302	NON	60	MIN
288	7B	2.52	2.00	0.00	22.724	24.628	25.956	31.903	32.054	30.594	32.909	27.074	34.087	NON	60	MIN
289	7C	3.76	2.00	0.00	31.245	34.769	36.050	43.504	45.168	43.786	47.067	38.143	47.425	NON	60	MIN
290	6A	1.47	3.95	0.00	22.724	24.628	24.514	26.102	27.603	29.137	28.421	24.940	31.123	NON	60	MIN
291	6B	2.92	3.95	0.00	45.447	49.256	47.587	55.105	55.367	53.964	58.338	49.079	63.728	NON	60	MIN
292	6C	4.40	3.95	0.00	53.259	57.948	57.681	68.081	69.208	58.990	67.313	62.349	77.807	NON	60	MIN
293	5A	1.55	5.59	0.00	31.245	36.218	33.166	36.253	36.425	32.779	37.396	33.008	44.461	NON	60	MIN
294	5B	3.07	5.59	0.00	46.157	54.327	52.273	58.005	58.281	47.348	63.574	55.014	66.692	NON	60	MIN
295	4A	1.56	0.84	0.00	35.506	39.839	39.656	36.253	40.068	40.002	41.136	40.343	48.166	NON	60	MIN
296	8A	0.68	1.77	0.00	.710	.724	1.002	1.450	1.021	1.021	1.070	1.034	1.053	NON	240	MIN
297	0B	1.36	1.77	0.00	1.420	1.011	2.163	2.900	3.278	3.642	3.740	2.201	2.964	NON	240	MIN
298	0C	2.03	1.77	0.00	2.130	2.097	3.605	4.713	5.020	5.463	5.983	3.668	4.076	NON	240	MIN
299	7A	1.28	2.00	0.00	9.942	12.314	12.257	14.098	15.299	14.164	16.454	13.203	16.302	NON	240	MIN
300	7B	2.52	2.00	0.00	24.144	24.628	27.199	33.353	33.511	32.051	34.405	26.407	34.087	NON	240	MIN
301	7C	3.76	2.00	0.00	31.245	36.218	36.050	43.504	45.168	45.163	47.067	36.676	51.071	NON	240	MIN
302	6A	1.47	3.95	0.00	24.144	24.628	24.514	26.102	27.603	26.223	28.421	23.473	34.087	NON	240	MIN
303	6B	2.92	3.95	0.00	46.157	49.256	50.471	54.380	54.638	53.904	59.834	48.412	69.656	NON	240	MIN
304	6C	4.40	3.95	0.00	56.809	61.570	57.681	68.081	69.208	69.201	71.053	58.681	77.807	NON	240	MIN
305	5A	1.55	5.59	0.00	33.730	36.218	32.445	36.253	38.247	0.000	39.266	36.676	44.461	NON	240	MIN
306	5B	3.07	5.59	0.00	53.259	57.948	54.076	58.005	61.923	61.917	67.313	55.014	66.692	NON	240	MIN
307	4A	1.56	0.84	0.00	31.245	32.596	31.724	33.353	33.511	36.422	35.908	36.676	44.461	NON	240	MIN
308	8A	0.68	1.77	0.00	.710	1.007	1.002	1.013	1.021	1.021	1.070	.734	1.482	NON	480	MIN
309	0B	1.36	1.77	0.00	1.775	1.449	2.163	3.263	3.278	3.740	3.740	2.201	2.964	NON	480	MIN
310	0C	2.03	1.77	0.00	2.485	2.097	3.245	4.713	5.464	5.427	6.357	2.934	4.076	NON	480	MIN
311	7A	1.28	2.00	0.00	11.362	11.590	12.257	15.226	15.299	17.202	17.202	12.470	16.302	NON	480	MIN
312	7B	2.52	2.00	0.00	22.724	26.077	27.199	31.903	32.054	32.051	35.908	26.407	34.087	NON	480	MIN
313	7C	3.76	2.00	0.00	31.245	34.769	36.050	43.504	45.168	43.786	47.067	36.676	48.907	NON	480	MIN

314	6A	1.47	3.95	8.00	22.724	24.628	23.072	27.592	27.633	27.640	29.317	22.105	35.569	NON	4.33	MIN
315	6B	2.92	3.95	8.00	44.027	47.007	47.507	53.655	53.910	52.437	54.338	48.412	66.692	NON	4.10	MIN
316	6C	4.40	3.95	8.00	56.839	61.570	57.681	65.256	50.996	61.917	74.793	58.681	81.512	NON	4.30	MIN
317	5A	1.55	5.59	8.00	35.586	36.218	32.445	36.253	36.425	40.064	41.136	36.076	44.461	NON	4.80	MIN
318	5B	3.07	5.59	8.00	53.259	57.948	50.471	58.005	65.566	61.917	63.574	58.681	70.397	NON	4.30	MIN
319	4A	1.56	8.84	8.00	28.405	32.596	30.282	31.903	30.597	32.779	34.435	29.341	40.756	NON	4.80	MIN
320	7A	0.64	1.98	4.00	3.551	4.346	4.607	7.613	7.649	8.313	9.149	5.135	6.669	NON		
321	7B	1.26	1.98	4.00	6.391	7.968	9.371	14.501	15.299	14.569	17.950	8.792	12.597	NON		
322	7C	1.88	1.50	4.00	9.942	10.141	12.257	19.577	19.670	19.668	22.438	13.937	17.043	NON		
323	6A	0.74	2.40	4.00	8.521	8.682	10.094	11.601	13.113	13.112	13.463	11.003	11.856	NON		
324	6B	1.46	2.80	4.00	21.303	23.179	24.514	31.903	34.968	32.051	35.900	26.407	28.159	NON		
325	5A	0.78	3.55	4.00	17.043	18.833	17.384	20.382	21.855	21.853	22.438	17.604	20.749	NON		
326	5B	1.54	3.95	4.00	34.886	34.763	36.050	48.683	48.796	48.792	43.383	32.275	40.815	NON		
327	4A	6.78	6.25	4.00	17.043	17.385	17.384	20.382	20.398	18.939	20.942	20.534	19.266	NON		
328	4B	1.58	6.25	4.00	29.825	31.872	31.724	37.703	36.425	43.786	43.388	33.742	38.533	NON		

RUN,CASE,HEIGHT,PERIOD,DEPTH, P10,P9	P8	P7	P6	P5	P4	P3	P2	P1,FABRIC			
1 7A 1.90 2.60 8.00	26.136	26.769	26.710	25.156	24.327	23.293	22.626	20.531	20.468	20.290	GRV
2 7B 2.56 2.76 8.00	34.142	35.006	34.894	32.820	31.526	30.565	29.398	27.050	26.602	26.275	GRV
3 7C 3.18 2.78 8.00	45.432	46.434	46.302	43.688	41.919	40.517	39.127	36.361	35.684	35.311	GRV
4 6A 1.34 3.96 8.00	29.016	29.866	29.972	29.166	28.565	28.024	27.630	25.663	26.336	26.163	GRV
5 6B 3.03 3.98 8.00	59.328	60.664	61.041	58.972	57.972	56.764	55.937	52.891	53.385	53.174	GRV
6 6C 3.79 4.00 8.00	77.329	77.154	77.502	74.856	73.472	71.969	70.985	67.333	67.686	67.535	GRV
7 5A 1.67 5.58 8.00	37.526	38.524	38.889	38.129	37.742	37.269	37.112	35.010	35.847	35.937	GRV
8 5D 3.17 5.61 8.00	59.501	60.599	61.185	59.688	58.845	57.968	57.385	54.416	55.320	55.209	GRV
9 4A 1.63 8.85 8.00	42.725	43.942	44.588	44.150	43.976	43.653	43.433	40.898	42.620	42.499	GRV
10 7A 1.11 2.79 8.00	15.595	15.637	14.146	14.585	13.798	13.306	8.671	11.718	11.888	10.229	GRV
11 7B 2.43 2.81 8.00	33.667	33.979	30.470	31.387	29.927	28.925	18.823	25.846	25.933	21.194	GRV
12 7C 3.58 2.85 8.00	49.291	49.645	44.717	46.027	44.173	42.488	27.773	38.693	38.300	31.175	GRV
13 6A 1.36 3.94 8.00	29.434	29.740	26.599	28.710	28.124	27.624	18.227	25.283	26.160	21.478	GRV
14 6B 3.09 3.94 8.00	60.653	61.112	55.638	58.904	57.593	57.251	37.187	52.681	53.164	43.123	GRV
15 6C 4.14 3.98 8.00	77.198	76.681	78.276	73.442	72.296	71.564	46.704	66.568	67.023	54.158	GRV
16 5A 1.76 5.59 8.00	37.880	38.150	34.490	37.674	37.292	36.680	24.426	34.446	35.441	29.319	GRV
17 5B 3.29 5.58 8.00	59.875	60.122	54.692	58.871	57.838	56.955	37.858	53.674	54.727	44.561	GRV
18 4A 1.76 8.84 8.00	43.661	43.997	40.362	44.066	43.718	43.417	28.934	40.885	42.532	34.640	GRV
19 7A 1.11 2.83 8.00	15.768	15.845	15.694	14.870	14.149	13.533	13.009	11.756	11.668	11.597	PLS
20 7B 2.53 2.78 8.00	34.546	34.592	34.258	32.588	30.828	29.487	28.373	25.843	25.522	25.291	PLS
21 7C 3.44 2.78 8.00	44.554	44.658	45.077	42.145	40.845	38.246	37.885	34.062	33.515	33.283	PLS
22 6A 1.35 3.94 8.00	28.987	29.153	29.557	28.468	28.716	26.985	26.542	24.535	25.189	24.977	PLS
23 6B 3.11 4.00 8.00	59.328	59.775	60.199	58.269	56.756	55.198	54.139	50.839	51.230	51.083	PLS
24 6C 3.42 4.83 8.00	75.096	75.586	76.068	73.736	71.878	69.775	68.558	64.470	64.719	64.454	PLS
25 5A 1.73 5.58 8.00	37.526	37.668	38.812	37.426	36.873	36.187	35.949	33.665	34.436	34.641	PLS
26 5B 3.12 5.60 8.00	58.688	60.010	60.896	59.468	58.107	56.537	55.721	52.215	53.047	52.996	PLS
27 4A 1.65 8.84 8.00	43.776	44.079	44.728	44.115	43.766	43.281	43.045	40.473	41.951	41.983	PLS
28 7A 1.14 2.79 8.00	15.898	16.147	15.703	14.754	14.387	13.871	13.744	13.097	12.258	12.293	WHT
29 7B 2.57 2.76 8.00	35.122	35.618	34.888	32.719	31.835	30.767	30.594	29.029	27.193	27.077	WHT
30 7C 3.33 2.78 8.00	44.451	45.801	43.996	41.372	40.323	39.054	38.787	36.868	34.779	34.508	WHT
31 6A 1.41 3.95 8.00	30.240	30.554	-1.843	29.626	29.299	28.679	28.796	27.798	27.882	27.147	WHT
32 6B 3.20 3.96 8.00	60.523	61.323	61.817	59.121	58.363	57.105	57.390	55.288	53.987	54.023	WHT
33 6C 3.97 3.93 8.00	77.573	78.291	77.663	75.455	74.695	73.027	73.424	70.632	69.141	69.328	WHT
34 5A 1.79 5.59 8.00	38.174	38.699	38.538	38.234	37.989	37.407	37.785	36.394	36.185	36.466	WHT
35 5B 3.27 5.60 8.00	59.731	60.498	60.708	59.355	58.977	57.877	58.435	56.251	55.648	56.113	WHT
36 4A 1.66 8.85 8.00	43.661	44.202	44.686	44.137	44.170	43.518	44.124	42.443	42.718	42.986	WHT
37 7A 1.13 2.79 8.00	15.797	14.381	13.898	14.162	14.179	13.901	13.851	13.275	12.865	12.925	PLS
38 7B 2.56 2.76 8.00	34.920	31.888	30.257	30.752	30.447	29.931	29.890	28.783	27.629	27.814	PLS
39 7C 3.22 2.75 8.00	44.136	39.481	38.501	34.937	38.645	37.754	37.851	36.390	35.899	35.201	PLS
40 6A 1.37 3.98 8.00	30.818	27.318	26.962	27.419	27.672	27.364	27.639	26.841	26.667	26.768	PLS
41 6B 3.20 3.95 8.00	60.552	54.885	54.822	54.969	55.295	54.757	55.278	53.531	53.289	53.598	PLS
42 6C 3.96 3.56 8.00	77.227	69.696	68.268	69.558	69.893	69.177	69.964	67.794	67.266	67.816	PLS
43 5A 1.72 5.58 8.00	37.973	35.279	34.692	34.971	35.349	34.852	35.320	34.387	34.324	34.682	PLS
44 5B 3.21 5.60 8.00	59.774	54.998	54.981	54.936	55.128	54.200	55.131	53.285	53.179	53.845	PLS
45 4A 1.76 8.81 8.00	44.418	42.884	42.364	41.850	42.157	41.669	42.224	40.994	41.236	41.403	PLS

APPENDIX E

English/SI Unit Conversions

Area:	$1 \text{ ft}^2 = 0.0929 \text{ m}^2$
Density:	$1 \text{ slug/ft}^3 = 515.4 \text{ kg/m}^3$
Force:	$1 \text{ lb} = 4.4483 \text{ N}$
Length:	$1 \text{ ft} = 0.305 \text{ m}$
Mass:	$1 \text{ slug} = 14.60 \text{ kg}$
Pressure:	$1 \text{ lb/ft}^2 = 47.9 \text{ N/m}^2$
Specific Weight:	$1 \text{ lb/ft}^3 = 157.1 \text{ N/m}^3$
Stress:	$1 \text{ lb/ft}^2 = 47.9 \text{ N/m}^2$
Velocity:	$1 \text{ ft/s} = 0.305 \text{ m/s}$
Volume:	$1 \text{ ft}^3 = 0.0283 \text{ m}^3$